# $CO_2$ ADSORPTION CAPACITIES OF GASIFIED COAL CHARS

by

Pavan Pramod Sripada

A thesis submitted in partial fulfillment of the requirements for the degree of

Master of Science

in

Chemical Engineering

Department of Chemical and Materials Engineering
University of Alberta

# Abstract

Recent interest in the use of *post*-underground coal gasification (UCG) sites for carbon capture and storage (CCS) has created a need to fundamentally understand the carbon dioxide ($CO_2$) adsorption on gasified and pyrolysed coal chars. More specifically, in this work, the effect of coal properties on the surface area development and subsequently the $CO_2$ adsorption capacities of coal chars are studied. In addition, some design considerations necessary for obtaining reliable adsorption measurements on a volumetric adsorption apparatus have been suggested based on sensitivity analysis on the accuracies on the components of the apparatus. $CO_2$ adsorption isotherms at 45.5°C were obtained for pyrolysed and gasified coal samples. Two pyrolysed chars and four $CO_2$ gasified chars were obtained from different coals at different temperatures. The sorption capacities were in turn compared with the respective raw coal samples. Results indicate that the adsorption capacity of both pyrolysed and gasified char is much higher in comparison to the raw coal samples. In addition, in the case of gasified chars, it was demonstrated that the chars from a sub-bituminous coal (characteristic of very high vitrinite content) had the highest sorption capacity followed by the lignite and bituminous char respectively. Moreover, the pore size distributions indicate enhanced micro and meso-porosity for the chars. The diffusivity decreased with increase in pressure for all the samples. The effective diffusivities in the raw coals were clearly a function of the mesoporosity in the coal. Further, the Dubinin-Astakhov model was found to be consistent with the experimental data.

**Keywords:** $CO_2$ adsorption, volumetric apparatus, pyrolysed coal char, gasified coal char, Underground coal Gasification-Carbon Capture and Storage.

# Preface

The results presented in this thesis comprises of three parts, namely, the sensitivity analysis and performance evaluation of volumetric adsorption apparatus (Chapter -4), adsorption behaviour of coal and coal char (Chapter – 5), and $CO_2$ adsorption in gasified chars (Chapter -6). The adsorption apparatus -2 was designed by P.P. Sripada in collaboration with Dr. S. Ramasamy. The literature review (Chapter-2), the sensitivity analysis and optimal operating procedures in Chapter -4, and the study on gasified chars in Chapter -5 are the original work of this study. The development of the horizontal tube furnace setup, the gasified char preparation, surface characterization and the adsorption measurements presented in chapter 5 were carried out by P.P.Sripada.

The research during this course of study resulted in two publications. The study on pyrolysed chars has been published in the form of a journal article as Ramasamy S, Sripada PP, Khan MM, Tian S, Trivedi J, Gupta R. "Adsorption behavior of $CO_2$ in coal and coal char" Energy and Fuels. 2014; 28(8):5241. Dr. S. Ramasamy designed and developed the volumetric apparatus -1. M.M. Khan performed the adsorption measurements for the samples presented. The samples were obtained from the M.Sc work of Tian S. P.P. Sripada carried out data processing and analysis with the assistance of Dr. S. Ramasamy, Dr. R. Gupta and Dr. J. Trivedi.

The results on performance evaluation of the coal sample in apparatus -1 presented in chapter -3 have been reproduced from a book chapter: Sripada, P. P., Khan, M. M., Ramasamy, S., Kanneganti, V., Trivedi, J., & Gupta, R. (2014). Comparison of $CO_2$ Storage Potential in Pyrolysed Coal Char of different Coal Ranks.*Gas Injection for Disposal and Enhanced Recovery*, 293. M.M. Khan and V. Kanneganti performed the sorption experiments and P.P. Sripada in collaboration with Dr. S. Ramasamy was responsible for data analysis and interpretation.

# Acknowledgements

At the outset, I would like to express my profound gratitude to Dr. Rajender Gupta for agreeing to supervise my research work. He has always been a source of great inspiration, encouragement, guidance and support. With his mentorship came great independence to work in the direction which interested me the most. This offered the ideal platform for any new grad student to explore, learn and grow without any form of pressure.

I would also like to thank my co – supervisor, Dr. Japan Trivedi, for his enthusiastic guidance and help during the course of this study. His constant participation in the discussions during the rebuttal to the reviewer's comments for the publication is gratefully acknowledged. He has been very kind in letting me build setups in his lab and use the facilities in the School of Petroleum Engineering.

I had the opportunity to work with some excellent colleagues who have contributed generously toward the project. Special thanks to Dr. Shan Ramasamy, a mentor par excellence. The sessions we had on data processing, academic writing, and apparatus design were great learning experiences. His constant motivation, guidance and support helped the work progress at a much faster pace. I would take the opportunity to express my gratitude to Monir Khan more an elder brother than a colleague. His excellent work ethics, sincerity, perseverance will always remain an inspiration. I would not have learnt the many life lessons without you.

Sincere appreciation is due to Dr. James Sawada for being a great help with solving any problem we had with the adsorption apparatus. The discussions with him were most enjoyable and his positive outlook helped boost our morale when things were not going as planned. Sincere thanks to Dr. Arvind Rajendran for the discussions on the design and the error analysis of the volumetric adsorption setup. Thanks Dr. Rajendran for agreeing to be a part of my examining committee and for the constructive remarks for improving the thesis.

The funding support from the Canadian Centre for Clean Coal/Carbon and Mineral Processing Technologies ($C^5$MPT) is gratefully acknowledged.

I am grateful to the CME department Machine Shop and Mr. Todd Kinnee of the School of Petroleum Engineering for helping us with all the machining needs in the apparatus.

Thanks to the Clean Coal Group members and post-doc; Dr. Moshfiqur Rahman, Dr. Deepak Pudasainee, Dr. Ben Wang, and Dr. Arun kumar Samata. You have been very patient with me and helped when I needed the most. Special thanks to my friends Nirlipt Mahapatra and Vinoj Kurian, your comments during the development of the gasification setup were very useful; Navjot Sandhu and Nitya Iyer you patiently let me complete the BET experiments despite your work loads. Thank you.

I would like to thank my dear friends and roommates Abhinandhan Raghu, Khushaal Popli, Rohan Gaikwad, Deepesh Kumar, Shivam Shahi and Manjeet Chowdhry for all the good times here in Edmonton and being very patient and tolerant with my cooking experiments. Thanks also for accompanying me to the lab in the late nights. Special thanks to Khushaal and Atreya Nittala for their help in wrapping up the thesis.

I am indebted to Chalapathi Rao uncle, Madhu Aunty and Pujita for being excellent hosts during my early days in Canada making the transition smoother. Thanks to Rekha Aunty and Dr. Raj Gupta for their invaluable support and encouragement. You were all my family in Canada making me feel at home every time I visit you. You were also the reason of moral strength for my parents on the other side of the planet.

Thanks to my parents and family for their infinite patience, constant support and encouragement. This would not have been possible without you all.

Edmonton, 2014

Pavan Pramod SRIPADA

# Table of Contents

# List of Tables

# List of Figures

# Chapter – 1

# Introduction

## 1.1 General Introduction

Increasing evidence on the effect of anthropogenic activities on climate change such as global warming and rise in sea levels has created a need to develop preventive measures to bring the situation under control (1). Greenhouse gases among numerous other agents are pointed responsible for the increasing global temperatures, which by the end of this century may be 1.1-6.3$^{o}$C higher (2). Among the greenhouse gases, Carbon dioxide ($CO_2$) contributes to two-thirds of the "enhanced greenhouse effect" (3). The concentration of atmospheric $CO_2$ has increased at a steady rate and as of September 2013 is 393 ppm against the upper safety limit of 350 ppm which has been surpassed by 1989 (4).

Some of the technological measures used to curb $CO_2$ emissions include (i) reduction in the energy consumption and improving energy efficiency (ii) switching to alternate non-conventional energy sources (iii) decreasing the use of fossil fuels (iv) carbon storage and sequestration options (1). The reduction in the energy consumption is an impractical proposition considering the economic policy viewpoint. Secondly, renewable energy sources like solar, wind, hydro, biomass and other alternate energy sources like nuclear energy hold enormous potential for catering to the global energy needs. However, there are a host of side-effects that arise as a result of the large scale implementation of alternate energy projects such as the unpredictable or intermittent supply of energy, environmental and economic concerns, land use and public conflicts (5, 6). Thus the use of fossil fuels as a back-up option is inevitable. Currently, 80% of the energy supply comes from the fossil fuels and is expected to rise in the near future (7). This is because of the low cost of fuel and the burden to supply for the energy demands of the present generation. The energy supply and the association $CO_2$ release can be partly compensated by the carbon storage sequestration option. Carbon sequestration involves the removal of $CO_2$ by creation sinks through biological and media or artificial measures for temporary or permanent storage. In this way, lower net carbon content is achieved in relatively short time spans without many changes to the existing system.

Terrestrial carbon sequestration options include the natural storage mechanisms in trees by the photosynthetic agents and ocean fertilization to enhance the growth of planktons which absorb $CO_2$ and get deposited on the ocean floor. On the other hand, carbon capture and storage (CCS) aims to achieve the lower carbon levels by capturing the $CO_2$ released from the major carbon dioxide producers like power plants and employing subsequent storage and sequestration measures. Some avenues for long term carbon storage include geological storage, ocean storage, and mineral carbonation (1). Mineral carbonation and ocean storage are subject to issues such as the availability of suitable minerals, hefty operational costs, and poorly understood efficiency, environmental impact respectively (1, 8). Geological storage in deep saline aquifers, coal beds and natural cavity formation provide cost effective, environmentally benign prospects which can be implemented in the required scale and may be the best long term solution for carbon sequestration (9). Moreover, the understanding of such systems can be obtained from past experiences in operations like natural gas storage, acid gas injection, and liquid waste disposal (3). Furthermore, storage of $CO_2$ in coal beds and sedimentary basins can yield additional benefits like enhanced coal bed methane recovery (ECBMR) and enhanced oil recovery (EOR) which is due to the greater adsorption affinity of $CO_2$ over methane in coal and the reduction in the viscosity of oil on $CO_2$ absorption respectively (10, 11). The $CO_2$ adsorbed in coal during the ECBMR process will remain stored if left undisturbed. However, if the coal is to be mined at a later date, the adsorbed $CO_2$ will be released. It is thus preventing the utilization of the coal resources although the available methane has been recovered. Thus, there is a need to find a way to effectively use the coal reserves and facilitate carbon sequestration for meeting the energy demand and at the same time decrease the net carbon content.

Underground Coal Gasification (UCG) technology is a promising clean coal technology for the future use of unused and un-minable coals (12). Early studies on the potential of the UCG suggest an increase in world's coal reserve estimates by about 70% corresponding to 600 Gt (13). In this technique, the coal is gasified underground (*in-situ*) in the presence of the oxidants supplied through a vertically drilled well, called the injection well and the products of gasification, known as *syngas* is transported through the production well. The syngas is then used for energy conversion through a power plant at the UCG site. The post-gasification site consists of a cavity with the debris of ash and leftover char. This technology is capable of utilizing the energy in an economic and environmentally sustainable manner. For example, the UCG process is known to release 25% less $CO_2$ as compared to a coal fired power plant (14). In addition, the UCG carries with it other environmental benefits such as the reduction of sulphur and $NO_x$ emissions, no solid waste discharge, and decrease in pollutant content (15).

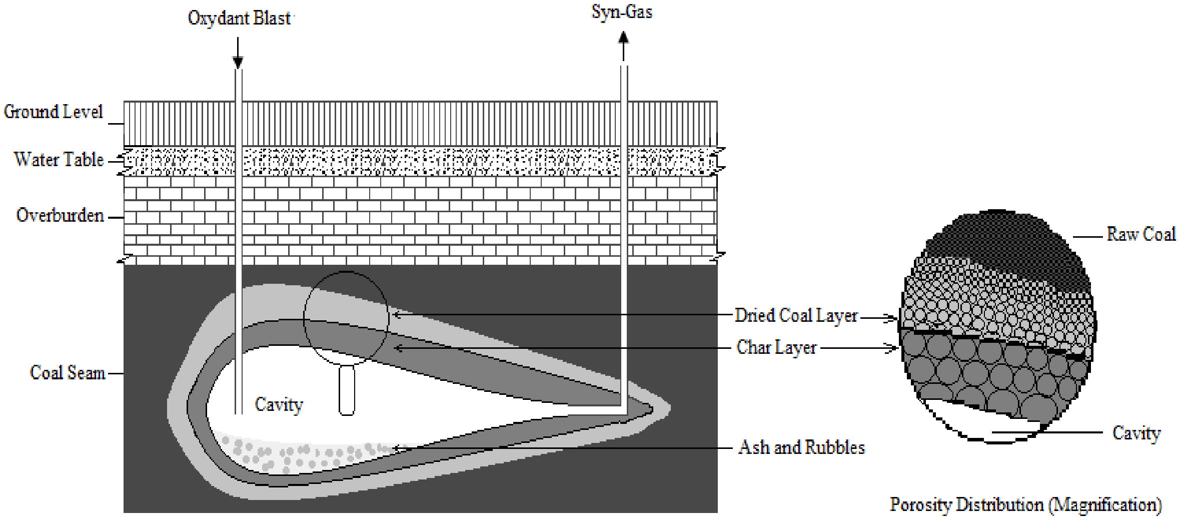

**Figure-2.1** The post burn cavity for Linked Vertical Well (LVW) UCG process

The earliest conception of underground gasification was by a German scientist Sir William Siemens in 1868 in an address to the British chemical society (13).At around the same time, the famous Russian chemist Dimitri L. Mendeleev suggested the gasification of coal underground and the transportation of gas to the consumers through pipes (14). Later, in the early 20th century, Sir William Ramsay, a British scientist, suggested that the smoke menace could be overcome by gasifying underground instead of burning of coal (14). The early experiments for developing the UCG began in the Soviet Union in 1932. Between 1944-1960, the energy shortage in Western Europe, resulted in the renewed interests with test runs being carried out in Czechoslovakia, France, Italy and Poland. First attempt towards the commercialization of this process was made in the UK in 1958-59. After an abeyance of two decades, the European work resumed and culminated in a test at El Tremedal in Spain. On the other side of the Atlantic, in the USA, thirty field tests were carried out during the period 1972-1989. The tests were carried out to assess the various configurations and were thought to be ready for commercial demonstration. However, due to the lower price of natural gas, the programme was terminated. Today, the development and commercialization of the UCG process is being actively being considered by many countries such as Russia, Australia, U.S.A, India, South Africa, China and Canada (16).

In the recent times, with the stringent environmental regulation and the ever increasing the demand for energy, CCS in *post*-UCG sites has been discussed but is not actively pursued mainly due to the limited quantitative understanding of the capacity, geo-mechanics, economics, and environmental concerns like the release of gases into the water table. The *post*-UCG site, is characteristic of enhanced porosity, permeability and larger surface area for gas sorption owing to the previous thermal treatment. In the UCG process, under steam and an oxidising atmosphere the coal is gasified to give mainly a mixture of $H_2$, CO and $CO_2$ commonly known as *syn-gas*. Post- gasification, a tear-drop shaped cavity is formed with the ash and rubble left in the bottom (See Figure 1.1). The remaining coal seam can be stratified as the partly gasified char layer, the pyrolysed char layers and the raw coal layer. The partly gasified char layer consists of coal that hasn't completely converted under the reactive atmosphere. Next, the pyrolysed char layer comprises of coal seam which has been exposed to high temperatures due to the temperature gradients in an inert atmosphere. The pyrolysed char layers will have varying characteristics in different regions as they have been exposed to different time- temperature histories (See Figure 1.2).

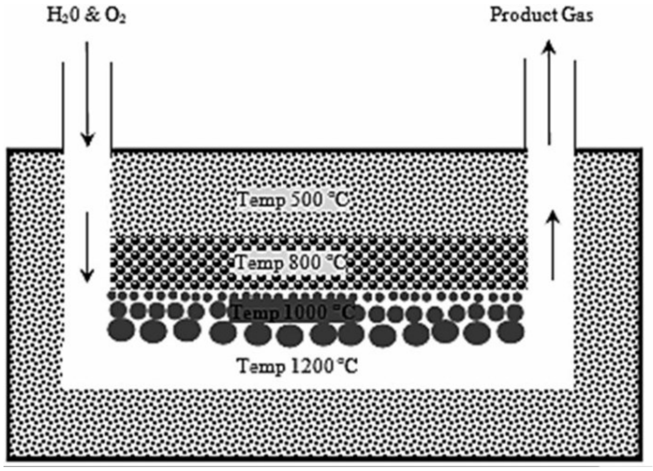

**Figure 1.3**: Pyrolyzed char layers in the post –UCG site

Further away from the burn cavity is the raw coal seam which has only experienced very mild or no changes during the gasification process. Coals' inherently microporous have reasonable adsorption capacity of $CO_2$ which is higher in comparison to other gases like methane and nitrogen (17). This has enabled technologies like ECBMR for the implementation of CCS. Moreover, the adsorption capacity is dependent on the nature of the coal, surface area and the porosity of the coal (18). For coal chars, however, the porosity and surface area will be greater as there is an expansion and generation of new pores during pyrolysis (19). This will enhance the adsorption of $CO_2$ on coal chars in comparison to the virgin coals. The above discussion help understand the advantages a UCG-CCS program would hold compared to the storage in a raw coal seam.

## 1.2 Objectives and Thesis Outline

The broad objective of this study is to demonstrate the effect of coal properties on the sorption capacities of the gasified chars obtained from large coal particles as applicable to a UCG-CCS system. Although the implementation of CCS in *post-* UCG sites is considered as a potential CCS alternative since the early 2000s, there have been barely a handful of reports that demonstrate the proof of concept through systematic investigation. There are many challenges that remain for the implementation of this technology such as the sorption capacity of the debris, the temperature and pressure conditions in the gasified site, geo-mechanical response, ground water risk and the $CO_2$ fate (20). In order to address some of these gaps in understanding, this study specifically aims the following:

1. To understand the influence of the raw coal properties on the sorption capacity of pyrolyzed coal char at different temperatures.
2. To determine the sorption capacities and sorption kinetic parameters of coal char gasified under $CO_2$ atmosphere for coals of different ranks and understand the influence of raw coal properties.

Chapter 2 details the research progress toward the development of the UCG-CCS technology apart from presenting the techniques that have been conventionally used for the measurement and analysis of sorption isotherms. In addition, a note is also presented on the influence of the coal properties on the chars from earlier studies in literature.

Chapter 3 describes the experimental methods that have been employed during the course of the study. In addition, the design specifications and the procedures for the adsorption apparatus and the horizontal tube furnace (used for preparation of the char) have been provided.

Chapter 4 discusses the design considerations for reliable sorption measurements on a volumetric adsorption apparatus. This has been done through a sensitivity analysis on the various parameters affecting sorption measurements and a performance evaluation of the apparatus through blank runs, inert samples and standard sorbents.

Chapter 5 discusses the $CO_2$ sorption of pyrolyzed coal chars. In particular, two coals, a coking and a non-coking have been pyrolyzed at two temperatures 800 and 1000$^{o}$C to simultaneously assess the influence of coal properties and pyrolysis temperatures on sorption capacities.

Chapter 6 deals with the supercritical $CO_2$ sorption on four coals (of different rank) gasified under $CO_2$ atmosphere at 800$^{o}$C. In addition, the sorption isotherms were analysed through adsorption potential theories and the diffusion coefficients were determined. Moreover, the overall discussion was presented in the perspective of the influence of coal properties.

Chapter 7 discusses the conclusion of the study and possible future directions.

# Chapter – 2

# Literature Review

## 2.1 UCG-CCS

The concept *post*-UCG CCS is emerging as a potential clean coal technology. The UCG combined with CCS is considered one of the most efficient and cost effective ways to use to the worlds vast coal reserves without emitting significant amounts of $CO_2$ (21). However, the storage of $CO_2$ can be effective only when it assumes supercritical form as the density is close to that of a liquid and compressibility is close to that of a gas (1). In other words, for an effective storage, a minimum depth of around 800 m would be required as the injected $CO_2$ obtained from power station flue gas may not be pure (12, 22). This fact can be play to the advantage as both the optimal depth for UCG operation and effective CCS is in the same range. In addition, the concept is considered feasible as the $CO_2$ can be permanently stored in the cavity and the more permeable left over seam. Moreover, the UCG goaf and the overburden potentially develop permeabilities between one and three orders of magnitude greater compared to the permeable hydrocarbon reservoirs (22). Furthermore, the debris of the process and the coal char has enhanced porosity leading to higher adsorption (23-25). However, it is expected that the pore volume needed to store supercritical $CO_2$ derived from the UCG process would require four times the pore volume occupied by the raw coal; all of this $CO_2$ cannot be stored in the UCG cavity alone (22). The storage would have to be carried out in the overlying strata. For instance, if the porosity of the overlying strata is assumed to be 15%, then the storage has to take place in strata to the height of 20 times the seam thickness (22). Apart from the above mentioned positives, the supercritical $CO_2$ injected for CCS can play a crucial role in dissolving the coal – derived chemical contaminants, thus reducing environmental risk.

Although the UCG-CCS is an attractive prospect in both the economic and environmental sustainability view points, there are a number for challenges and uncertainties to be alleviated. Burten et al. (20) suggest a few potential challenges in the implementation of CCS, namely: sorption capacity of the debris, the temperature and pressure conditions in the post –gasification site, geo-mechanical response, ground water risk, and the $CO_2$ fate. In addition, it is also necessary to understand the rate of adsorption for the various coals for which UCG may be implemented. Quantitative data on the contaminant dissolving capability of supercritical $CO_2$ is not yet reported (20). It is important for the implementation of UCG-CCS that the criteria for both the UCG operation and CCS capability are met at the same time. Sharifovich and Verma (16) list some of the site selection criteria for the UCG process implementation. Some of the important criteria are thickness of coal seam, depth of coal seam, coal properties, dip of coal seam, ground water availability, amount of coal, and land use restrictions. Naturally, most of the criteria listed here are subjective to the location of the coal seam and only the influence of coal properties can be generalised with the understanding from either open literature or experiences from other UCG pilot scale operations. Coal properties would decide the optimal operating parameters for the process. From the CCS standpoint, the coal properties of the seam such as the porosity and permeability after gasification would influence the extent to which CCS is feasible; in addition to controlling operating parameters such as the rate of injection. Unfortunately, the current level on understanding on the sorption capabilities of gas is very limited. Only recently, Kempka et. al (26) provides the proof of concept through experimental investigation. Nevertheless, a fundamental understanding on the effect of coal properties on sorption capabilities is essential.

## 2.2 Methods for adsorption measurement

The physical adsorption of high pressure fluids on solids finds application in the chemical and biochemical separations, purification of gases and solid-phase extraction. The actual properties of the adsorbed gas such as the size and volume at the molecular level cannot be determined by today's technology. As a consequence, the experimentally measured 'adsorbed amounts' reflect a change in bulk parameters due to adsorption of a gas, and not the actual adsorbed phase quantities (see Figure 2.1). Gibbs in 1928, recommends the quantification of adsorption by variables called the Gibbs Surface Excess (GSE) that can be unambiguously measured (27). Gibbs Surface Excess adsorption is defined as the difference between the amount adsorbed at actual adsorbed gas phase density and the amount adsorbed at bulk gas phase density.

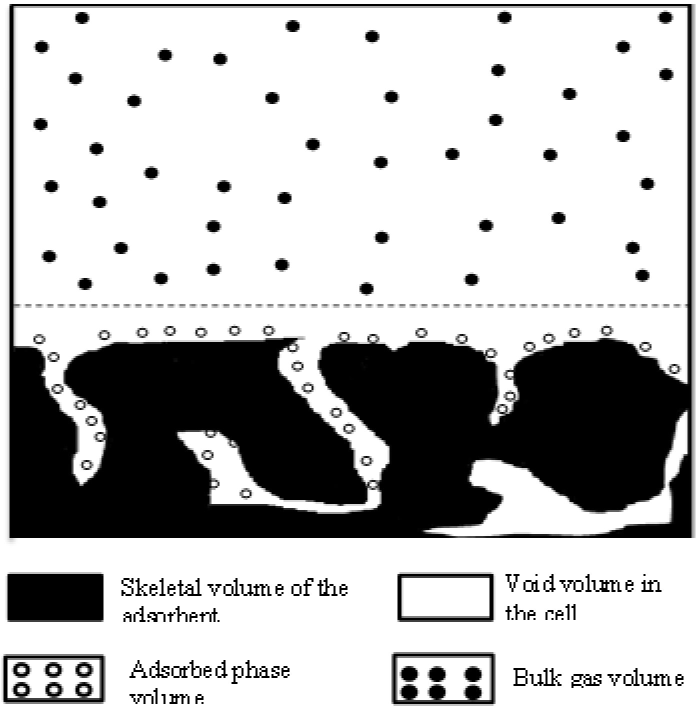

**Figure 2.1:** Illustration of the presence of gas in phases during adsorption. The dotted line represents the Gibbs interface.

Many researchers have developed different techniques for the measurement of adsorption. Some of the conventional methods to measure the sorption on adsorbents include: gravimetric method, volumetric method, gravimetric – volumetric method, chromatographic methods, Peizometric methods and IR spectroscopy (28, 29). Some of the recently developed methods include Frequency response technique (FRT), Zero Length Column (ZLC) technique, Total Desorption (TD) method (30). The advantages and disadvantages of these methods area described in Table 2.1. 2.1 adopted from (27). Among these methods, the volumetric and the gravimetric methods have been frequently used for studying the equilibrium sorption and kinetics. The gravimetric methods involve the determination of sorption through the measurement of the increase in weight of the adsorbent as the gas is adsorbed on the surface. The measurement of weight is performed through extremely sensitive microbalances. This method, however, requires a buoyancy correction factor to be incorporated (28, 31). Although, the use of sensitive microbalances result in reliable sorption measurement, the method is however, cost intensive.

**Table 2.1** Advantages and disadvantages of various method used for adsorption measurements (28).

| **Methods** | **Adsorption equilibria** | | **Adsorption Kinetics** | |
|---|---|---|---|---|
| | **Advantages** | **Disadvantages** | **Advantages** | **Disadvantages** |
| Gravimetric | Simple | Pure gas only, no control over final state, difficult to repeat | Simple | nonisothermal data, difficult to repeat |
| Volumetric | Simple, multicomponent gas | No control over final state, random data, difficult to repeat | | Nonisothermal data, complex, difficult to repeat |
| Piezometric | Ideal for high-pressure data | Pure gas only | | Not useful |
| Gravimetric-Volumetric | No gas analysis needed, simple | Binary gas only, random data, no control over final state, diffucult to repeat | | Not very useful, non- isothermal data, complex boundary conditions |
| Total desorption | Multicomponent gas, final state controlled, easy to repeat | Not simple | | Not very useful |
| Column dynamic | Good for trace adsorbents in bulk gas, relatively easy to repeat, constant P,T | Requires precise flow rate and composition measurement | Directly gives column dynamics, isothermal for trace | Model-dependent analysis |
| Closed loop recycle | Good for multicomponent trace adsorbates in bulk gas, constant P,T | No control over final state, difficult to repeat | Isothermal, constant P,T | Good for multicomponent trace adsorbates in bulk gas, difficult to repeat |
| Isotope exchange | Multicomponent bulk or trace, final state under control, easy to repeat, constant P,T,$y_i$ | Needs isotopes and their analysis | Multicomponent gas, isothermal, final state under control, easy to repeat, constant P,T, $y_i$ | Needs isotopes and their analysis |

Volumetric method on the other hand, uses the measurement of changes in the gas pressure to determine the amount of gas adsorbed on the sample. In this method, two cells of known volume are connected in series. The gas is injected in to the first cell, called the reference volume at a pressure measured through a pressure transducer of high accuracy. After constancy in pressure and temperature is attained, the gas is let into the second cell, the sample cell, where the adsorbent of known mass is placed. Based on the difference in pressure, the amount adsorbed in calculated. The volumetric method has been used in many studies for determining the sorption of multicomponent gases on adsorbents due to its simplicity for lab scale implementation (32-34); however, the accuracy of the volumetric system is known to be lesser than the gravimetric systems. The errors in the volumetric devices originate from the uncertainty in the gas phase density, uncertainty in the volume and accuracy of the pressure transducers (35).

## 2.3 Analysing adsorption isotherms

### 2.3.1 Langmuir Theory

The Langmuir model was developed in 1916 by Irwin Langmuir to determine the monolayer sorption capacity of a non-porous solid (36). In this model, the surface of solid adsorbent is considered to be consisting of an array of adsorption sites. Further, it is considered that the rate at which the molecules arrive from the gas phase and condense on the active site is equal to the rate at which the molecules evaporating from the surface. The condensation of the gas molecules is a product of the condensation coefficient (fraction of incident molecules condensing on the surface), the rate constant from the kinetic theory and the fraction of vacant active sites. The evaporation term is modeled as an Arrhenius type equation with the activation energy term being the isosteric heat of adsorption. Upon simplification, the Langmuir equation is of the form:

$$\frac{n}{n_m} = \frac{Bp}{1 + Bp} \qquad (2.1)$$

Where, $B$ is a product of the constants in the condensation and the evaporation terms. $n$ is the amount adsorbent per unit mass, $n_m$ is the monolayer capacity, and $p$ is the pressure. Although the Langmuir theory has been developed for non-porous solids, it had found application for microporous solids. According to the classical view, the monolayer theory is plausible explanation as the limit exists because of the pores being so narrow that they cannot accommodate more than a single layer of adsorbate. However, the degree of conformity of the Langmuir mechanism has been found to vary considerably as the heat of adsorption is considered to be constant with the degree of coverage; which is not the case (37).

The Brunauer, Emmett and Teller in 1938, simplified Langmuir's equation for multilayer adsorption (based on the same evaporation- condensation theory) by introducing several assumptions (detailed elsewhere (37)), commonly known as the Brunauer, Emmett and Teller (BET) equation.

$$\frac{n}{n_m} = \frac{c(\frac{p}{p^o})}{(1 - \frac{p}{p^o}) + (1 + (c-1)\frac{p}{p^o})} \qquad (2.2)$$

Where, c is parameter of the equation, analogous to B in the Langmuir equation. In order to test the models to the experimental results of amount adsorbed per unit mass versus pressure, the above are equations are simply rearranged into a linear equation form.

## 2.3.2 Adsorption Potential Theory

Contrary to Langmuir theory of surface coverage through the formation of layers of the adsorbate, Dubinin (38) postulated that in very fine pores, the adsorption takes place through pore filling. Dubinin's theory is an adaptation the previously developed theory by Polanyi in which considered the existence of a potential field on the surface of the solid in which the gas would enter. The adsorbed volume is represented as the space between each set of equi-potential surfaces. The differential molar work of adsorption is related to the decrease in the free energy in adsorption provided the bulk fluid is in equilibrium with saturated vapor. In addition, a second parameter, known as the degree of filling has been defined as the ratio of the volume that has been filled to the total volume of the micropore system. The degree of filling is postulated to be a temperature independent function of the differential molar work of adsorption. An expression for this function was given by Dubinin and Radushkevich (39) by assuming the pore size distribution to be Gaussian. By combining the above postulates, the DR formulation is as follows,

$$W = W_o \exp\{-(\frac{RT}{\beta}\ln\frac{p^o}{p})^2\} \qquad (2.3)$$

Where, W is the adsorbed volume of the adsorbate, $W_o$ is the micropore volume, $\beta$ is the scaling factor that reduces the characteristic curves of degree of filling versus the adsorbed amount in coincidence with a standard adsorbent. Originally, the standard adsorbent was taken as benzene for which$\beta = 1$. T is the temperature, R is the universal gas constant, and $p^o$ is the saturation vapor pressure. However, the DR equation is known to be limited to the case when the degree of filling is less than 0.15 (40). Moreover, it does not reduce to the Henry's law at low pressures in order for thermodynamic consistency (40).

On the other hand, the Dubinin and Astakhov considered the pore size distribution to be a Weibull distribution rather than a Gaussian, giving rise to the Dubinin- Astakhov (DA) equation:

$$W = W_o \exp\ \{-(\frac{RT}{\varepsilon} \ln \frac{p^o}{p})^n\} \qquad (2.4)$$

$\varepsilon$ is the characteristic free energy of adsorption corresponding to the value at degree of filling is 1/*e*= 0.368. The DA equation is a generalization of the DR equation (where *n*=2). $n$ in the is referred to as the heterogeneity factor since it has been suggested to be related to the heterogeneity in pore size distribution. $n \sim 2$ for carbonaceous materials (37). It has to be noted that the saturation pressure is to be determined for the test conditions.

Many studies on the sorption of adsorbates such as methane and $CO_2$ on activated carbon or coal have checked the validity of both the potential theory and the Langmuir theory. The DA equation was found to yield the best curve fit for the experimental data for both methane and $CO_2$ sorption in many cases ((41-43)). For instance, Clarkson and Bustin (44) analysed the sorption of methane on dry coals through DA, DR, BET and Langmuir models. By plotting the characteristic curves for these equations, they found that the surface of adsorption is not energetically homogeneous; thus demonstrating the fallacy of that Langmuir theory assumption. Moreover, in their study of sorption with different gases on activated carbon Agarwal and Schwarz in 1988 (41) emphasized the use of characteristic curves for the validation of these models and found that the DA model yielded better representation of the data. The adsorption theory models were consistently found to represent data better, however, their use becomes subject to the empirical estimation of the saturation vapor pressure. With many studies being carried out for the supercritical $CO_2$ on coals where the definition of saturation pressure becomes meaningless. However, in the previous reports a pseudo – saturation pressure was defined for the gases using empirical equations. Some of the methods for the determination of the pseudo – saturation pressure include reviewed by Li and Gu (45); i) Antoine equation; ii) Dubinin's method; iii) method by Rieche et. al (46)

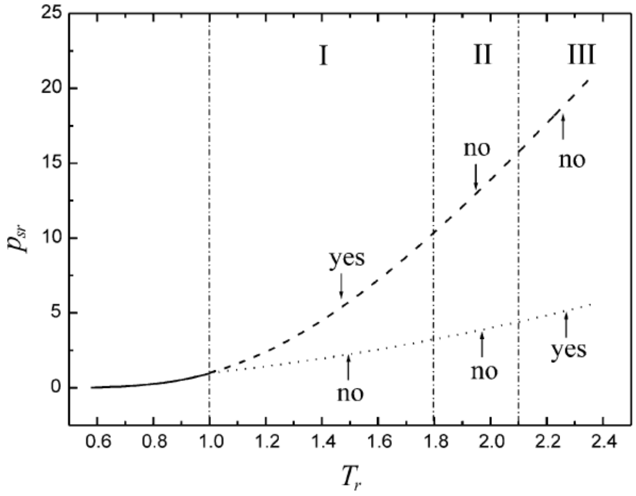

**Figure 2.2:** Suitability of empirical methods for the determination of pseudo-saturated vapor pressure (45). The solid line is the Antoine equation curve. The dashed and dotted line is the plot of pseudo – saturated pressure by Dubinin method and Rieche et. al (46). [Reproduced with permission]

$$\ln p^o = B - C/(D + T) \qquad (2.5)$$

Where, B, C, and D are the Antoine equation constants. The Antoine equation constants for $CO_2$ are listed in (41). T is the temperature. Dubinin method for estimation of pseudo-saturated vapor pressure is given by equation.

$$p^o = (\frac{T}{T_c})^2 P_c \qquad (2.6)$$

Where, $T_c$ and $P_c$ are the critical temperature and pressure. The method by (46) is presented in equation.

$$p^o = P_c \exp[h\left(1 - \frac{T_c}{T}\right)] \qquad (2.7)$$

Where $h$ is defined by the equation given below.

$$h = \frac{T_b}{T_c}\,(\ln P_c/(1 - \frac{T_b}{T_c})) \qquad (2.8)$$

The calculation of the pseudo-vapor pressure was extensively analysed by (45). Figure 2.2 illustrates their conclusions where it was suggested that the Antoine equation is appropriate to use till a reduced temperature of 1. For reduced temperatures in the range of 1-1.8, the Dubinin method is recommended. On the other hand, the equation by (46) is considered appropriate above reduced temperatures of 2.1. However, neither of the methods was considered good enough at reduced temperatures in the range of 1.8-2.1.

## 2.4 Gas sorption in coals

Coal is solid, brittle combustible organic sedimentary rock that is formed as a result of the decomposition and alteration of vegetation by the effects of temperature and pressure. Coal is known to be highly heterogeneous with the mineral matter randomly distributed within the organic matrix. Apart from the mineral and the organic components coal also possesses significant moisture content. The organic matter is derived into the volatile matter and fixed carbon sub groups. The organic matrix consists of three principal components known as the macerals, namely, vitrinite, liptinite, and inerinite. Vitrnite is composed mainly of hydrogen whereas inertinite is composed of carbon and possesses greater aromaticity. On the other hand, liptinite is characterized by greater hydrogen content, volatile matter content and heating value (47). Coals are principally classified on their rank as Lignite, Sub-bituminous, Bituminous and Anthracite. The classification is based on the degree of coalification in the coals and is measured by the reflectance of the vitrinite maceral (48).

Coal is known to be a predominantly microporous solid with the capability of adsorbing a variety of gases for coals with higher carbon content (19) . Gan et.al (49) measured the surface area of $CO_2$ at 298 K indicating the molecular sieve character i.e., coals behave as organic macromolecular systems and not at as rigid inorganic rocks; with the average porosity varying about 4.1 – 23.2%. Further, coals are considered to be consisting of isolated pores instead the generally accepted model of coal pores existing as interconnected network (50). Many reports have indicated that there is a significant change in the surface area with coal rank (51). For applications such as the storage of $CO_2$ in coal, it becomes necessary to develop a sound understanding on these fundamental properties of coal.

### 2.4.1 Influence of rank

Several previously reported studies such (52) and (53) studied the influence of rank on the sorption of carbon dioxide on dry and moist coals. The sorption decreases with the rank with the transition from lignite to the sub-bituminous region. There after the sorption increases with rank till the anthracite. It was found that a minimum on the sorption capacity was observed at a vitrinite reflectance range of 1.2 – 1.4. Prinz and Littke (52) also found that the microporous volume is a minimum in this region. The microporous volume decreased till 1.2 -1.4% and increased with the reflectance thereafter. Ozdemir et. al (53) noted that the sorption capacity was lower for bituminous coals when compared to the sub-bituminous and the lignites. Larson (18) also reported a "broad minima" at 1.2% reflectance. Saghafi et. al (54) performed sub-critical sorption measurements on the Sydney basin coals. However, they did not report any strong correlation between the rank and the sorption capacity. Recently, Jian et. al in 2012 (55) found that the medium rank coals had the least sorption capacity and attributed this behaviour to the higher oxygen content in the coals. The higher rank coals with more aromatic hydrocarbons, short aliphatic chains and depleted oxygen content may be responsible for the greater sorption. Laxminarayana and Crosdale (56) pointed out that this phenomenon may arise due to the 'plugging' of the pores in the medium rank coals. These pores open up as the coalification process continues leading to higher sorption capacities in high rank coals. In addition, the study by (57) also indicates that as rank increases the micropore density increases, thus leading to better gas sorption capacities.

### 2.4.2 Influence of mineral matter

As mentioned earlier, coal consists principally of three components, namely, the organic matter, mineral matter/ash, and moisture. In general, a observed negative correlation of the gas sorption capacity with the increase in ash content. Gurdal and Yalcun (58) state that a more consistent trend was observed in the sorption - ash content relationships in comparison to other coal properties. Laxminarayana and Crosdale (56) have studied coals with ash content ranging from 1.5% to 54% and have observed consistent decreasing trend in sorption capacity with ash percentage. It is well known that the carbon dioxide tends to adsorbs on the organic rather than the inorganic part of the coal matrix. Naturally, higher ash content is going to impede the adsorption of gases by acting as a diluent (59). Moreover, evidences presented by (11) show clear decreases in the sorption amounts with mineral matter content (34) point out that significant variation in the sorption isotherms when the coals were plotted on an ash free basis. This indicates that the organic composition of the coals also plays a critical part in gas sorption. Carroll and Pashin (60) suggest that the mineral matter and the moisture content play a critical role in determining the sorption capacity of coals whereas the maceral composition in the organics was relatively insignificant.

### 2.4.3 Influence of maceral composition

Maceral groups in coal grouped into three main categories: the vitrinite, inetrinite and liptinite. Several reports suggest that the maceral composition plays a crucial role in determining sorption in coals (61), whereas some suggest that there is no correlation between the maceral composition and sorption capacity (18) and (58). Considering the first maceral group, the vitrinites, (32) reports increasing carbon dioxide sorption of the coals with vitrinite content ranging from 2- 92 %. It was also found that the adsorption is greater for vitrinite rich coals (11, 44, 55). Gurdal and Yalcun (58) showed the relationship between the maceral composition and the microporous capacity. They too found that the vitrinite content increased sorption in spite of the large scatter in their data. Clarkson and Bustin in 1997 (57) suggested that the general increase in gas sorption with vitrnite is because vitrnites possess greater micropore volumes in comparison to other prominent maceral components like inertinites and liptinites. In addition, (44) and (61) found that bright banded coals had higher microporous volumes in comparison to the dull isorank coals. Laxminarayana and Crosdale (56) did not find any consistent trend when the vitrinite alone was plot against Langmuir volumes. However, they did observe increasing Langmuir volume with vitrinite between coals of the same rank. They also pointed out that a decreasing trend was observed semi anthracite and anthracites for the limited number of coals that were tested. Day et. al (18) did not find any correlation for the variation of the sorption with the vitrinite content for the coals that were tested. On the other hand, (34) interestingly noted that the highest adsorbing coals did not necessarily contain the highest vitrinite content.

The variation in $CO_2$ sorption with inertinites was also undertaken previously by several research groups. In general, it was found that the sorption decreases with increasing inertinite content (18). However, (58) did not find any trend with respect to sorption and inertinite content for the coals that were studied. Bhebhe (32) observed an extremely weak negative correlation for the coals that were analysed. The lower sorption in inertinites may be attributed to the nature of porosity, cross-linking density and surface functionality (57). Saghafi et. al (54) indicated that the contribution by the macro and the meso pores is around 5% of the total sorption. Inertinites being meso and macroporous in nature have a lesser influence on the sorption of gases in coal(62). Further, (11) and (34) found that sum of vitrinite and inertinite contents correlated better with $CO_2$ sorption in comparison to the individual maceral components. Moreover, (11) suggested that the telocollinite, a maceral in the vitrinite group, yielded a high correlation constant with sorption suggesting the influence of this maceral on gas adsorption applications.

In the cases of the liptinite group of macerals, (11) reported a gentle decreasing trend with increasing liptinite content. Liptinite being a maceral with large volatile matter content with primary aliphatic constituents, (63) and mesoporous nature (62), possesses less surface area; might be leading to lesser sorption quantities. However, (58) observed a positive correlation with in the increasing liptinite content. The sample that were analysed by them ranged from 2% to 40% liptinite. Further, they suggested that the effect that was observed might be due to the influence of other maceral components in the coal samples.

## 2.5 Sorption Capacities of Pyrolysed/Gasified Chars

As the coal is pyrolysed, i.e., being treated at high temperatures in an inert atmosphere, the volatile matter release takes place due to the decomposition, saturation and the cross-linking of the aromatic chains within the coal matrix. Gases like $CH_4$, $H_2$, CO and $CO_2$ are emitted (64, 65). In addition to the mentioned products, pyrolysis also results in the production of tar. Tar essentially consists of room temperature condensable saturated organics that result because of the reaction of matrix with hydrogen (65). The above processes are also accompanied by structural changes in the coal like the generation of new pores and the formation of macropores because of the coalescence of original pores (19, 66). However, at high temperatures, the crosslinks are broken between the aromatic rings and the chains now structurally rearrange themselves to reduce the surface area of the chars. Therefore, the pyrolysis process is expected to yield a maxima in the surface area at a critical temperature. In addition to these chemical changes, structural changes of the coal matrix take place simultaneously. As a result, the coal chars will have enhanced porosity and thus giving rise to better carbon dioxide sorption capacities. Porosity of the coal chars is extensively studied and reviewed in (19, 64, 66-69). The enhanced gas sorption capacities on coal char dictates a fundamental understanding on mechanics and the dynamics behind chars' internal structure. It would also be pertinent to note the porosity development for different coal ranks in order to predict, at least qualitatively, the surface areas and therefore the $CO_2$ sorption capacities.

$CO_2$ sorption on coal chars was studied by (70). In their study, the sorption on the chars was much greater than the virgin coal samples. However, they observed that the sorption decreased with the pyrolysis temperature for the temperatures greater than 1000K. Gutierrez et. al (71) studied the effect of carbonization on sub-bituminous on the apprarent surface areas. For the coals that were tested by them, the surface area increased to reach a maxima at 1073 K followed by a sharp dip in the surface areas at 1173 K. For the samples tested by (72) maxima in the surface area variation with the pyrolysis temperature was observed in the range of 600 – 700 $^{o}$C. Toda et. al (73) and Miura and Silveston (69) reported the same with their studies on the porosity distribution variation with temperature on caking and coking coals. It was observed by (69), for one char, the total pore volume increased with temperature continuously and for the other, the pore volume increased till 800$^{o}$C and then dropped. The volatile matter content in coals was attributed for the difference in behaviour. It is interesting to note that the coals were found to exhibit different behavior. Coking coals tend to develop greater fluidity on heating and produce more tar (74, 75). Jiang et. al (70) postulated that the tar decomposes to give carbon, which deposits on the micropores to reduce their number.

Gasification is a process by which the coal is converted to gases on the reaction with oxidants such as steam, air or carbon dioxide. During gasification, the carbon is consumed as it reacts with the oxidant, thus leading to structural changes in the char as the reaction progress.

$$C + CO_2 \rightarrow 2\ CO$$

$$C + H_2O \rightarrow CO + H_2$$

This is also clearly seen in the scanning electron micrographs in (76) for the chars at different conversion levels for $CO_2$ gasification. In addition, de Koranyi in 1989 (77) studied the structural changes in the char as a function of conversion on three British bituminous coals. It was found that the surface area versus burn off level had a maxima varying from 30-50% for two of the samples tested. Further analyses suggest that this could be either due to creating of newer pores or larger pore arising due to pore coalescence. This observation was also similar to comments made by (78).

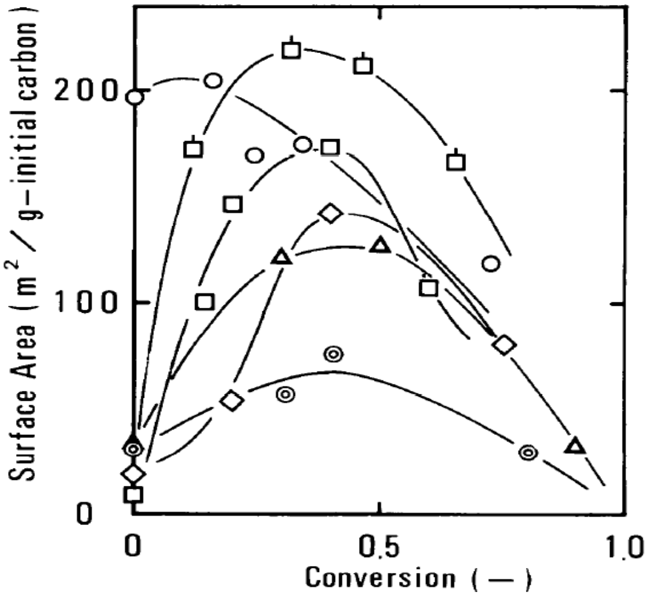

**Figure 2.3:** Variation of surface area with conversion for coals at different temperatures (79). [Reproduced with permission]

Adschiri and Furusawa (79) observed an increase in the surface area of $CO_2$ gasified chars with conversion and gasification temperature (shown in Figure 2.3). Further, (80) studied the $CO_2$ and $O_2$ gasification of South African coals and reported increase in micropore volumes after $CO_2$ and $O_2$. Feng and Bhatia (81) studied the pore structure development on $CO_2$ and air gasification for several chars subject to different levels of heat treatment. It was observed that for one of the coals the pore structure development for gasification at different temperatures was different. However, for other coals that were tested, the char surface area decreased at higher temperatures. The dependence on the surface area on the coal type is also observed by (82). Moreover, the gasification reacitivity, and hence the surface area of the char is a function of the gasification conditions such as heating rate, particle size and pressure (83).

# Chapter – 3

# Experimental Methods

## 3.1 Volumetric Adsorption Apparatus

The adsorption capacities of the coal and the coal char samples were determined using a volumetric adsorption setup. The apparatus was developed to handle large samples sizes in comparison to commercial volumetric and gravimetric adsorption measurement devices. Volumetric adsorption method was chosen because of its advantages like simplicity in laboratory scale implementation and cost effectiveness in contrast to gravimetric devices which require extremely sensitive microbalances (85). Figure 3.1 depicts the principal elements of the volumetric adsorption setup.

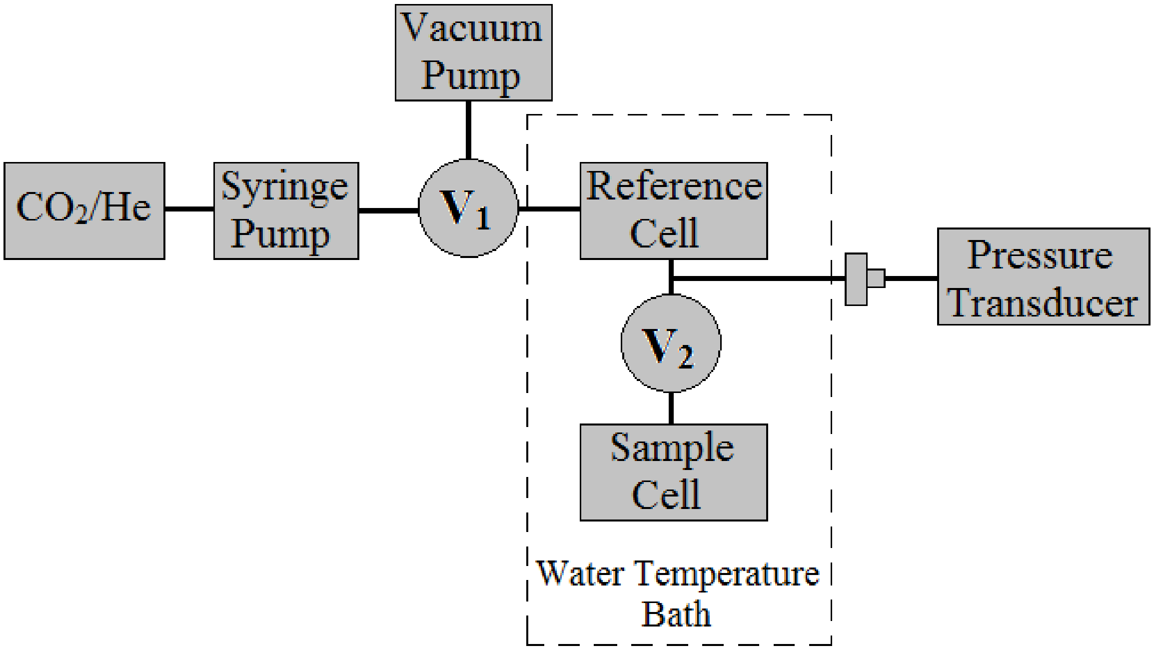

**Figure 3.1**: Principle of a volumetric adsorption apparatus

The volumetric adsorption apparatus consists mainly of a sample cell, a reference cell, a pressure transducer, and temperature control highlights the basic components of a volumetric adsorption apparatus. The sample is placed in the sample cell and the reference cell is employed in order to determine amount of gas in the system based on pressure readings from the transducer. It is essential to determine the exact volume of the reference cell and the sample cell with the maximum possible accuracy. The temperature control can be achieved by either using a heat exchanger in the inlet section of set-up or by placing the cells in a controlled water bath. The operating procedure in brief would involve the following three steps. To begin with, a known amount of sample is placed into the sample cell. Secondly, the gas is pressurized and held in the reference cell till stable gas temperature and pressure are attained (approx. 2 hours). Thirdly, the gas is equilibrated into the sample cell where the gas adsorbs on the adsorbent. The gas is held in the sample cell for long duration till pressure constancy is attained. Finally, based on the pressure readings before and after equilibration, the adsorbed amounts are calculated.

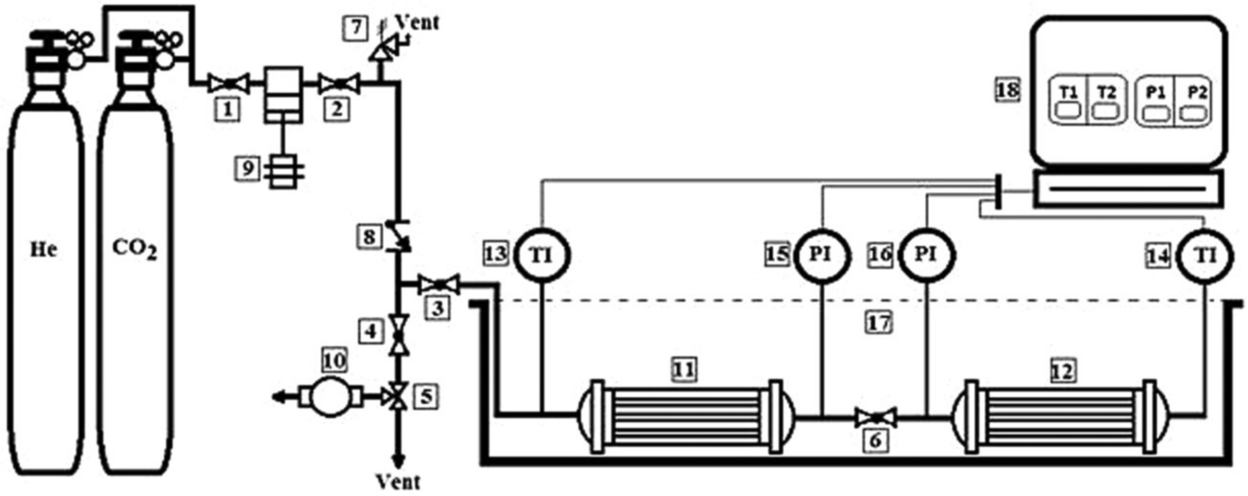

**Figure 3.2** Schematic of the volumetric adsorption apparatus. [1-6: Valves; 7: Pressure relief valve; 8: Check valve; 9: High pressure syringe pump; 10: Vacuum Pump; 11: Reference cell; 12: Sample cell; 13 & 14: Temperature sensor; 15 & 16: Pressure transducer; 17: Water bath; 18: Data acquisition system]

The equipment consists of four segments namely the gas injection, isothermal section, evacuation section, and data acquisition system, as shown in Figure 3.2 The gas injection system consists of a high pressure syringe pump (ISCO 500D) which has a rated delivery pressure of 3750 psig. To ensure safety, a pressure release valve was installed at the output of the syringe pump. In the isothermal segment the components like reference cell, sample cell, pressure transducers, thermocouples, and valves are placed in a water bath with high precision temperature controller (Thermo scientific Model 253). In addition, the inline thermocouples were integrated next to each cell (i.e., reference cell & sample cell) for measuring the gas temperature, which play a vital role in determining the error due to temperature sensitivity in the sorption measurement. Further, the reference and sample cells were incorporated with an in-line filter to avoid fine solid particles entering the tubing and valves. The evacuation segment consists of vacuum pump and vent. The vacuum pump helps in evacuating the presence of trace gases in the adsorption setup. During the experiment, the excess gases were removed through a vent which was directed to the fume hood. Both temperature and pressure were continuously monitored with the help of TRH central and lab view program.

**Table 3.1:** Specifications of the two designed apparatuses

| **Parameter** | **Apparatus – 1** | **Apparatus – 2** |
|---|---|---|
| Reference Volume, $V_R$ | 40.5849 cc | 24.0972 cc |
| Sample volume, $V_S$ | 36.7981 cc | 39.8894 cc |
| Volume Ratio ($V_S/V_R$) | 0.9066 | 1.655 |
| Pressure Transducer accuracy | 0.14% of span | 0.0025% of span |
| Span | 0-2500 psia | 400-3000 psia |
| Temperature accuracy | $\pm 0.1^{o}C$ | $\pm 0.1^{o}C$ |

In this study, adsorption studies have been carried out on two volumetric adsorption devices. The design specifications of the two devices are mentioned in Table 1. Comparing the two devices, it can be seen that there is a significant difference between the pressure transducer accuracy, equilibration times and the ratio of sample cell to reference cell defined as volume ratio. The pressure transducer accuracy in case of apparatus - 1 and apparatus - 2 would result in error in pressure measurement of ±3.5psia and ±0.065psia. Moreover, the cell volumes determined in apparatus - 1 contains an error of 5% compared to an error of 2% in apparatus - 2. In addition, the volume ratio of the cells were varied since it was found that volume ratio in the cells influences the final measurement accuracy (35). However, the temperature sensitivity for both the apparatus is $\pm 0.1^{o}C$ since the same water bath was used.

### 3.1.1 Volume Calibration Methodology

In this study, the volume calibration is performed principally by physical volume measurement and pycnometry. In the physical volume measurement, the volume of the reference and the sample cell is determined by the summation of the volumes of respective process components such as valves, tubes and tube fittings. Volume of the components is determined either from the dimensions specified in the respective drawings or by physically measuring the dimensions. On the other hand, in the pycnometric technique a helium blank test is carried out with a calibrated volume at one end and an unknown volume at the other in order to back calculate the unknown volume. At first, a blank test is carried out with calibrated volume and the reference volume to determine the reference volume. Finally, with the now calibrated reference volume, the sample cell volume is determined through the same procedure. Further, from both the methods, the sample and reference volumes with least error in a $CO_2$ blank test mass balance are chosen.

### 3.1.2 Operating Procedure

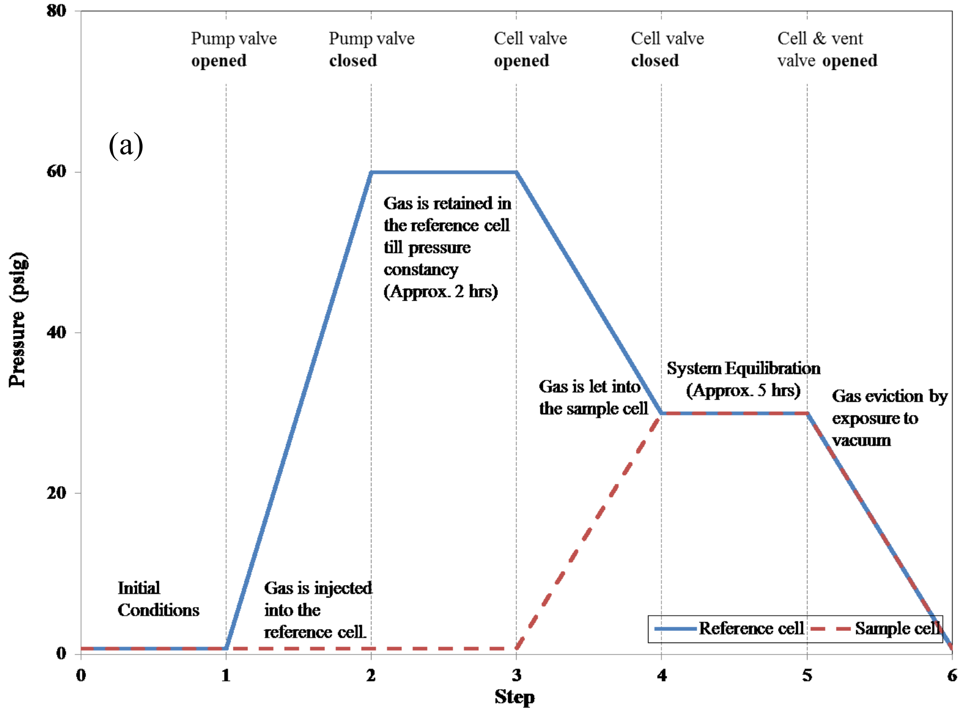

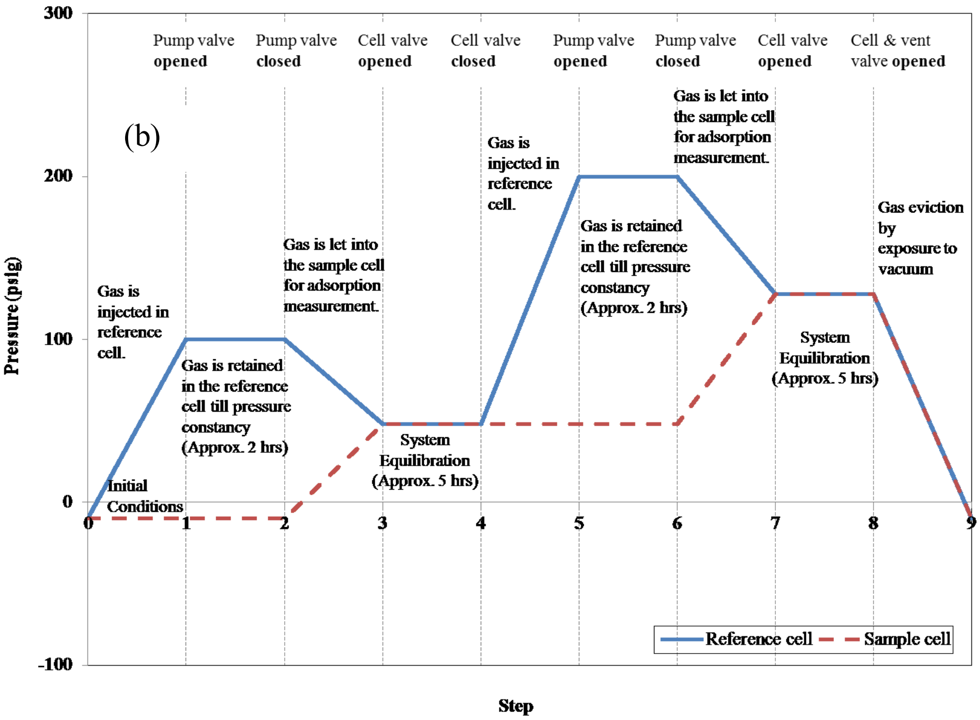

**Figure 3.3** Procedure for gas adsorption measurement in (a) single pressure mode and (b) cumulative pressure mode

The volumetric adsorption apparatus can be operated in several ways to calculate the amount of gas adsorbed by a solid; however the mass balance and hence the calculation method would be different in each case. In this study, the volumetric apparatus has been operated in the single pressure method and cumulative mode. The respective operating procedures have been illustrated in Figure 3.3. The main difference between the two modes lies in the location of the pressure injection step. The isotherms reported in this study have been carried out in the single pressure mode unless otherwise mentioned. Prior to any adsorption measurement, the trace gases were evacuated from the experimental setup through a vacuum pump. Subsequently, the gas was injected into the reference cell for a desired pressure with the help of gas injection system. Further, the gas was retained in the reference cell to obtain an isothermal condition. Later, the gas was allowed to equilibrate with the sample cell for a prolonged period (i.e., approx. 5 hrs.) till equilibration was obtained. Further, the procedure was repeated to obtain the adsorption isotherm for the subsequent pressure points. On the other hand, in the cumulative pressure mode, the procedure remains the same except the last step where instead of system evacuation, gas is injected into the reference cell in order to proceed to the next pressure point in the isotherm (See Figure 3.3(b)).

In the volumetric adsorption method, it is essential to predetermine the void volume in the sample cell for measuring the sorption capacity of a sample. Void volume is defined as the space available in the sample cell for the gas to occupy. The sample cell and the definition of the associated volumes have already been detailed in Figure 2.1. For instance, if a porous sample is considered, void volume is going to be the volume occupied by the gas apart from the solid surface. In this study, the void volume was determined through helium expansion method. Helium being a gas which behaves almost ideally under ambient conditions was widely used to determine the void volume due to the size of the gas molecule and poor adsorption on coal (86-88). In this study, the helium void volume was estimated by the single pressure operating mode at six different injection pressures from 1500-2000 psia. Such high pressures were chosen because of two reasons: the variance in the calculated void volume was observed to be less (See figure 4.7) and the void volumes estimated for glass beads at pressures in this range produced the mass balance residue (MBR) closest to zero for the $CO_2$ glass beads isotherm. At first, the helium gas is injected into the reference cell at pressure above 1500 psia. The system is then allowed to stabilize for 1 hour till constant temperature is attained. The gas is then equilibrated into the sample cell where a known quantity of sample is placed (typically 20 g). Assuming the helium does not adsorb on the surface of the adsorbent, the empty volume in the sample cell, or the void volume can be estimated through a simple mass balance (See equation 3.20). The void volume of the system is calculated by determining the void volumes obtained at each pressure. Table B.3 in Appendix B provides a typical helium void volume calculation.

To obtain the porosity of the coal sample, the bulk density measurements were also carried out using glass bead displacement technique adopted by Ramasamy et. al (89). In this study, a known packing density of 30-50 μm glass beads was used to determine the irregular surface within the cleats of the coal sample to obtain bulk density. Further, it was correlated with helium void volume to obtain the porosity of the coal sample.

### 3.1.3 Gibbs Surface Excess

During adsorption, two different components of the gas phase are known to exist. As illustrated in figure 2.1, the gas present directly on the coal surface is referred as the adsorbed phase. On the other hand, any gas that is not adsorbed on to the coal surface is a part of the bulk gas phase. Properties of the adsorbed phase are going to be different from that of the bulk gas phase. The density of the adsorbed phase decreases with distance till it reaches the bulk phase density (See figure 3.4). However, it is difficult to distinguish the bulk gas phase and adsorbed phase macroscopically, thus it becomes impossible to experimentally measure the properties of the adsorbed phase like its density, and volume. This limitation prevents the representation of adsorption amounts directly in terms of adsorbed phase properties. In this manuscript, the experimentally determined amount of gas adsorbed on coal and coal char samples are denoted by Excess Adsorption or Gibbs Surface Excess (GSE) Adsorption.

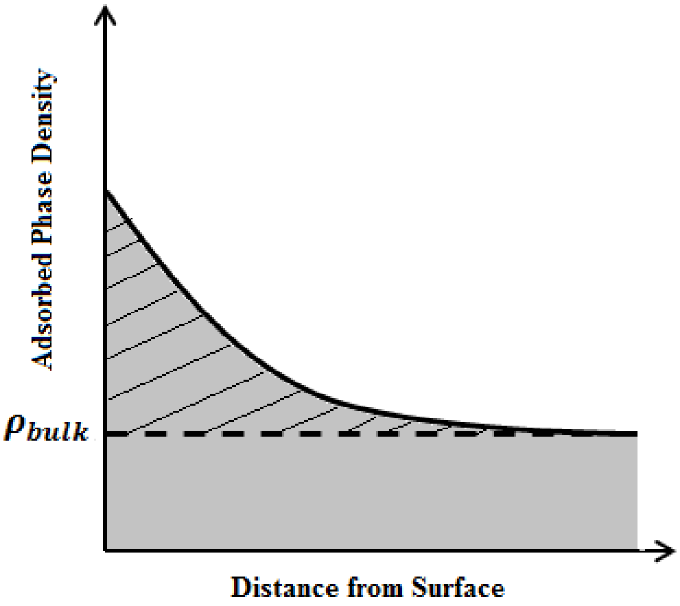

**Figure 4.4**: Gibbs Surface Excess Adsorption

In the Gibbs Surface Excess model, there exists an interface separating the adsorbed gas phase and the bulk gas phase which is called the Gibbs interface. The GSE model assumes that the adsorption occurs at the bulk gas phase density rather than the actual adsorbed phase density.

Thus, the Gibbs Surface Excess adsorption is defined as the difference between the amount adsorbed at actual adsorbed gas phase density and the amount adsorbed at bulk gas phase density. The Gibbs Surface excess would thus correspond to the adsorption as a function of the portion with the shaded portion of Figure 3.4, whereas the absolute adsorption would be the area in gray.

*Single Pressure mode*

For a volumetric adsorption system operated in the single pressure mode, the amount of gas present initially in the reference cell (i.e., before injection) can be written as

$$n_{inital} = \rho_1 \times V_R \tag{3.1}$$

Where, $\rho_1$ is the molar density of the gas at the corresponding temperature and pressure. $V_R$ is the volume of the reference cell (inclusive of all tube fittings).

After gas equilibration, the mass balance for the gas in the system can be written as,

$$\rho_1 \times V_R = \rho_1^* \times V_R + \rho_1^* \times (V_{cell} - V_{solid} - V_a) + \rho_a \times V_a \tag{3.2}$$

In equation 3.2, $V_{cell}$ is the total volume of the sample cell (inclusive of all tube fittings). $V_{solid}$ is the skeletal volume of the coal (does not include the volume in the pores). Free space available in the system is given by $V_{cell} - V_{solid} - V_a$. Where $V_a$ and $\rho_a$ are the volume and density of the adsorbed phase. Moreover, the term $V_{cell} - V_{solid}$ is referred to as the void volume in the sample cell. As described earlier, the void volume is determined using the helium expansion method.

From the definition of Gibbs excess,

$$n_{excess} = V_a(\rho_1^* - \rho_a) \tag{3.3}$$

the mass balance in equation (3.2) can be rearranged as,

$$n_{excess} = V_R \times (\rho_1 - \rho_1^*) - \rho_1^* \times (V_{cell} - V_{solid}) \tag{3.4}$$

Gibbs surface excess can be treated as a quantity that is a good representative of the adsorption in a system and this can be used for the determination of thermodynamic and kinetic parameters related to adsorption.(27)

*Cumulative Pressure Mode*

In case of cumulative pressure injection mode, the initial conditions gas in the first run is the same as equation (3.1).

$$n_{initial} = \rho_i * V_R \qquad (3.5)$$

Where, $\rho_i$ is the density of gas at the injection pressure for the current pressure point.

Post - equilibration mass balance for the $i^{th}$ step, can be written as:

$$\rho_i \times V_R = \rho_i^* \times V_R + \rho_i^* \times \left( V_{cell} - V_{solid} - V_{a,i} \right) + \rho_{a,i} \times V_{a,i} + \rho_{i-1}^* \times ( V_{cell} - V_{solid} ) + n_{excess,i-1} \text{ ....(3.6)}$$

Where, $\rho_i^*$ , $\rho_{i-1}^*$ refer to the gas density after equilibration at the $i^{th}$ point and *i-1*$^{th}$ point. $V_{ai}$ and $\rho_{ai}$ are the adsorbed phase volume and density. $n_{excess,i-1}$ is the excess adsorption amount in the *i-1*$^{th}$ point. The excess adsorption in a cumulative injection method can be computed with equation (3.7)

$$n_{excess,i} = V_R \times (\rho_i - \rho_i^*) - (\rho_{i-1}^* + \rho_i^*) \times ( V_{cell} - V_{solid} ) - n_{excess,i-1} \qquad (3.7)$$

## 3.1.4 Estimation of diffusion coefficients

The effective diffusivity is conventionally determined by the application of the unipore diffusion model to transient volumetric adsorption data. The unipore model is based on the solution to the Fick's second law for spherical particles. (90)

$$\frac{D}{r^2} . \frac{\partial}{\partial x}\left(r^2 \frac{\partial C}{\partial r}\right) = \frac{\partial C}{\partial t} \qquad (3.8)$$

Where, r is the radius, C is the concentration, and t is the time. In this equation, it is assumed that the diffusion coefficient is independent of concentration. In addition, it is assumed pore size is uniform, isothermal conditions prevail. It is also assumed that the diffusion coefficient is independent of concentration. The solution to equation is given by:

$$\frac{V_t}{V_\infty} = 1 - \frac{6}{\pi^2}\sum_{n=1}^{\infty}\frac{1}{n^2}e^{-\frac{Dn^2\pi^2 t}{r_p^2}} \qquad (3.9)$$

$V_t$ is the total amount of gas adsorbed at time t, $V_\infty$ is the total volume adsorbed. Equation is the unipore diffusion mode. The term $D/r_p^2$ is the effective diffusivity depicted by $D_e$ . For $\frac{V_t}{V_\infty}$ <0.5, equation may be approximated as.

$$\frac{V_t}{V_\infty} = 6\sqrt{\frac{D_e t}{\pi}} \qquad (3.10)$$

In this study, the quantity on the LHS of equation 3.10, is obtained from the adsorption rate data and plotted against time. Curve fitting is then performed on this plot with the effective diffusivity as the parameter to be estimated. Non –linear regression was performed with the limits for the estimates set to $10^{-7}$ to $10^{-2}$. The 95% confidence intervals and regression coefficients for all the samples have been tabulated in Table B 1-8 (Appendix –B).

### 3.1.5 Error Analysis

The error analysis for the volumetric adsorption isotherms has been carried out by using a multivariate error propagation approach. In this method, if y is any dependent quantity, a function of independent variables $x_1$, $x_2$, $x_3$, …, $x_n$ which inherently possess errors $\sigma_{x_1}$, $\sigma_{x_2}$, $\sigma_{x_3}$ and $\sigma_{x_n}$; then the error in y is given by:

$$\sigma_y^2 = \sum_{i=1}^{n}\left[\left(\frac{\partial y}{\partial x_i}\right)^2 . \sigma_{x_i}^2\right] (3.11)$$

In this analysis, the errors propagating in the volumetric adsorption setup due to the calibration and the experimental procedures have been considered. The calibration and experimental procedures are as follows:

1. At first, volume calibration carried out in the pycnometric method, where, a helium blank run was conducted with the reference cell on one end and a calibrated volume on the other. Based on a simple mass balance, the volume of the reference cell is estimated.

2. In the same way, the sample cell volume is then calculated based on the reference cell from a blank helium isotherm.
3. The void volume in the system is then calculated based on the calibrated reference and the sample cell volumes.
4. The adsorption measurements are then calculated based on the void volumes.

It is to be noted that the errors arising due to the calibrated volume are propagated till the final step of sorption measurements. In addition, at every step, the errors due to the pressure and temperature sensitivity of the gas have to be incorporated.

### 3.1.5.1 Error in Reference Cell Calibration

The reference cell calibration is done by performing a helium blank test with a calibrated volume on one side and the reference volume on the other. The reference volume consists of the reference cell, pressure sensor, thermocouple, and valves.

$$\rho_i \times V_{std} = \rho_i^* \times (V_r + V_{std}) \quad (3.12)$$

Where, $\rho_i$ , $\rho_i^*$ , $V_{std}$, $V_r$ are the injected gas density, equilibrated gas density, calibrated volume, and the reference volume. This can be rearranged to give the reference volume, provided there is no form of sorption by the metal parts.

$$V_r = (\rho_i - \rho_i^*) \times V_{std}/\rho_i^* \quad (3.13)$$

Therefore, the error in the reference volume is estimated by

$$\sigma_{V_r}^2 = \sigma_{std}^2 \, . (\frac{\partial V_r}{\partial V_{std}})^2 + \sigma_{\rho_i}^2 . (\frac{\partial V_r}{\partial \rho_i})^2 + \sigma_{\rho_i^*}^2 . (\frac{\partial V_r}{\partial \rho_i^*})^2 \quad (3.14)$$

Here, $\sigma_{std}^2$ is taken as a given, the value of which is obtained from the manufacturers specification and is listed in Table 3.1. The density is calculated from the equation and the error is given by

$$\rho = \frac{PM}{ZRT} \quad (3.15)$$

$$\sigma_{\rho}^{2} = \sigma_{P}^{2}.(\frac{\partial \rho}{\partial P})^{2} + \sigma_{T}^{2}.(\frac{\partial \rho}{\partial T})^{2} + \sigma_{Z}^{2}.(\frac{\partial \rho}{\partial Z})^{2} \quad (3.16)$$

Where, Z is the compressibility factor. In this study, the density values have been obtained directly from the NIST database (91). Hence, the third term in equation has been neglected.

### 3.1.5.2 Error in Sample Cell Calibration

The error in the sample cell volume is calibrated following a similar procedure as in the case of the reference volume calibration. In this case, a helium blank run is conducted with the reference cell in one end and the sample cell on the other. The mass balance is as given below:

$$\rho_i \times V_r = \rho_i^* \times (V_r + V_{cell}) \quad (3.17)$$

Where, $V_{cell}$ is the volume of the sample cell. The sample cell volume can be calculated from equation assuming there is no sorption by the metal parts.

$$V_{cell} = (\rho_i - \rho_i^*) \times V_{cell}/\rho_i^* \quad (3.18)$$

The error in the sample cell volume is thus given by:

$$\sigma_{V_{cell}}^{2} = \sigma_{r}^{2} \ .(\frac{\partial V_{cell}}{\partial V_r})^{2} + \sigma_{\rho_i}^{2}.(\frac{\partial V_{cell}}{\partial \rho_i})^{2} + \sigma_{\rho_i^*}^{2}.(\frac{\partial V_{cell}}{\partial \rho_i^*})^{2} \quad (3.19)$$

### 3.1.5.3 Error in Void Volume measurement

On the other hand, the void volume is calculated through a helium displacement method with the sample placed in the sample cell. Helium adsorption on either the adsorbent or the inert sample is assumed to be zero. Therefore, the void volume, $V_{void}$ can be calculated as

$$V_{void} = V_r.\frac{\rho_i - \rho_i^*}{\rho_i^*} \quad (3.20)$$

The error in the void volume estimation is given by

$$\sigma_{V_{void}}^{2} = \sigma_{V_r}^{2}.(\frac{\partial V_{void}}{\partial V_r})^{2} + \sigma_{\rho_i}^{2}.(\frac{\partial V_{void}}{\partial \rho_i})^{2} + \sigma_{\rho_i^*}^{2}.(\frac{\partial V_{void}}{\partial \rho_i^*})^{2} \quad (3.21)$$

### 3.1.5.4 Error in adsorption measurement

For a volumetric system, in a blank run or with an inert sample isotherm, the mass balance residue (MBR) is defined as the difference between the initial and final amounts in the system i.e., the amounts before and after equilibration into the sample cell.

$$\sigma_{MBR}^2 = \sigma_{n_{initial}}^2 . (\frac{\partial MBR}{\partial n_{initial}})^2 + \sigma_{n_{final}}^2 . (\frac{\partial MBR}{\partial n_{final}})^2 \quad (3.22)$$

Where $n_{initial}$ and $n_{final}$ is the initial and final amounts in the system.

Initial amounts in the single pressure mode and cumulative pressure mode is given by equation 3.23 and 3.24.

$$n_{initial} = \rho_i . V_r \qquad (3.23)$$

$$n_{initial}^{cumulative} = \rho_i . V_r + \rho_{i-1}^* . V_{void} \quad (3.24)$$

Hence, the error in the initial amount injected into the system in single pressure mode and cumulative pressure mode would be given by equation 3.25 and 3.26.

$$\sigma_{n_{initial}}^2 = \sigma_{\rho_i}^2 . (\frac{\partial n_{initial}}{\partial \rho_i})^2 + \sigma_{V_r}^2 . (\frac{\partial n_{initial}}{\partial V_r})^2 \quad (3.25)$$

$$\sigma_{n_{initial}^{cumulative}}^2 = \sigma_{\rho_i}^2 . (\frac{\partial n_{initial}^{cumulative}}{\partial \rho_i})^2 + \sigma_{V_r}^2 . (\frac{\partial n_{initial}^{cumulative}}{\partial V_r})^2 + \sigma_{V_{void}}^2 . (\frac{\partial n_{initial}^{cumulative}}{\partial V_{void}})^2 \quad (3.26)$$

Similarly, if $n_{final}$is the amount in the system, after equilibration, then the error in the final amounts would be given by, equation 3.29 and 3.30

$$n_{final} = \rho_i^* . (V_r + V_{void}) \quad (3.27)$$

$$n_{final}^{cumulative} = \rho_i^* . (V_r + V_{void}) \quad (3.28)$$

$$\sigma_{n_{final}}^2 = \sigma_{\rho_i^*}^2 . (\frac{\partial n_{final}}{\partial \rho_i^*})^2 + \sigma_{V_r}^2 . (\frac{\partial n_{final}}{\partial V_r})^2 + \sigma_{V_{void}}^2 . (\frac{\partial n_{final}}{\partial V_{void}})^2 \quad (3.29)$$

$$\sigma_{n_{final}^{cumulative}}^2 = \sigma_{\rho_i^*}^2 . (\frac{\partial n_{final}^{cumulative}}{\partial \rho_i^*})^2 + \sigma_{V_r}^2 . (\frac{\partial n_{final}^{cumulative}}{\partial V_r})^2 + \sigma_{V_{void}}^2 \quad (3.30)$$

It is to be noted that in the volume calibration and the void volume estimation, only single pressure procedure was followed. The adsorption measurements on the other hand were conducted in both the cumulative and single pressure fashion.

The equations from 3.22 to 3.30 represent the case when either the sample is non- adsorbent or there is no sample. In the case when an adsorbing sample is used, the excess sorption would replace MBR in equation. In addition, conventionally, the sorption is reported on a per unit mass basis, $n_{sorption}$. Therefore,

$$\sigma^2_{excess} = \sigma^2_{n_{initial}} . (\frac{\partial excess}{\partial n_{initial}})^2 + \sigma^2_{n_{final}} . (\frac{\partial excess}{\partial n_{final}})^2 \quad \text{(A.21)}$$

$$n_{sorption} = excess/m \quad \text{(A.21)}$$

Where, m is the mass of the adsorbent. Thus,

$$\sigma^2_{n_{sorption}} = \sigma^2_{excess} . (\frac{\partial n_{sorption}}{\partial excess})^2 + \sigma^2_{m} . (\frac{\partial n_{sorption}}{\partial m})^2 \quad \text{(A.22)}$$

In this analysis, the error in mass measurement was set to zero.

**Table 2.2:** Systematic errors that have been assigned in the error calculations.

| Error Source | Value |
|---|---|
| Error in calibrated volume | 0.5 cc |
| Error in Pressure measurement | 0.004 bar |
| Temperature sensitivity | 0.1 °C |
| Mass measurement | 0 g |

## 3.2 Sample Preparation

### 3.2.1 Raw coal Samples

Five coals of different ranks have been used in the study, namely, to a low volatile sub-bituminous coal A, low volatile bituminous coal B, medium, high - volatile subbituminous coals C and D, and lignite coal E. The selection of coals with diverse characteristics (See table 3.2) was done in order to facilitate a fundamental understanding on the effect of coal properties on the sorption capacities. The sorption measurements on raw coals were carried out on large particles, typically in the size range of 22 to 4.75 mm. The samples were placed in the refrigerator after communition (to prevent oxidation) and were heated at 110°C for 8 hours (moisture removal) before being tested for adsorption.

### 3.2.2 Pyrolysed char samples

The selected coals for adsorption measurements of the pyrolysed coal char study in chapter -5 were low rank non-coking coal (Coal A) and higher rank coking coal (coal B). The size of the coal sample ranges from 22 mm to 32 mm respectively. Coal samples were pyrolyzed at 800°C in a nitrogen environment for 20 min under an estimated heating rate of 2.5°C/s using a drop tube furnace (92). During pyrolysis, coal develops plasticity and further re-solidifies to form char. The degree of plasticity depends on the coal nature and has a significant impact on the coal char structure (93). It was observed that the higher rank coals develop greater plasticity compared to the low rank coals at high temperature, which can potentially block the pores in high rank coal during the pyrolysis process.

### 3.2.3 Gasified char samples

For the study reported in chapter 6, i.e., for the estimation of the sorption capacity of gasified coal chars, four coals namely, coal B, coal C, coal D and coal E were used. All the coals were gasified in a horizontal tube furnace setup, schematic shown in figure 3.5, at 800 °C under $CO_2$ atmosphere for 10 minutes. The heating rate was maintained at 5°C/min for all the samples and the $CO_2$ flow rate was maintained at 2 l/min. The particle size of the raw coals was in the range of 3.35 – 4.75 mm. The coals of diverse ranks were selected in order to determine the effect of coal properties on the sorption capacity of gasified char. The gasification setup consists of a horizontal tube furnace, in which the heating mechanism is electrical. A quartz tube of 59mm diameter and 80 cm length is placed in the furnace to hold the sample crucible and a thermocouple to measure the temperatures at the sample location. In addition, the quartz tube provides a sealed environment for the gasification to take place.

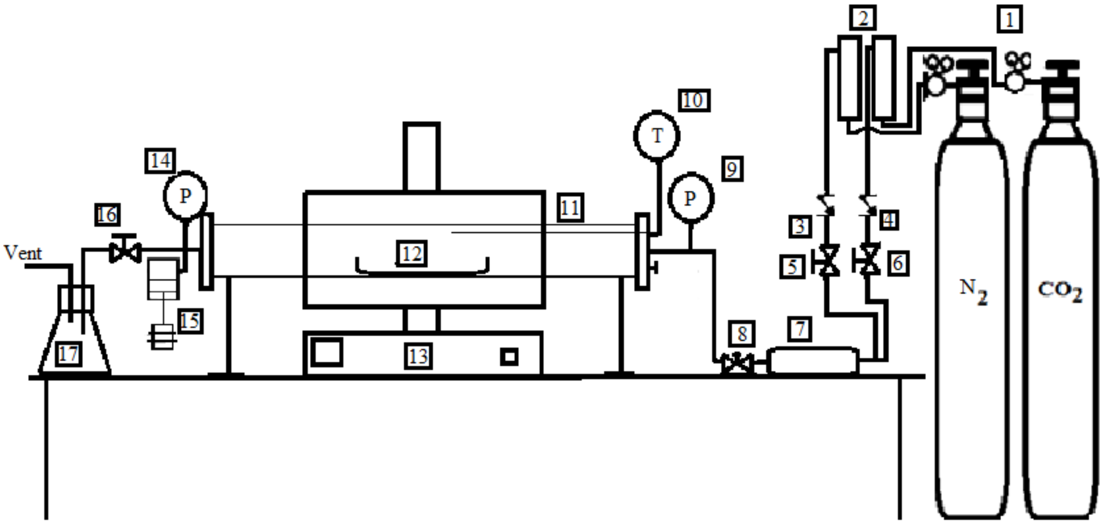

**Figure 3.5** Schematic of the Horizontal tube furnace Gasification setup.
[1.Gas Cylinders 2.Rotameters 3,4.Check Valve.5,6.Ball Valve 7.Mixing Tank 9,14 Pressure Guages 10.Thermocouple 11.Quartz tube 12.Sample holder 13.Tube furnace 15.Pressure Release Valve 16.High Temperature ball valve 17.Scrubbing solution]

The quartz tube is sealed at the both ends with two flanges and kaowool discs were used as gaskets. The gas is injected through the right end of the tube (as shown in the figure 3.5) at a constant flow rate set on the rotameter. Two rotameters are provided in order to set the $N_2$ and the $CO_2$ flow rates independently. In addition, the setup is also equipped with two pressure gauges 0-60 psig at both ends of the quartz tube. However, it is made sure that atmospheric pressure is maintained at all times. The left hand side of the quartz tube, i.e., the rear end of the setup consists of the venting section. The venting section is comprised of the pressure release valve and a scrubbing solution. The line form the scrubbing solution is sent to the fume hood.

The procedure followed for preparing the char samples is as follows. At first, a known mass of raw coal particles of 3.35-4.75 mm were spread to form one layer on the crucible and placed into the furnace. The samples were then purged for 30 mins with $N_2$, at 500 ml/min. Next, the furnace temperature was raised to $800^{o}C$ at a ramp rate of 5 $^{o}C$/min. During the temperature ramping period a constant nitrogen flow of 500 ml/min was maintained. When the furnace reached a temperature of $800^{o}C$, $CO_2$ was injected at 2 l/min for 10 mins in addition to the nitrogen flow, in order to ensure constant flow in the system. After 10 mins, $CO_2$ flow is terminated and the furnace is allowed to cool down. The final mass of the sample was measured after cooling. The conversion of the samples is measured by taking the weights before ($W_o$) and after ($W$) the gasification by the equation,

$$\chi\,(\%) = \frac{W - W_o}{W_o} * 100 \qquad (3.24)$$

## 3.3 Sample Characterization

A variety of coal samples have been used in this work in order to highlight the effect of coal properties. The proximate, ultimate and the petrographic analysis of the coals have been listed in the Table 3.2. The characterization results for coals A and B were obtained from (92). In addition, surface area and surface morphology was studied using low pressure sorption analysers and Scanning Electron Microscopes.

*Surface area determination*

The surface area samples in Chapter – 5 was measured by low pressure sorption isotherms that were carried out in Micromeritics ASAP 2020 using nitrogen as the probe molecule at 77 K. Initially, samples were heated to 250°C at a ramp rate of 5°C /min until a vacuum level of 0.5 Pa was reached. After reaching the vacuum set point the samples were outgassed for 4 hours. Surface area and micropore analyses were carried out on ~ 400 mg samples using a fixed dose quantity of 0.25 cc per step with a maximum equilibration delay of 1 hour per step.

On the other hand, the $CO_2$ surface area was measured for samples in Chapter -6. The low pressure $CO_2$ isotherms were carried out in Quantachrome Autosorb iQ instrument. Prior to the sorption measurement, the samples were degassed at 200°C at 2°C/min for 10 hours under high vacuum. The isotherms were carried out on 500 mg of samples with a fixed dosing of 0.5 cc per step, with maximum equilibration of 10 mins. The adsorption data were obtained in both $N_2$ and $CO_2$ isotherms were obtained by maintaining constant test conditions, which allow the comparisons to be made between the respective samples in each study.

**Table 3.3**: Proximate, Ultimate and Petrographic analysis of raw coals.

| **Parameter** | **Coal A** | **Coal B** | **Coal C** | **Coal D** | **Coal E** |
|---|---|---|---|---|---|
| *Proximate Analysis (wt. %)* | | | | | |
| *Moisture (ad)* | *5.01* | *1.26* | *4.45* | *2.81* | *6.9* |
| *Ash (ad)* | *10.39* | *14.07* | *15.40* | *10.58* | *19.2* |
| *Volatile Matter (daf)* | *31.0* | *27.0* | *28.89* | *39.60* | *42.8* |
| *Fixed Carbon (ad)* | *58.39* | *61.85* | *50.26* | *52.31* | *57.1* |
| *Ultimate Analysis (wt %, dry basis)* | | | | | |
| *Sulphur* | *0.56* | *0.61* | *0.54* | *0.84* | *1.15* |
| *Carbon* | *66.8* | *79.4* | *63.29* | *64.34* | *54.3* |
| *Hydrogen* | *3.86* | *4.48* | *3.97* | *4.11* | *3.91* |
| *Nitrogen* | *0.78* | *1.46* | *1.07* | *0.95* | *1.22* |
| *Oxygen* | *8.99* | *3.83* | *15.73* | *19.18* | *20.26* |
| *Petrographic Analysis* | | | | | |
| *Vitrinite(%)* | *32.2* | *44.8* | *65.20* | *67.8* | *53.2* |
| *Inertinite(%)* | *52.1* | *44.9* | *22.10* | *17.90* | *36.4* |
| *Liptinite(%)* | *4.5* | *5.1* | *2.10* | *7.50* | *7.0* |
| *Maximum Virinite Reflectance* ($R_{max}$ %) | *0.57* | *1.24* | *0.56* | *0.69* | *0.44* |

*Surface morphology*

The sample morphology images for the raw coals and the gasified char particles were obtained from a Zeiss EVO MA 15 stationed at the Earth Sciences department at the University of Alberta. The images were obtained in the variable pressure mode in order to avoid carbon coating. Most images were taken at a magnification of around 150 -500X; primarily to view the surface changes on the large coal particles.

# Chapter – 4

# Sensitivity Analysis and Performance Evaluation of a Volumetric Adsorption Apparatus

Several commentaries are available in the literature on the reliability of the volumetric apparatus compared to the gravimetric adsorption measurement system. It has been well established that although the volumetric system is cost effective and can be custom designed for the needs of the study, there are certain inherent error sources in the system that reduce the reliability of measurement. For instance, in this study, the volumetric apparatus is chosen to represent large volumes of the coal sample to capture the heterogeneity in coal, and at the same time, study the sorption on large samples. On the other hand, the error sources in the system include, the error in the pressure measurement, isothermal sensitivity, and the errors in the volume calibration. Moreover, apart from these errors further complications can also be introduced with the effect of the PVT behavior of the adsorbate. However, in order to benefit from the flexibility of the volumetric system through meaningful and reliable data, it is essential to overcome the challenges stated above. This chapter presents an analysis on the error contribution of the various sources on the sorption measurements through a sensitivity analysis. Further, the performance evaluation procedures developed have been used to compare two apparatus designed during the course of the study. Such a study would help in improving the apparatus performance by at least reducing, if not eliminating the errors through better equipment selection. At first, emphasis is placed on the effect of PVT behavior of the gas on the sorption blank run as this helps understand the sensitivity of dealing with gases such as CO2 which transition into supercritical phase in the operating conditions.

## 4.1 $CO_2$ Gas Behaviour

$CO_2$ gas transitions into the supercritical phase at temperatures and pressures above 31°C and 73 bar. In the case of geological sequestration of $CO_2$ the adsorption pressure comes under this region. Hence, it would be worthwhile to understand effect of the transition into the supercritical phase on the PVT behavior as observed in a volumetric apparatus. Further, the emphasis of this transition can be highlighted through the comparison with an ideal gas such as Helium. The errors in the blank runs of apparatus 1 and 2 with Helium and $CO_2$ have been compared in Figure 4(a) and (b). In addition, the volumetric error due to the PVT behavior of the gas has been depicted in the respective plot. The volumetric error due to Helium/$CO_2$ is calculated from the product of volume and partial differential of molar density with respect to a pressure change of 0.5 bar $(\frac{\partial \rho}{\partial P}).V$. On the other hand, the error in the blank tests is estimated by the difference in gas amounts before and after equilibration at a particular pressure, otherwise known as the mass balance residue (MBR). Obviously, the MBR for any blank test should be zero, provided the system is perfectly sealed.

From Figure 4.1(a) it can be seen that the error decreases as a pressure increases. The Helium molar density results in a maximum error at 1.5 mmole at pressure around 5 bar decreasing thereafter. On the other hand, the errors on the cumulative blank tests are much lower in the range of 0.5 mmole. In the case of single pressure blank test, it is observed that the error is higher than the cumulative pressure at lower pressures; however, the errors in single pressure are lower at higher pressure compared to the cumulative pressure blank tests. In general, the blank tests have lesser error compared to the Helium molar density profile. This is because, the errors in the pressure measurement in apparatus -1 and 2 are lesser than 0.5 bar. In the case of $CO_2$, for all the tests reported in figure 4.1(b), the error is the least at low pressures around 10 bar, increases steadily thereafter till about 60 bar. Subsequently, a sharp rise in the error is noted from 60 – 80 bar to result in a maxima around 85 bar. The error decreases steadily after the maxima. It can be seen that the volumetric error due to $CO_2$ density profile results in an error close to 16 mmole. This observation may only be explained by the transition of $CO_2$ from the gaseous to the supercritical phase at 73 bar at any temperature above 31.1°C. Carlés (94) suggests that the critical phenomena can even be felt far from the critical point and "induce unexpected dynamic responses". The properties of the supercritical fluids are sensitive to minute changes in the properties. Although the temperature of the isotherm is 45.5 ($T/T_c$=1.5), is generally considered to be far enough from the critical point to have any form of abnormality in the sorption isotherm (95).

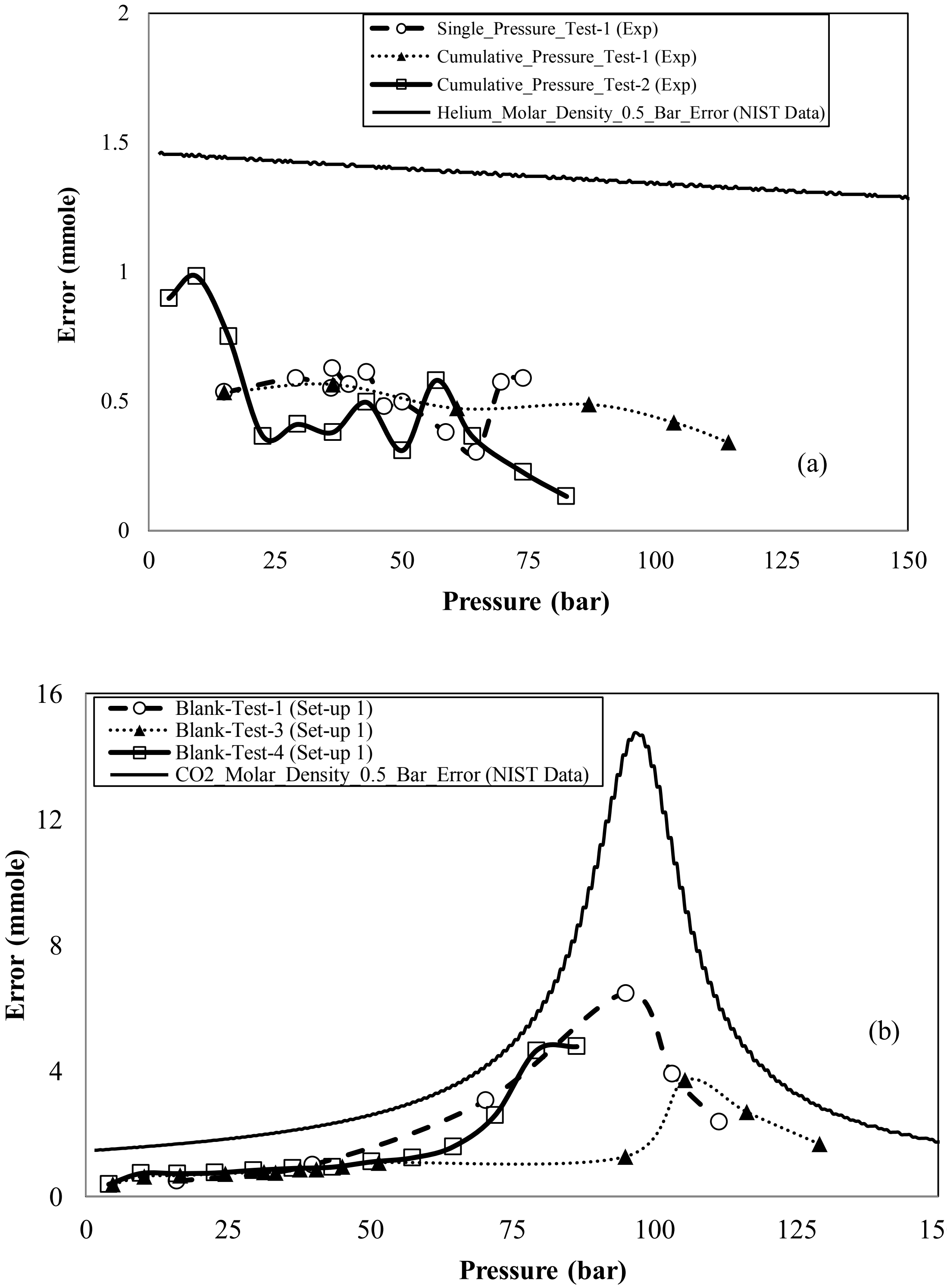

**Figure 4.1**: Comparison of the volumetric errors due to Helium gas behavior at pressures up to 100 bar in apparatus 1 and apparatus 2, (b) Comparison of the volumetric errors due to $CO_2$ gas behavior at pressures up to 100 bar in apparatus 1 and apparatus 2

Furthermore, this observation also leads to an understanding on the sensitivity of $CO_2$ to an error in pressure sensing. The effect is amplified as the sensitivity of $CO_2$ density to pressure, given by $\left(\frac{\partial \rho}{\partial P}\right)$ is multiplied with a large volume (adsorption setups in this study). However, in the case of blank tests, i.e., blank test -1, blank test-3, and blank test - 4 performed in apparatus -1(in cumulative operation mode) result in the next highest error at 7, 5 and 4 mmole respectively. On the other hand, the blank tests performed in apparatus -2 (in single pressure operation mode) have maximum errors in the range of 0.065 mmole. It is to be noted that the errors in the blank tests are considerably less than the $CO_2$ molar density curve. This is because the pressure sensors used in apparatuses 1 and 2 have accuracies in the range of 0.137 bar and 0.004 bar. The difference between the blank isotherms of apparatus -1 and apparatus -2 may be attributed to method of operation (i.e., single pressure or cumulative pressure) and the difference in the accuracies of the pressure transducers .Thus, higher accuracy in the pressure transducer can lead to lesser errors in the case of blank tests and sorption isotherms in general. Although the pressure transducer is an important component in the volumetric adsorption apparatus, there are several influencing parameters such as the accuracy in volume calibration of reference manifold and sample cell, efficiency of temperature control, and accuracy in determination of void volume. Of these, the accuracy in volume calibration, pressure sensor accuracy and efficacy of temperature controller are the basic errors introduced into the system the rest are derived from these basic errors. Thus it would be worthwhile to carry out a sensitivity analysis on the effect of above mentioned parameters on the total error in the isotherm.

## 4.2 Sensitivity Analysis

At first, the error contribution due to the pressure sensor accuracy on a blank run is studied as a function of pressure (See Figure 4.2 (a)). The errors have been calculated based on the multivariate error analysis method presented in section 3.1.5. The pressure sensor errors have been arbitrarily set at 1, 10, 100 and 200% increase from the initial error set at 0.01 bar. In addition, other influencing parameters such as the temperature sensitivity and volume calibration error are set to constant values of 0.1°C and 0.05 cc. The temperature of the isotherm is set to 45.5 °C. Moreover, the error calculations have been carried out for operation on a single pressure mode. From Figure 4.2(a), it is to be noted that as the pressure sensor error increases, there is a significant increase in the total error in the isotherm.

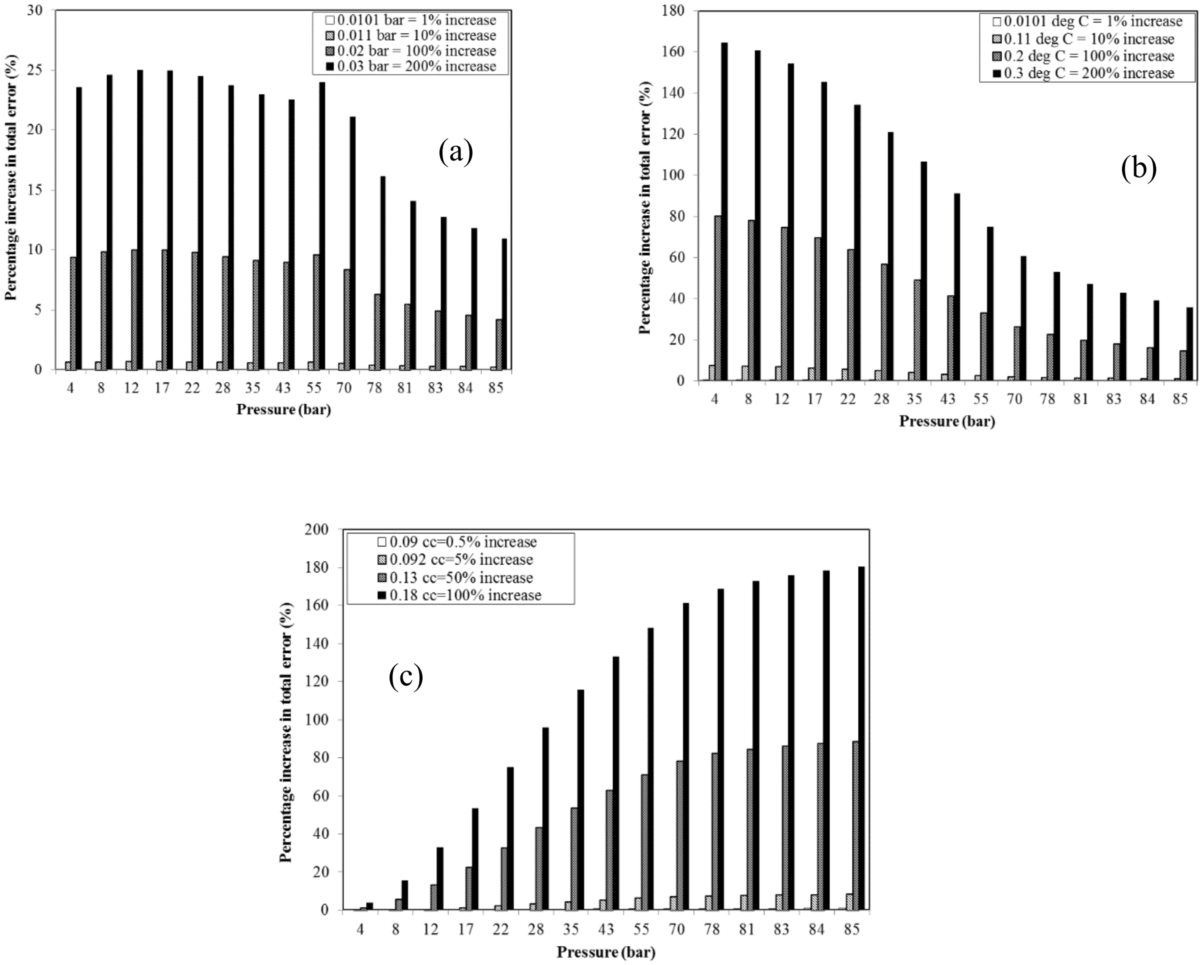

**Figure 4.2(a,b,c):** Sensitivity analysis of the pressure, temperature, and volume calibration influence on the overall error of the system.

In addition, the percentage increase in error rises initially till a point of 17 bar and steadily declines thereafter till 80 bar. However, a small peak is noticed in the range 50 – 75 bar for all the cases of pressure errors. It can be seen that for a 1% increase in the pressure sensor error (i.e., 0.0101 bar), the total error in the system increases by a maximum of 0.073% in the range of 10-20 bar and reaches a minimum of 0.028% at 85 bar. With an increase of 100% in the pressure sensor error, the total error increased by a maximum of 10% to a value to 0.252 mmole from 0.25 mmole. Comparing the plots with pressure sensor errors increasing from 100 to 200%, the percent increase in error increased from 10% to 25% resulting in an error of 0.3 mmole. The pressure sensor error is significantly influencing the total error in the system. In particular, the pressure sensor error influences the error in the density of gas which in turn influences the calibration accuracy of the reference cell (pycnometric calibration); initial and final amounts measured in the system. It is to be noted that the nature of influences are quite fundamental and it is critical to ensure that the pressure measurements are accurate to the desired tolerances. If not, the error would accumulate and result in extremely unreliable results. The magnitude of such influence can be inferred from results of the multivariate error analysis presented in Figure 4.2(a).

Figure 4.2(b) shows the percentage increase in the total error in the system when the error due to temperature fluctuations have been increased by 1, 10, 100 and 200% from the initial error that was set at 0.1 $^{o}$C. In addition, other influencing parameters such as the pressure sensor and volume calibration error are set to constant values of 0.01 bar and 0.05 cc. The temperature of the isotherm is set to 45.5 $^{o}$C. As in the case of pressure sensor error variation, the total error in the system increases with increase in the error due to temperature fluctuations. However, the total error in the system decreases with increasing pressure for all the cases of temperature fluctuation errors introduced. This decrease is relatively steep at lower pressures compared to the high pressure regions of the plot. With a 1% increase in the error due to temperature fluctuation, the total error in the system increases by a maximum 0.75% at 4 bar and a minimum of 0.10% at 85 bar. However, it is to be noted that the absolute error in the system increases in magnitude with pressure, however, the sensitivity (as depicted by % increase in error) decreases with pressure. In other words, the errors are more sensitive at lower pressure than at higher pressures. Comparing the plots with pressure sensor errors increasing from 100 to 200%, the percent increase in error varied from 80% to 164% at a pressure of 4 bar and 14-35% at 85 bar. The temperature fluctuations in the system mainly induce variations in the density of the gas/supercritical fluid. The variations in density, caused either through the temperature fluctuations or pressure measurement or prediction through an EOS, affect the overall quality of the resulting isotherms.

Figure 4.2(c) shows the percentage increase in the total error in the system as a function of pressure where the error in the reference volume calibration has been varied by 0.5, 5, 50 and 100% from the initial error that was set at 0.08 cc. In addition, other influencing parameters such as the error due to temperature fluctuation and pressure sensitivity are set to constant values of 0.1$^{o}$C and 0.01 bar. The temperature of the isotherm is set to 45.5 $^{o}$C. It can be seen from Figure

2(c) that as the error in reference volume increases, there is an increase in the total error in the system. In this case, both the absolute error and the percentage increase in the error increase with increasing pressure. For a 0.5% increase in the error in reference volume, which amounts to 0.09cc, there is a maximum increase of 085% at 85 bar. Similarly, for a 50 and 100% increase in the error in the reference volume (0.13 cc and 0.18 cc) the total error in the system increases by 88 and 180% respectively. It should be noted that such a small change in volume can lead to errors in the range of 2-3 mmole at high pressures. This is due to the fact that the volumes associated with such systems are large, and any small change in volume is going to contribute significantly towards the total error. From all the graphs in Figure 4.2, it can be inferred that the greater uncertainty in volume calibration can have substantial impact on the isotherm compared to that of the pressure and temperature effects. It is also to be noted that the impact of pressure and temperature errors on the density profile is subject to the location from the critical point. Being closer to the critical point, the minute errors due to temperature fluctuations or pressure sensor sensitivity can impact the isotherm to a greater extent.

## 4.3 Performance Evaluation

This section of the chapter details the procedures used to characterize the performance of an adsorption apparatus. The two adsorption apparatus developed have been compared based on blank runs, isotherms with inert samples such as glass beads and isotherms on standard adsorbents.

### 4.3.1 Blank isotherms

The $CO_2$ blank runs carried out in apparatus 1 and 2 at a temperature of 45.5 $^{o}$C have been compared in Figure 4.3(a). The comparison is made by plotting the MBR against pressure for each apparatus. The blank isotherm in apparatus -1 have been carried out in a cumulative fashion, whereas the blank from apparatus-2 in a single pressure mode. As stated earlier, the MBR is defined as the difference between the initial amount (before equilibration) and final amount (after equilibration) in the volumetric apparatus. Ideally, the MBR should be equal to zero, provided there are no leaks in the system. From figure 4.3(a) it can be seen that in the apparatus -1 blank isotherm, the MBR is close to zero till a pressure of 51 bar. At pressure close to 60 bar, there is a sharp decrease to reach a minima at -2.53 mmole around 80 bar. After the minima, the mass balance residue in apparatus – 1increases sharply to cross the abscissa at 100 bar and continues to rise till 120 bar to reach a maximum of 5.75 mmole. Moreover, the very trend is followed by the apparatus-2. However, the magnitude is lesser initially. In this case, the descent starts around 45 bar to reach a minima of -3.9 mmole at a pressure of 81 bar.

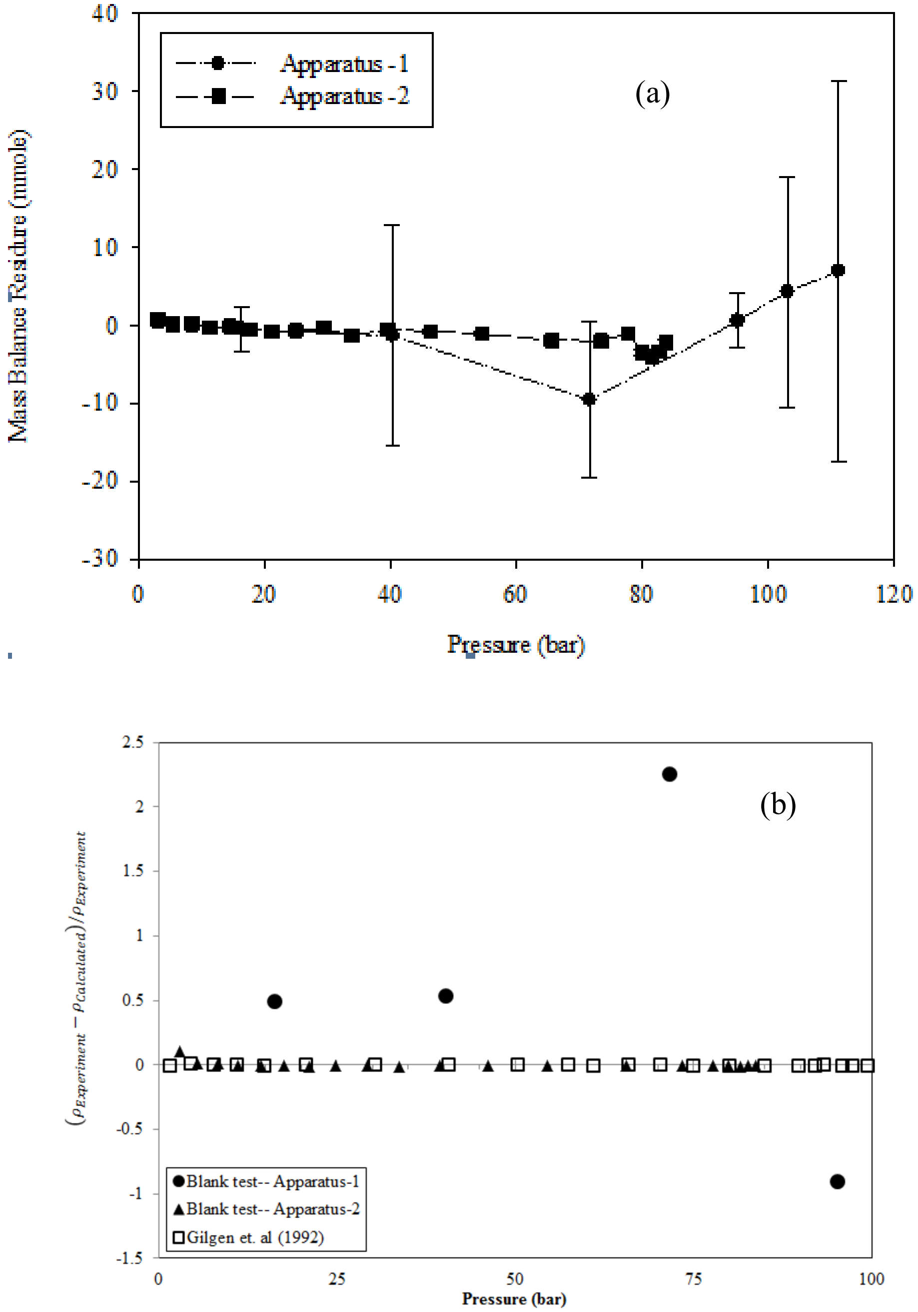

**Figure 4.3** Comparison of the blank tests from the apparatus -1 and apparatus -2

Subsequently, the mass balance residue increases to reach a maximum around -2 mmole. This trend in a blank was reported by other researchers, however, the cause for such a dynamic trend has not been inspected. The reason might be because of the interplay of all the errors in the system discussed in the previous sections. The error bars in the plot have been calculated based on the multivariate errors present in the apparatus – 1 and apparatus-2. It can be seen that the error bars are minimal in the low pressures; however, they are larger as the pressure goes beyond 60 bar. This indicates the pressures in the range of 60-80 bar are the most susceptible to the effects due to the errors in density measurement at 45.5°C. The difference in the magnitude between the two apparatus may be because of the enhanced pressure sensor accuracy in apparatus -2.

Figure 4.3(b) depicts the error in the equilibrated density measurement as a function of pressure. The error in the equilibrated density is computed by the expression:

$$\left(\rho_{Experiment} - \rho_{Calculated}\right)/\rho_{Experiment} \qquad (4.1)$$

Here $\rho_{Experiment}$ is the equilibrated density obtained from the experiment, $\rho_{Calculated}$ is the density predicted from a mass balance with a known injected density and volumes (depicting an ideal case). Ideally, the density obtained from the experiment should be equal to the one predicted from a mass balance, thereby resulting in an error of zero. In figure 4.3(b), the error in equilibrated density has been presented for the blank isotherms in apparatus -1 and 2 apart from a PVT data obtained from (96). It can be seen that for the apparatus -1, the error varies from 5% in the lower pressures upto 35 bar. The error reached a maximum negative value of 15% at 40 bar and a maximum value of +20% at 50 bar. Overall, the error as a function of pressure seemed un-correlated for apparatus -1. On the hand, for apparatus -2, the maximum error is 10% at 10 bar. The error consistently stayed close to zero line mark for higher pressures with the errors in the range of 0.4 – 1%. The literature data taken from (96), have been obtained from a blank isotherm in a gravimetric apparatus. The data from literature and the data from this study are obtained through different measurement techniques; however, the comparison is only made to emphasize the errors in a volumetric system relative to a gravimetric. The error in the literature data is much lesser to the data obtained from this study.

## 4.3.2 Isotherms on inert samples

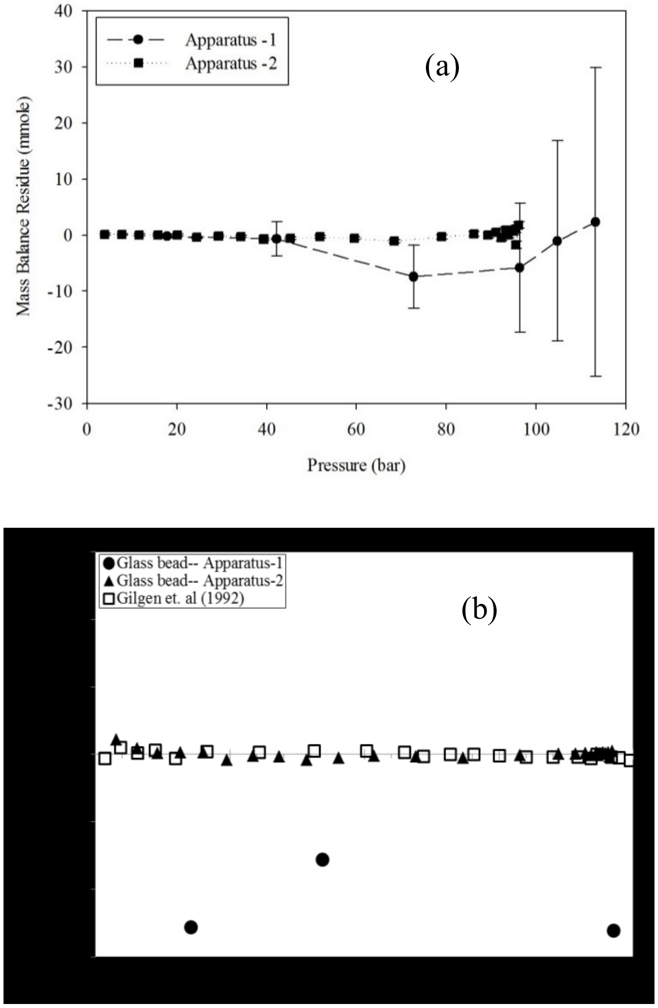

**Figure 4.4 (a), (b):** Comparison of the glass bead from the apparatus -1 and apparatus -2

The isotherms of an inert sample (non-adsorbent) sample under $CO_2$ on apparatus -1 and 2 at 45.5$^{o}$C have been compared in Figure 4.4(a). In this study, approximately 20 g of 6 mm glass beads were used as inert samples since the glass beads are incapable of adsorbing helium or $CO_2$. In this case too, like the blank isotherms, the apparatus -1 isotherm were carried out in a cumulative injection method, whereas the apparatus -2 isotherms were carried out in single pressure mode. The isotherms are being compared by plotting the MBR versus pressure. It can be seen from figure 4.4(a) that in apparatus -1 the MBR is around -0.5 mmole at 42 bar. The value goes on to decrease till a minimum of -7 mmole at 70 bar. The MBR increases till a value of 2.33 mmole. A similar trend was observed with the glass bead isotherm in apparatus -2, although the magnitude of deviation from zero was much lesser. It is also worthwhile comparing the MBR values of a blank isotherm and the glass bead isotherm. The values in the glass bead isotherm on an average are much lower. This is possible because, the inert glass beads occupy a part of the total volume that is inaccessible to the gas. This reduces the void volume in the system, thereby reducing the error and hence the deviation of the MBR values from zero. It is to be noted that the error bars in the case of apparatus -1 are larger than those in apparatus -2. The error bars have been a result of the calculations from the multivariate error propagation method described in the materials and methods chapter.

Figure 4.4(b) compares the errors in the equilibrated density in glass bead isotherms carried out in apparatus -1 and apparatus -2 in a similar manner as shown in figure 4.3(b). It can be seen from the glass bead isotherm in apparatus -1 that the density error is fairly large around 20-30% compared to the glass bead isotherm carried out in apparatus -2. It has to be noted that only three out of six points in the glass bead isotherm could be presented in the graph. The rest three points were beyond the scale. In the case of apparatus -2, the density error for the isotherm is less than one percent. The literature data from (96), the same data presented in Figure 4.3(b), has been used to compare the errors in density measurement. The large errors in density can be partly attributed to the pressure sensor accuracy, void volume determination error and insufficient equilibration times.

### 4.3.3 Isotherms on a commercial adsorbent

Silica gel was considered as a standard commercial adsorbent for comparing the sorption magnitudes estimated in both apparatus 1 and 2. In addition, the experimental data have been compared to ones earlier reported in literature [97]. The excess adsorption vs pressure plot for comparing the $CO_2$ isotherms on silica gel carried out at 45.5°C the have been shown in Figure 4.5.

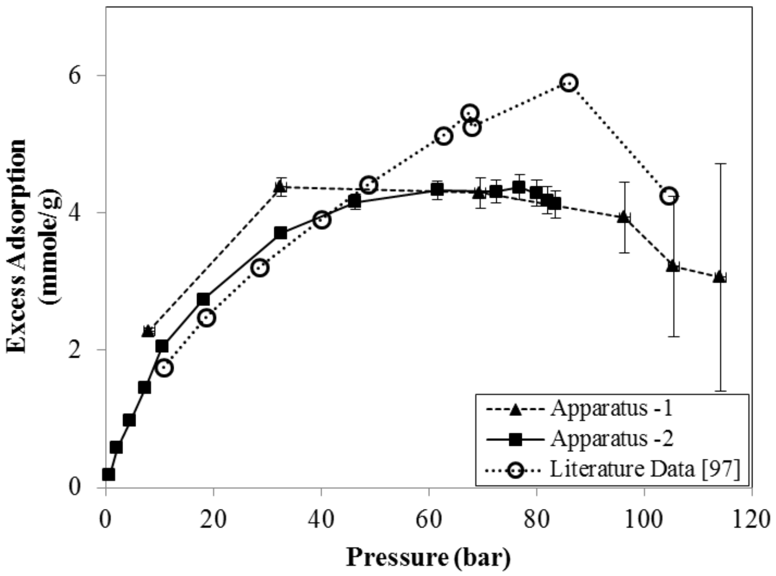

**Figure 4.5:** Comparison of Silica gel isotherms from apparatus -1 and 2 with the literature data

In addition, the isotherms obtained in this study were compared with the silica gel isotherm reported in literature (97) at 47.3°C. There is a good agreement between the isotherms from apparatus -1 and 2. It can be seen that there is a steep increase in the sorption till 30 bar in the case of both the samples from this study and from literature. The sorption magnitudes in all the case lie with in a deviation of ±5% from each other till 50 bar. The maximum sorption for the samples from this study is observed to be around 4.2 mmole/g (apparatus-1). Subsequently, the sorption decreases steady as the pressure increases. However, in the literature sample, the sorption magnitude continues to rise as the pressure increases. This difference in the sorption trend may be due to the difference in the nature of the sample and the errors in the measurement apparatus. Further, it is to be noted that the abnormal trends that were found in the blank and the glass bead isotherms (See Figure 4.3 and 4.4) are not reflected in the silica gel isotherms. This is because; the errors in the systems are lesser than the adsorption capacity of silica gel. However, the deviation due to the errors in the systems may be apparent in the sorption on absorbents with lesser adsorption capacity. In order to validate this, $CO_2$ sorption on raw coal samples was carried out at 45.5°C.

### 4.3.4 Isotherms on raw coals

Figure 4.6 compares the excess adsorption magnitudes of a raw coal carried out in apparatus -1 and 2 at 45.5°C. The isotherms were run on cumulative and single pressure modes in apparatus 1 and apparatus -2 respectively. In the case of apparatus -1, the sorption increases till a pressure of 45 bar reaching 0.65 mmole/g. Subsequently, a sudden decrease in the sorption magnitude is then observed around a pressure of 72 bar. The sorption then increases in magnitude to reach 1.32 mmole/g at 96 bar and 1.86 mmole/g at 113 bar thereafter. However, in the case of isotherms from apparatus -2, the sorption magnitude steadily increases from 0.09 mmole/g at 2 bar to 0.8 mmole/g at 87 bar. Following which is a steep rise to 1.15 mmole at 91 bar. A large number of experiments in the past have been reported (98). On the other hand, the trend of an isotherm such in apparatus -2 has been reported; however, the reason behind the abnormal dip in the sorption magnitude around 70 bar has not been examined comprehensively till date. Most certainly this trend cannot be explained by the Gibbs Surface Excess model. In a typical Gibbs surface excess isotherm would increase with pressure as long as the bulk gas density is less than the adsorbed phase density. A maximum would be attained when the bulk gas density equals the adsorbed phase density. Subsequently, the sorption magnitude would decrease as the bulk gas density is greater than the adsorbed phase density. Moreover, it is to be noted that the trend in the coal isotherm is similar to the blank and glass bead isotherm (both trend and magnitude)

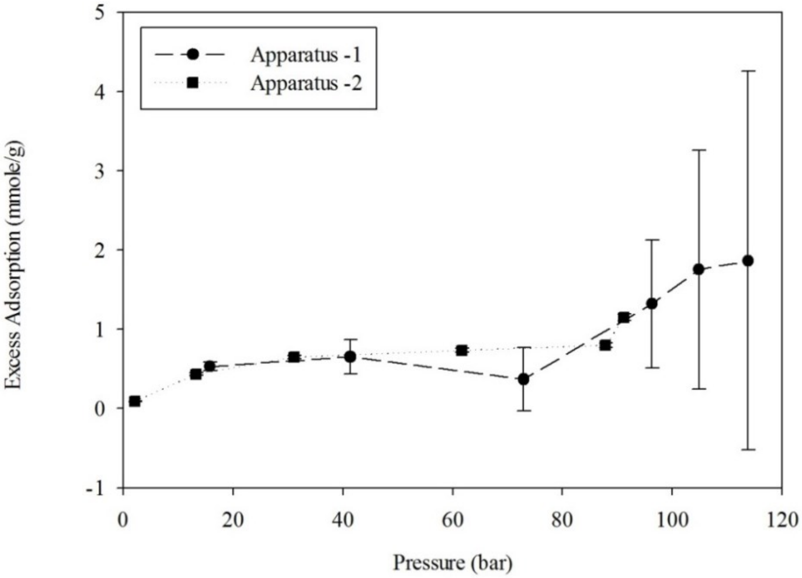

**Figure 4.6:** Comparison of raw coal isotherms from apparatus 1 and 2

presented earlier in Figure 4.3 and 4.4. Interestingly, the trend in blank test is not reflected in the silica gel isotherm.

## 4.4 Optimized Operation Procedures

Based on the understanding from the sensitivity analysis and the performance evaluation procedures, it was understood that the volume calibration and the pressure sensor accuracy played a crucial role in the final error in measurement. In addition, errors would also be introduced due to the estimation of helium void volume in the sample. This section deals with the optimum procedure for volume calibration and void volume estimates.

### 4.4.1 Void Volume Estimation

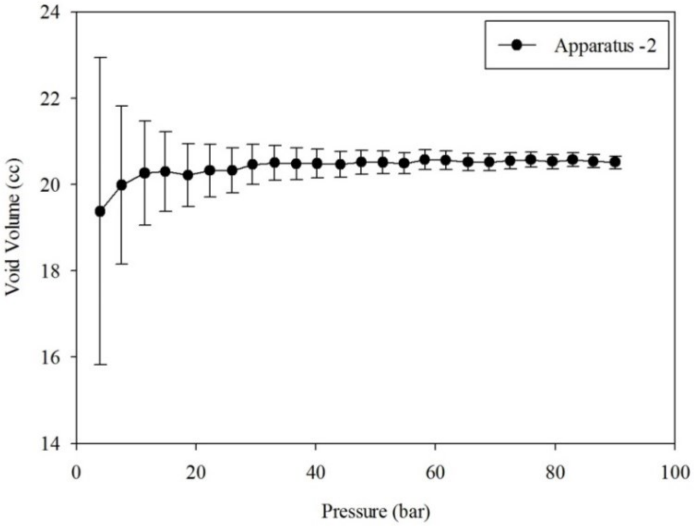

**Figure 4.7**: Variation of void volume against pressure for glass beads

Variation of the void volume in the case of glass beads isotherm is depicted in Figure 4.7 as a function of pressure. The void volume has been determined in apparatus -2 in a single pressure operating mode. As stated earlier, the void volume is determined by the Helium expansion method where a known amount of helium is injected into the sample cell at first. Subsequently, the gas is equilibrated into the sample cell and based on this equilibration pressure the void volume or free space in the sample cell is back calculated. From Figure 4.7, it can be seen that as the pressure increases, the void volume determined through Helium expansion method increase till 30 bar and remains constant thereafter. In this case, the void volume reached a maximum value of around 21 cc before flattening out. The choice of a unique value for the void volume should be based on the range of pressures which yield the lowest average MBR. Usually, the optimized pressure range is located toward the higher pressures (above 60 bar) as the values are more consistent in this region. Moreover, it is to be noted that the error associated with the void volume at lower pressures is much higher than those at higher pressures. This methodology of determining void volume at a certain pressure range based on volumetric tests on non-adsorbent samples (glass beads) would only be valid for adsorbents which do not adsorb significant amounts of helium. Carbon based adsorbents such as coal; activated carbon, coal char, and shale are a few materials which are poor adsorbents of helium (87). However, in the case of samples that adsorb significant amounts of helium, lower pressures have to be preferred for void volume determination as the sorption magnitude would be lower thus resulting in better estimates of the void volume.

### 4.4.2 Volume Calibration

The importance of volume calibration in the accuracy sorption measurements has been demonstrated through the sensitivity analysis presented earlier. Volume calibration procedures have to be carried out in order to determine both the reference as well as the sample volumes at the maximum possible accuracy**.** Figure 4.8 compares the efficacy of various volume calibration techniques adopted in this study by comparing the MBR values of blank test using these volume sets. Ideally, the optimized volume set should result in the average MBR value of zero. Figure 4.8(a), shows the MBR on a Helium blank isotherm on apparatus -1 for different sets of volumes generated by the different techniques used for calibration; namely, pycnometry, physical volume estimation and the mass flow meter method.

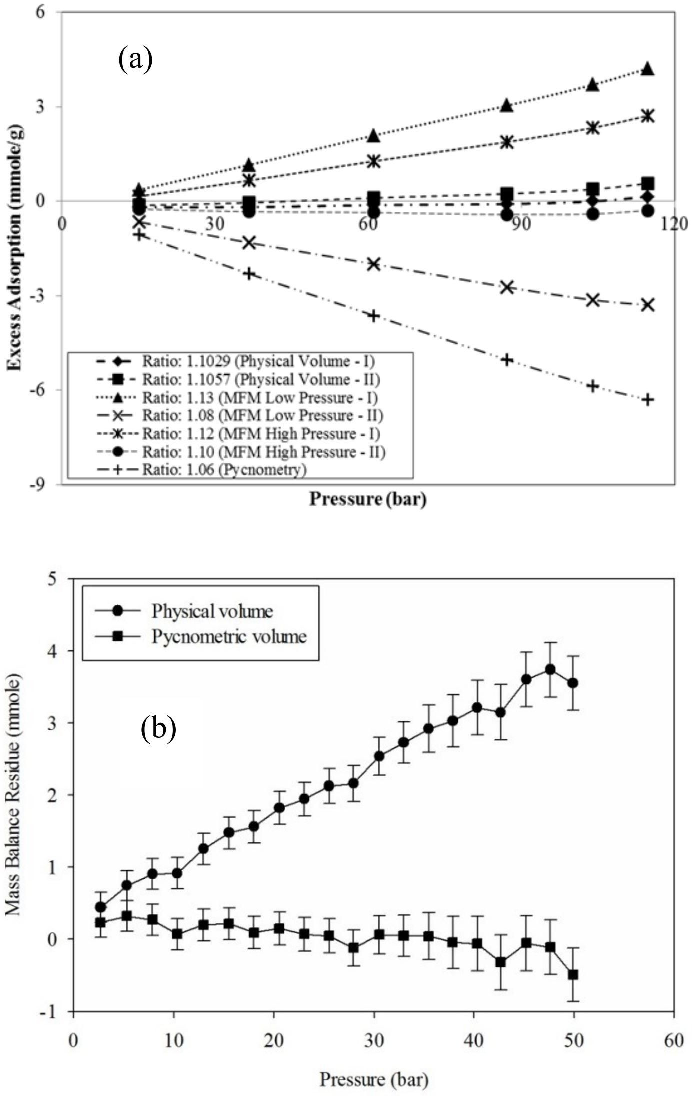

**Figure 4.8:** Suitability of various volume calibration methods

It can be seen that the physical volumes yield the MBR closest to zero and the volume obtained by the pycnometric technique gives the larges MBR. In addition, it is to be observed that the volume ratios in all the techniques, the volume ratio varies only by 10%. On the other hand, in the case of apparatus -2, the MBR for the helium blank was in better in the case of pycnometric volume compared to the physical volume estimation. However, in the case of apparatus -1, because the poor pressure sensor accuracy yield erroneous estimates compared to other techniques.

# Chapter – 5

# Adsorption Behavior of $CO_2$ in Coal and Coal Char[1]

Coal has gained significant importance in $CO_2$ sequestration due to its unique pore structure and fissure system. In the case of pyrolysed coal chars, there is an increase in the porosity and the surface area compared to the raw coal as a result of the structural changes in the coal matrix that accompany the volatile matter release. The quantification of the $CO_2$ sorption capacity of pyrolysed chars is essential as they form a significant part of the post-UCG site. The pyrolysed chars are stratified in various layers due to the exposure to different time temperature histories. This chapter details the sorption capacities of the raw coal and the effect of coal character and the pore structure on the sorption capacity of $CO_2$. In addition, $CO_2$ sorption capacities of two pyrolysed chars from coal A and B obtained at 800 and 1000°C have been obtained. Further, the sorption capacities of the pyrolysed chars have been analysed to determine the effect of raw coal properties.

## 5.1 Adsorption Behaviour of Raw Coal Sample

The adsorption capacities of four raw coals are estimated at 45.5°C and are depicted Figure 5.1 as a function of gas density. Within the reported samples (see Figure 5.1), coal A, coal B, coal C and coal D are obtained by experiment at 45.5°C, on the other hand, A3 Australian coal, S2,S3 Switzerland coal represents the literature data (31) obtained at 45°C. The term density here refers to the isothermal molar density of carbon dioxide as a function of pressure. The figure clearly shows a significant rise in excess adsorption capacity with an increase in density for the reported samples. Even though, the magnitude of adsorption is different, the increase in excess adsorption per unit rise in density is almost identical for the experimental samples (i.e., coal A, coal B, coal C & coal D).

---

[1] The results presented in this chapter are published elsewhere (84)

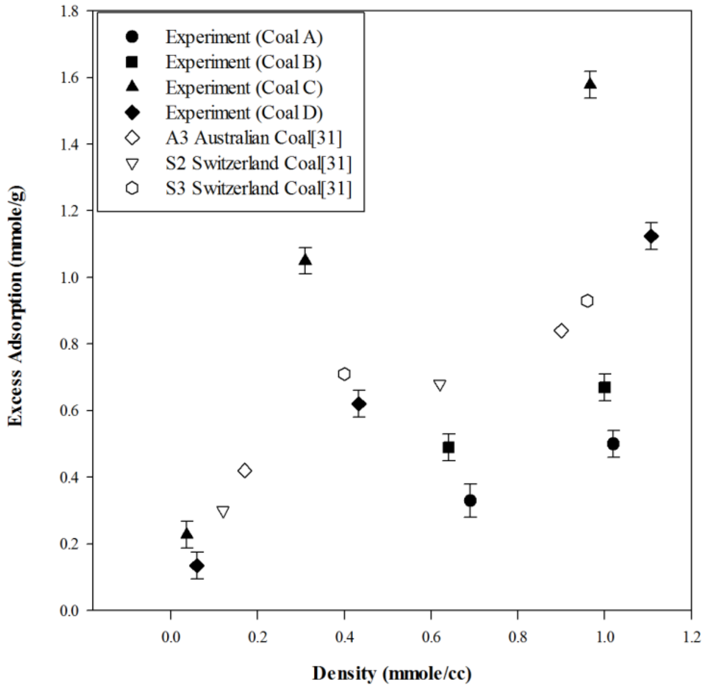

**Figure 5.1:** Comparison of excess adsorption data for experiment and literature in virgin coal sample.

Within the studied range of density, except for coal C and coal D, it was observed that the excess sorption capacity for the reported virgin coal samples is below 1mmole/ gram. The high adsorption in coal C and coal D can be due to the influence of the inherent coal properties which increase the microporous surface area. However, from literature it was understood that the storage potential in virgin coal is comparatively less than other commercial adsorbents (99). In addition, the adsorption magnitude is much higher in the case of literature in comparison to coal A and coal B. However, the adsorption of coal C and coal D is greater than all the literature samples. This difference in adsorption magnitude within the experimental and literature samples may be only attributed due to the properties of the coal sample. Among the reported samples, coal C has the highest adsorption capacity and coal A has the least. It was understood from Table 2 that the percentage of ash is much higher for coal C than that of coal A. However, the moisture, volatile matter and the fixed carbon are greater for coal A. It was understood from Table 3.2 that the percentage of ash is much higher for S3 Switzerland coal than coal A. However, the moisture, volatile matter and the fixed carbon are greater for coal A. Many researchers have shown that the adsorption decreases with the increase in macroscopic properties like moisture, ash, and volatile matter content (58, 60, 100). However, considering the ash and fixed carbon content, the trend from literature is in contradiction for coal A and S3 Switzerland coal (See Figure 5.1). This observation suggests that the microscopic properties like maceral content might have a stronger influence on the $CO_2$ adsorption (61). Hence, there is a need to understand the effect of vitrinite, inertinite, liptinite and the mineral matter composition on the adsorption capacity.

## 5.2 Effect of coal properties

Among the coal properties, coal rank is a broad classification of the coals in terms of the degree of coalification they might have undergone. The rank is measured through the reflectance of the vitrinite maceral. The adsorption capacities of the raw coals are plotted again the vitrinite reflectance (%) in Figure 5.2. In addition, experiment data obtained from this study are compared with the data reported in literature (31,101). Experimental data and literature data (31) was obtained at 350 psi and a temperature of 45.5$^{o}$C and 45$^{o}$C respectively, On the other hand, literature data (101) was obtained at a pressure of 300 psi and a temperature of 25$^{o}$C (101, 102). From Figure 6, it can be seen that a weak correlation is exhibited by the experimental samples which lie in the sub-bituminous to bituminous region. Coal A and coal C have almost the same reflectance but the sorption capacity of coal C is much higher. The reason behind such a large difference in adsorption magnitudes can be attributed to disparity between the properties of coal A and coal C. Further, coal D and coal B have increasingly higher reflectances than that of coal C, however, there is a steady decrease in the sorption capacity. This can be explained by the fact that the amount of vitrinite is very high in C and D followed by the amount in coal B. It is not only the reflectance, but the amount of vitrinite also plays an important factor in determining the amount of $CO_2$ adsorbed. Further, a very weak correlation is exhibited by the three coal samples considered in literature data (31). In the case of reported literature data (101), a sharp rise in adsorption level was only observed for low volatile bituminous and the semi-anthracites (i.e., $R_{max}$ 1.5% to 2.5%). However, a weak correlation is observed for the coals with the reflectance below 1.5% (54)**.** The higher rank coals with more aromatic hydrocarbons, short aliphatic chains and depleted oxygen content may be responsible for the greater sorption (55). Many researchers have observed a 'U-trend' for the relationship between adsorption and reflectance for coal ranging from lignite to semi anthracite (18, 52, 53). This phenomenon may arise due to the 'plugging' of the pores in the medium rank coals. These pores gradually open up as the coalification process continues leading to higher sorption capacities in high rank coals (56).

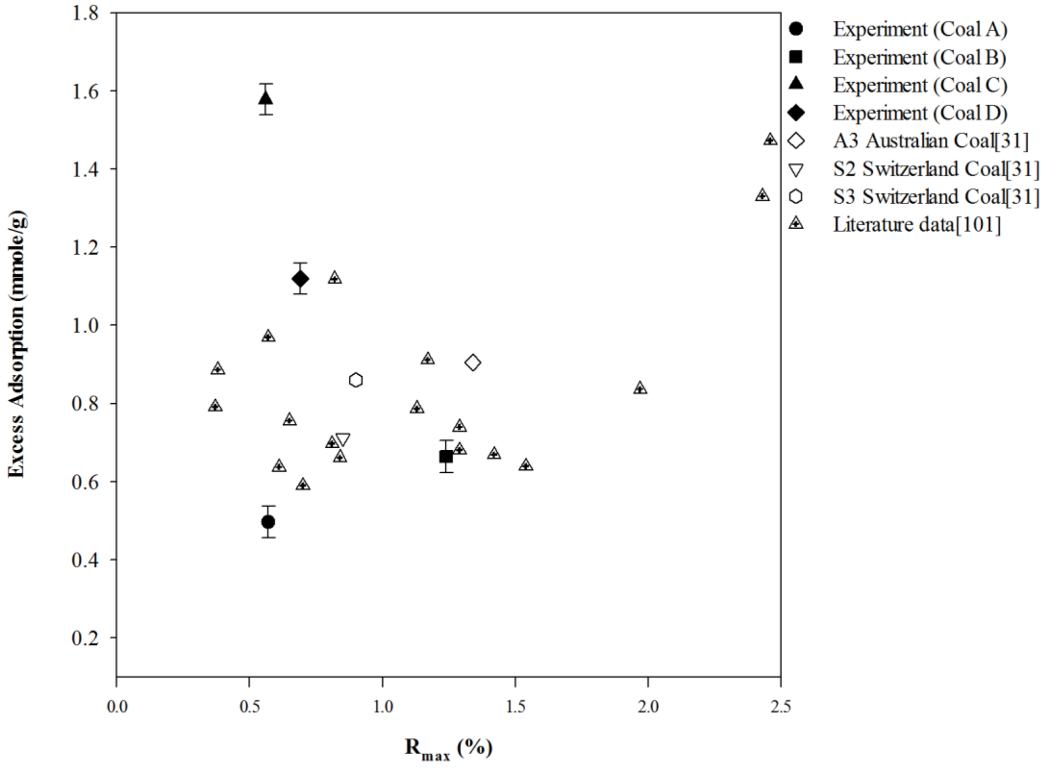

**Figure 5.2:** Excess adsorption behaviour of virgin coal as a function of coal rank

Figure 5.3a compares the adsorption capacity as a function of volatile matter on AR (as received) and AF (ash free) basis in virgin coal for both experimental and literature samples. The experimental data from this study were obtained at a pressure of 350 psi and a temperature of 45.5°C. Further, it was compared with a literature data (31,100) obtained at a pressure of 350 psi and a temperature of 45°C and 26°C.

The trends of AR and AF basis obtained from Figure 5.3a clearly show that the excess adsorption decreases with increase in volatile matter for both experimental and literature samples. In addition, it is to be noted that there is a large difference in the adsorption magnitudes between coal A and coal C. The large difference may be due to few properties of coals (i.e., minerals or macerals content) that dominate the sorption in coals. However, the general decrease in adsorption with volatile matter can be explained by the fact that the macropore volume increases with increase in volatile matter content the fact that the macropore volume increases with increase in volatile matter content (52, 57). Since, high volatile coals tend to have higher liptinite content which is mainly composed of macropores (63). As noted earlier, adsorption in coal is highly influenced by the micropore content. As noted earlier, adsorption in coal is highly influenced by the micropore content. The difference in the excess adsorption magnitudes within the experimental samples and between the experimental and literature data is attributed mainly to the coal property rather than the minor variations in the test conditions (i.e. temperature). In specific, for the literature data (31) and (100), even though there is a notable difference in the test conditions, the excess adsorption magnitudes are similar. This suggests that the influence in coal property is much more pronounced.

In addition, the very similar trends seen in Figure 5.3a between AR and AF basis indicate that the presence of ash does not seem to contribute to the adsorption capacity. However, from Figure 5.3b, it can be seen that the excess adsorption decreases slightly with increase in ash content for almost all samples in experiment and literature except for coal C. Coal C has a significantly higher sorption capacity than most coals in spite of higher ash content. This observation suggests that the maceral components may have a much more pronounced impact compared to the influence of mineral components. In general, the decreasing trend in sorption capacity vs ash content is almost identical to the studies reported in the literature (56,58). It can be speculated that the ash hinders the presence of active sites for adsorption in coal. Thus, implying that the greater the ash content lesser the number of active sites per unit volume of coal, resulting in lesser adsorption. Further, the inorganic components like ash in coal have a negative impact on adsorption (11) and $CO_2$ adsorption in coal mainly takes place on the organic phase (59).

Figure 5.4 shows the impact of vitrinite content on the excess adsorption of virgin coals obtained from experimental and literature data (59). As stated earlier, the experimental data have been obtained at a pressure of 24 bar and a temperature of 45.5$^{o}$C. From Figure 8, it can be seen that, the higher the vitrinite content, the greater the adsorption for both experimental and literature data. Within the studied samples, coal C and coal D have much greater vitrinite content than coal A and coal B leading to a larger adsorption capacity. Particularly, the greater vitrinite content in coal C is probably the cause for large adsorption magnitudes compared to the other experimental samples. Moreover, despite the similar vitrinite content in coal C and coal D, there is a notable difference between their adsorption magnitudes. The difference may be due to the influence of other major macerals components like inertinite and liptinite. However, it may be speculated that the presence of greater vitrinite overpowers the role of other coal properties in determining the adsorption capacity in virgin coals. Furthermore, it is reported in literature that vitrinites possess greater micropore volumes in comparison to other prominent maceral components like inertinites and liptinites (57).

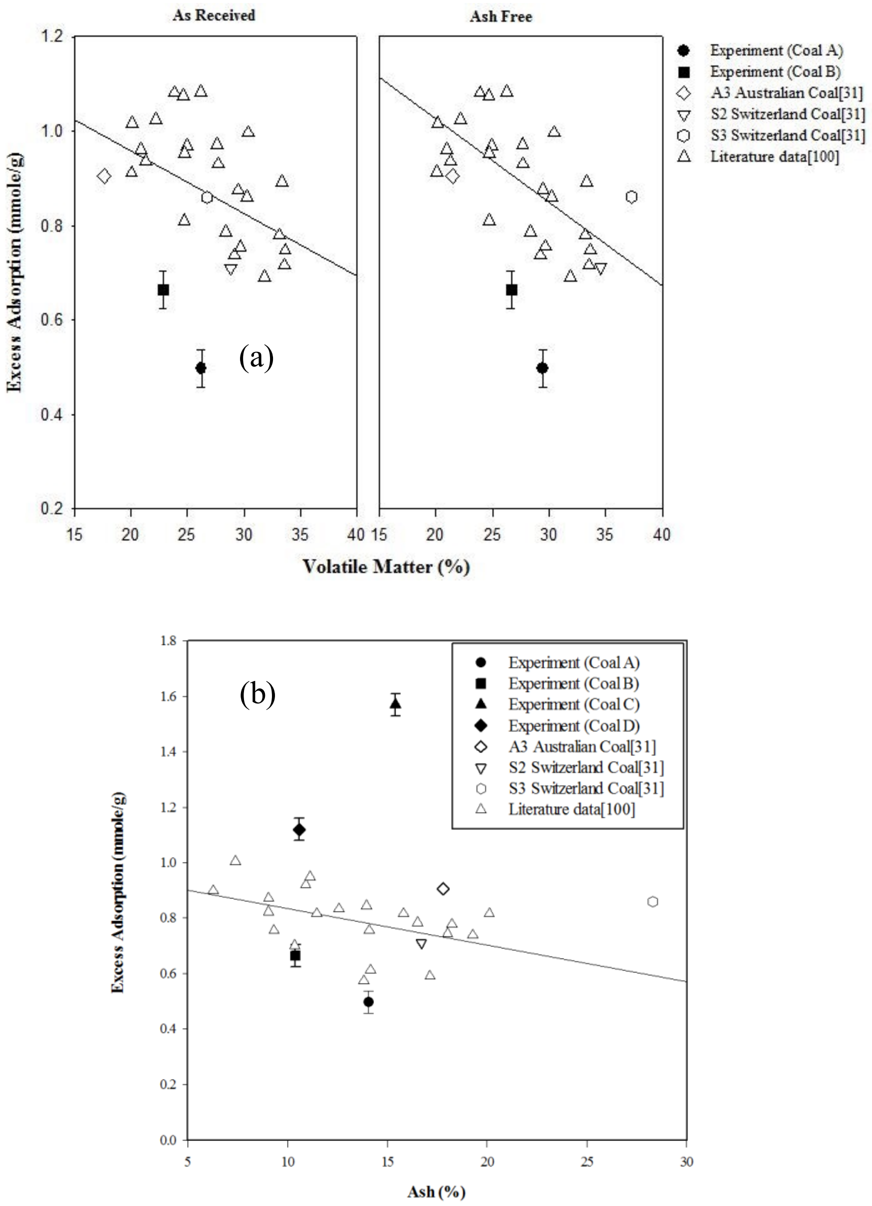

**Figure 5.3** Excess adsorption behaviour of virgin coal as a function of (a) volatile matter and (b) ash content

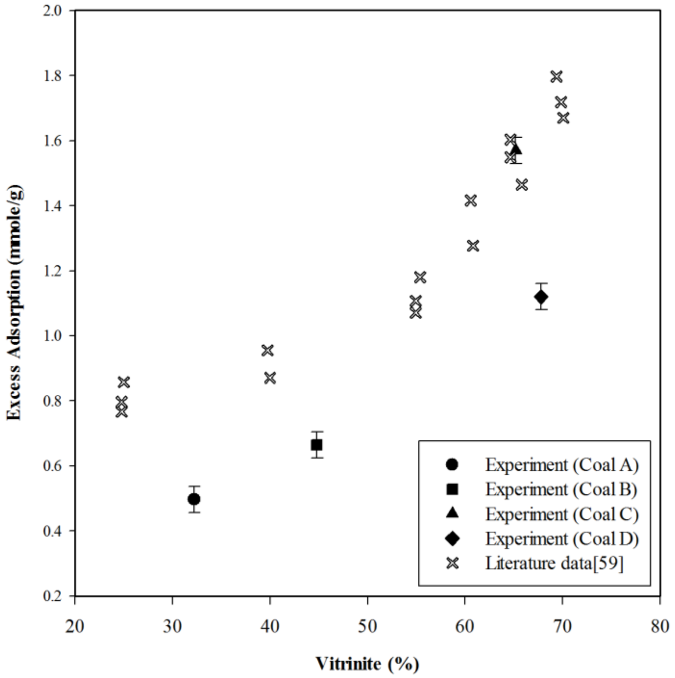

**Figure 5.4** Comparison of excess adsorption data for experiment and literature in virgin coal sample as a function of vitrinite content.

Vitrinites possess greater micropore volumes in comparison to other prominent maceral components like inertinites and liptinites (57). For instance, from DFT surface area analysis, it was understood that the amount of micropores in coal B is much higher than the coal A. This observation can be used corroborate the relationship between the higher vitrinite content and higher micropores in virgin coals. In addition, it was noted that the micropores in coal account for a greater fraction of adsorption compared to the macro and mesopores (54). Moreover, it was also observed that brighter banded coals containing vitrinite had higher microporous volumes in comparison to the dull isorank coals (44), (61). The vitrinite trend is consistent with the work reported in the literature (11, 32, 44, 55). However, few studies have reported that the influence of vitrinite content was rank dependent (56).

Adsorption studies on macerals have brought out some interesting observations. For instance, there was also a report suggesting that the telocollinite content may have a strong impact on gas adsorption magnitudes (11). Furthermore, the combination of vitrinite and inertinite contents gave a better correlation for adsorption in comparison to the individual maceral components (11), (34). In inertinite, the lower adsorption may be attributed to the nature of porosity, cross-linking density, and surface functionality(57). On the other hand, liptinite having large amount of volatile matter and primary aliphatic constituents possesses greater amount of mesopores leading to lesser surface area and lower adsorption (63), (62). These reports help in explaining the notable difference in the adsorption magnitudes between coal C and coal D. From Table 1, it can be seen that coal C and coal D have almost similar vitrinite and inertinite contents but the liptinite content varies significantly. Since liptinite has a negative impact on adsorption, the greater liptinite content in coal D leads to lesser adsorption compared to coal C.

## 5.3 Adsorption behaviour of coal char sample

The sorption capacities of coal char samples were determined at 45.5$^{o}$C till a pressure of 20 bar. Figure 5.5 shows the variation in excess adsorption capacity of Coal A and Coal B samples at different pyrolyzed temperature. As noted earlier, the samples used in this study were pyrolyzed at 800$^{o}$C and 1000$^{o}$C. The trend in Figure 5.5 shows a sharp rise in excess adsorption with an increase in CO$_2$ pressure. For the studied range of pressures, the higher the CO$_2$ pressure, the greater the adsorption. The impact of CO$_2$ pressure on excess adsorption is much more pronounced for char samples in comparison to the virgin sample for both Coal A and Coal B. This behaviour can be attributed to the pore structure changes that occur during pyrolysis, where, the volatile matter release is accompanied by structural changes like the generation of new pores

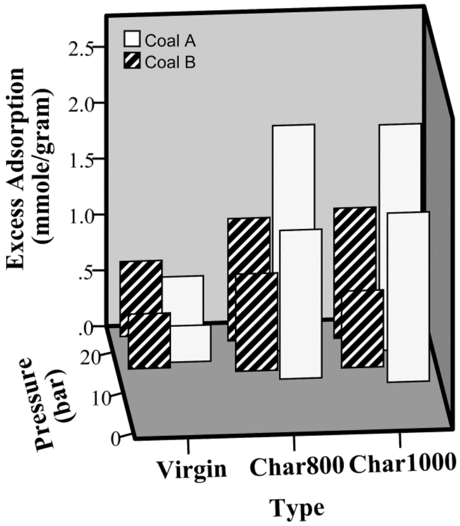

**Figure 5.5** Comparison of excess adsorption data for coal and coal char samples

and coalescence of pores to form larger pores leading to enhanced surface area (19, 66). Yet, from Figure 5.5 it can be seen that the impact of $CO_2$ pressure between char 800 and char 1000 were almost identical for both Coal A and Coal B. Since at higher temperatures, the crosslinks are broken between the aromatic rings and the resulting structural rearrangement reduces the surface area of the chars. Within the studied coal samples, the adsorption trend is much steeper for Coal A char samples than the Coal B counterparts. However, in the case of virgin sample, the adsorption capacity for Coal B is greater than Coal A. In brief, this observation can be partly assigned to the nature of the virgin coals which dictates the surface area of the produced coal char. In conclusion, it is essential to understand the influence of surface area and the coal nature on adsorption.

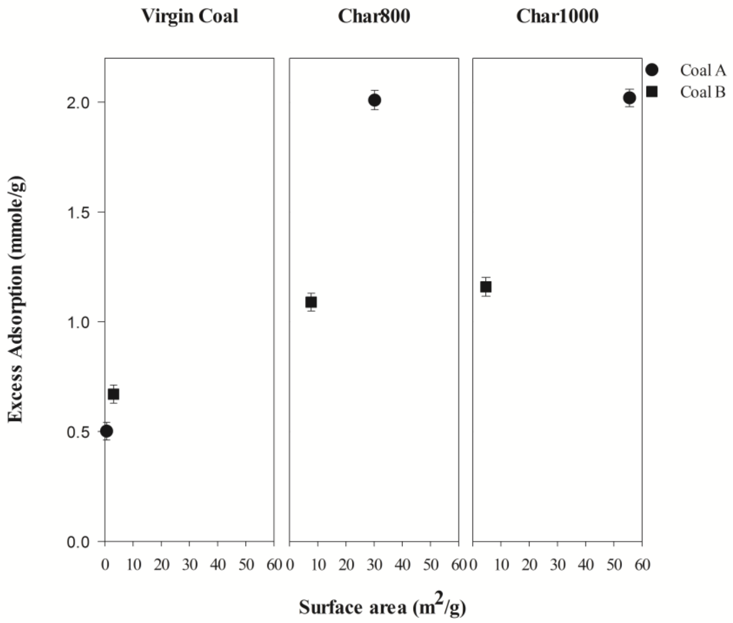

**Figure 5.6** Excess adsorption behaviour of virgin coal and coal char samples as a function of surface area.

Figure 5.6 illustrates the excess adsorption as a function of surface area for both virgin coal and coal char obtained by pyrolysis at a temperature of 800°C and 1000°C. Adsorption measurements were performed at a pressure of 300psi and an isothermal temperature of 45.5°C. The trend in Figure 5.6 shows that there is a direct linear relationship between excess adsorption and surface area. In general for coal samples, greater the surface area, the higher the excess adsorption. Figure 5.6 clearly shows that the surface area is much higher for Coal A char samples in comparison to Coal B char samples. On the other hand, in the case of virgin coal samples, Coal A has a lower surface area than Coal B. Within Coal A samples, there is a significant rise in the surface area between virgin and char 800 by 30 times. In contrast, the increase in surface area was only 1.8 times in the case of Coal B sample. However, an abnormal behaviour was observed for char 1000 samples unlike char 800, despite the rise in surface area the adsorption was insignificant for Coal A. Similarly, the effect of pyrolysis temperature on surface area was inconsequential for Coal B. The above observation confirms that the characteristics of surface area was influenced by the nature of the coal and its pyrolysis temperature, where, Coal B being a coking coal, tends to develop lesser pores compared to the lower rank non-coking coal (Coal A). Further, it was also understood from the literature that the surface area increases as pyrolysis temperature increases till a critical temperature and decreases further (69-73).

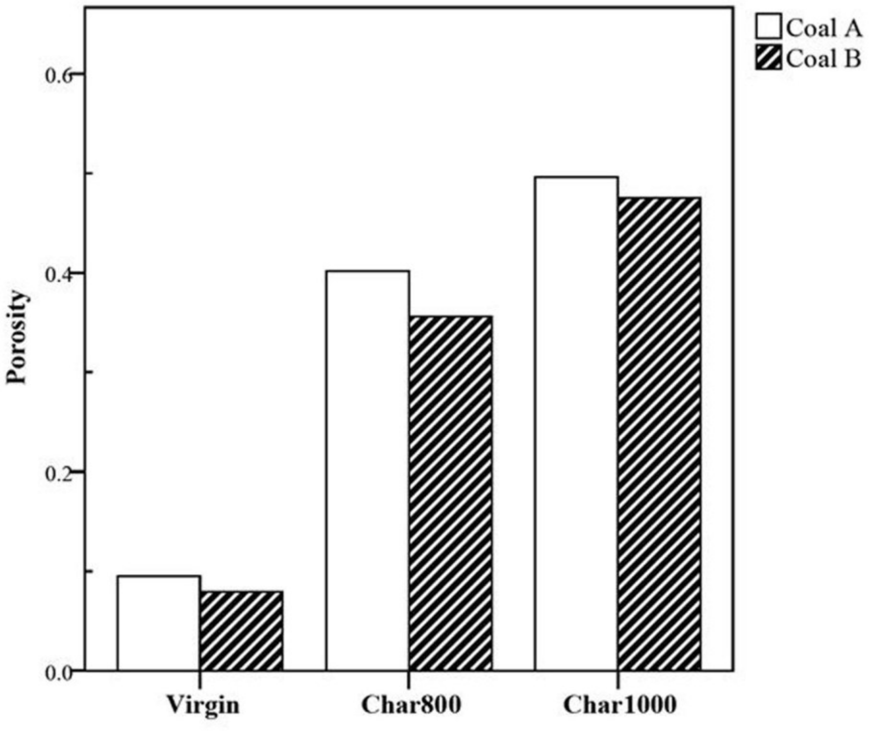

**Figure 5.7** Porosity of the char species of coal A and coal B compared with the respective virgin coal samples.

As stated earlier, this behaviour is due to the high temperature structural rearrangement of the char matrix during pyrolysis process (70). Although, the relationship between the adsorption capacity and pyrolysis temperature can be explained in terms of surface area, a detailed interpretation of pore properties like porosity and pore size distributions will help to understand the adsorption behaviour in char samples.

The enhanced porosity of the char samples obtained at 800 and 1000 °C compared to the raw coal samples are depicted in Figure 5.7. The most significant feature is that the porosity of char samples was much higher than virgin samples for both coals. It was also found that the rise in porosity is around 4 times for char 800 from the virgin sample. However, it is only 1.2 times between char800 and char 1000. As explained earlier, the increase in the porosity is due to the development of macropores and the growth of micropores which has caused due the pore expansion and new pore generation in char 800 samples. Further, the growth in porosity was effected due to the structural rearrangement at higher temperature for char 1000 samples. Within the studied samples, the porosity is much more pronounced for Coal A in comparison to Coal B.

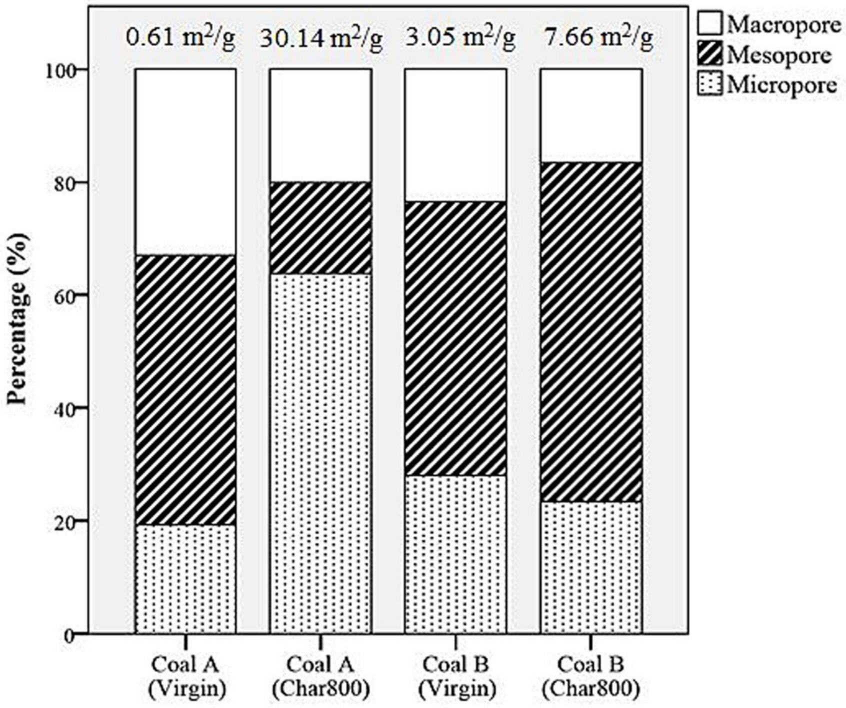

**Figure 5.8** Porosity distribution in terms of surface area for virgin coal and coal char of coal A and coal B

This can be attributed due the nature of the coal samples. Since, coal B being a coking coal, tends to expel more tar which upon condensation may block the pores. However, it can be seen that the porosity of coal A and coal B vary marginally but there is a substantial increase in the surface area. This is because, coal A tends to develop more micropores than coal B which is responsible for the increase in surface area for adsorption. Therefore, it can be concluded that the pore distribution and the nature of the coal has a substantial impact on adsorption behaviour.

Figure 5.8 quantifies the percentage of micro, meso, and macro pore distribution in virgin and char800 sample for both Coal A and Coal B. The observation confirms (see Figure 14) that there is a substantial change in the pore distribution between virgin and char 800 samples particularly for Coal A. The rise in the surface area for Coal A is more pronounced in micro pores compared to the reduction in the surface area for meso and macro pores. However, a significant rise in the surface area was only observed for mesopores between Coal B samples. Within the studied virgin samples, the micro pores in Coal B are reasonably higher than Coal A. The higher micropores in Coal B can be attributed to the greater vitrinite content compared to Coal A, since vitrinites are known to be composed of more micropores. It was found from experiment that during pyrolysis at $800^{o}$C, the distribution of meso and macro pore was partly transformed into micro pores in Coal A. As explained earlier, this behaviour can be attributed to the structural changes like the generation of new pores and coalescence of pores that occur during pyrolysis(19, 66) . Conversely, this behaviour was not observed for Coal B, since, being a coking coal, the excess tar produced may condense to form more mesopores (74, 75). Further, the decomposition of metaplast (a viscous fluid expelled during initial stages of pyrolysis) produces carbon that may plug the pores and cause reduction in the micropore surface area(70). Therefore, it can be concluded that micropores have the greatest influence on adsorption since they offer a higher surface area compared to other pore sizes. Moreover, the pore distribution plays a vital role in understanding the impact of coal nature on the adsorption behaviour.

# Chapter – 6

# $CO_2$ Adsorption Capacities of Gasified Chars

This chapter discusses the increase in $CO_2$ sorption capacities of gasified coal chars. The gasified chars represented by char800, have been obtained by $CO_2$ gasification for 10 mins at 800°C. The procedure of the char gasification is detailed in section 3.2.3. In addition, the sorption capacities have been analysed based on the pore size distributions and $CO_2$ surface area. Further, the diffusivities of the raw coals studied and the coal char have been estimated by fitting the unipore diffusion model.

## 6.1 Raw coal isotherms

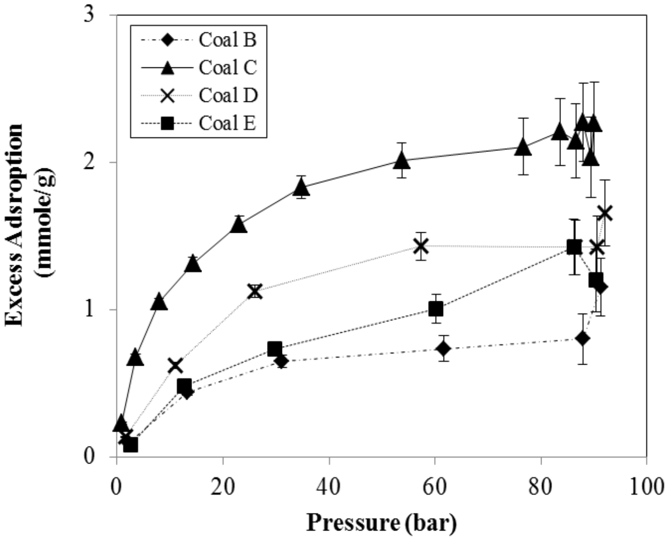

**Figure 6.1:** $CO_2$ adsorption isotherms for raw coals. Interpolation lines have been indicated between data points.

In this part of the study, four raw coals namely, coals B, C, D and E have been considered. Figure 6.1 compares the raw coal isotherms of $CO_2$ adsorption at 45.5 °C for the four different coals used for analysing the sorption capacities of their respective gasified chars. It can be seen that among all coals, coal C has the highest sorption capacity with a maximum of 2.26 mmole/g followed by coal D, coal E and coal B by 1.65, 1.42 and 1.15 mmole/g respectively. As discussed in the last chapter, the difference in the sorption magnitudes of different coals because of the inherent properties of coal. It was noted in this study as well as other reports in the literature that the sorption in coal is a strong function of the maceral components particularly vitrinite and the mineral matter acts as an inert toward gas sorption (84). Moreover, it was also observed that sorption for all the coals increases steadily till a pressure of 70 bar after which the curve tended to flatten out before reaching an abnormal peak around 90 bar. The reason for the sudden rise in adsorption capacity is either a characteristic of supercritical fluid adsorption.

## 6.2 Gasified coal chars

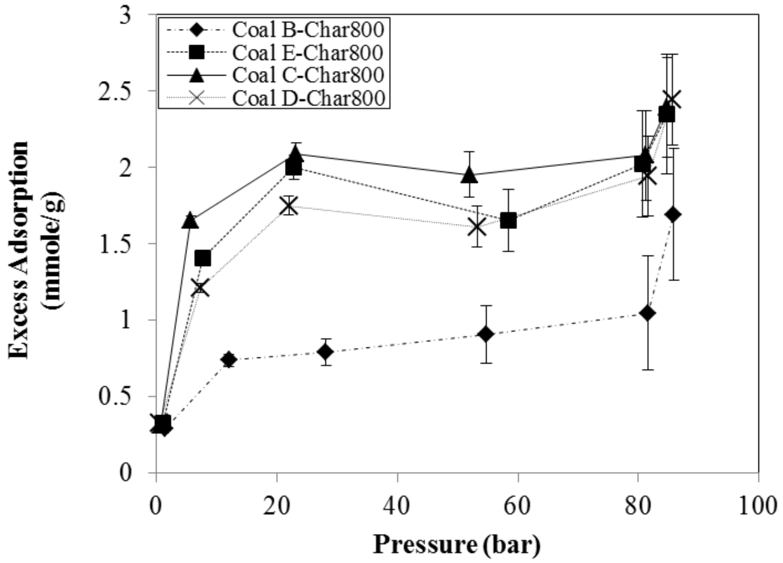

**Figure 6.2:** Comparison of the sorption capacities of raw coal and gasified coal char at 800$^{o}$C. Interpolation lines have been indicated between data points.

In the case of gasified chars the isotherms have been obtained at 45.5$^{o}$C and it is observed that among the chars, coal C char800 has the highest sorption capacity followed by the chars of coals E, D and B respectively(see Figure 6.2). In addition, in comparison to the sorption capacities of the raw coals, shown in Figure 6.1, the sorption capacities are significantly higher compared for coals B D and E. However, in the case of coal C, the sorption capacity is almost same till a pressure of 70 bar. The sorption capacity of char C 800, reached a peak of 2.5 mmole/g at 80 bar. The sharp increase in the sorption capacity is observed for all the chars at 80 bar. The increase in the sorption of gasified char is because of the increase in the surface area of the char800 species. The char800 species have undergone thermal treatment at 800$^{o}$C at a slow heating rate in an inert atmosphere followed by $CO_2$ gasification for 10 mins. As mentioned earlier, during formation of chars volatile matter is released resulting in the development of the pores. This development of the pores occurs by opening originally closed pores, creating new pores and increasing pore size of existing and newly formed pores (22). In addition, the $CO_2$ gasification would consume a part of the char to open up of the closed pores thus increasing the surface area and the porosity char. This phenomenon is not just common to coke but all organic fuels. Several studies in the literature have reported in the increase in surface area during gasification. For instance, (79) reported the increase in the surface area of $CO_2$ gasified chars as a function of conversion and gasification temperature. Later in 1998, (80) compared the increase in micropore volumes after $CO_2$ and $O_2$ gasification on South African coals. Recently, (103) reported the increase in the surface area of gasified petcoke chars at different conversion levels. It is understood from these reports and the study reported in the last chapter that the surface area and the porosity of char are bound to be greater than the raw coal. However, it would be interesting to look at the magnitude of increase in the sorption capacity as a function of coal properties. Moreover, the marginal or insignificant increase in the sorption capacity of coal C char suggests that the conversion in the char species may also play an important role.

## 6.3 Carbon Conversion in gasified chars

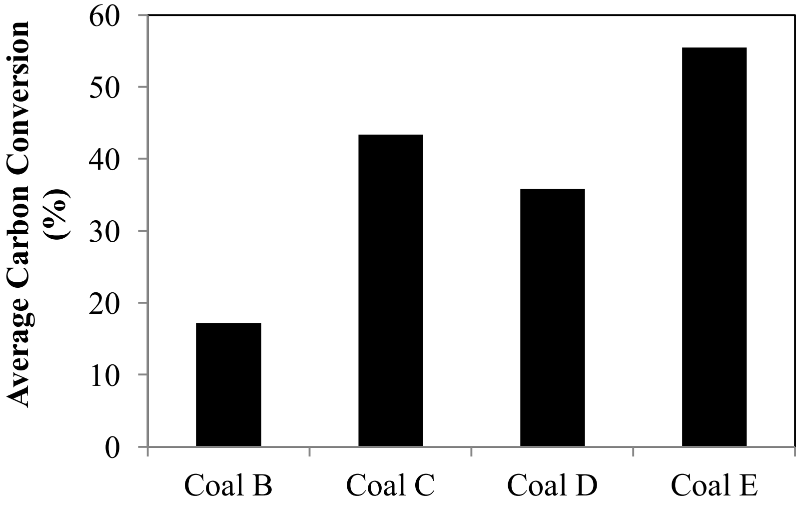

**Figure 6.3:** Carbon conversion for the chars of the four coals at 800°C

The carbon conversion for the chars has been calculated by the equation 3.24 and is represented in Figure 6.3. It can be seen that conversion level for the four coals is markedly different under the test conditions. Coal E char has the highest conversion at 54% followed by the chars of coal

C and D at 45 and 37% respectively. Coal B char has the least conversion after 10 minutes of exposure to $CO_2$. It is to be noted that Coal E is a lignite coal, coals C and D are medium and high volatile sub-bituminous coals and coal B is a bituminous coal. Thus, in terms of coal rank, the coals studied can be arranged in the following order: Coal E< Coal C< Coal D< Coal B. From the results presented in figure 6.3, it could be inferred that for the studied coals, as the rank increases, the reactivity decreases. Particularly, in the case of coal B which is a coking coal, the condensed volatiles on the surface would block most pores and thus decreasing the reactivity of the char. In addition, the reactivity of the char during gasification is a function of nature of pores, inherent minerals and the crystalline structure of the char (104). Lignites were found to have the higher reactivities compared to other coals during gasification by many researchers (104 -108). The results reported in (106) suggest that apart from the pore structure, the alkaline minerals such as Potassium compounds present in lignites have a profound impact the reactivity during steam gasification. Moreover, in another study by Takarada et. al (108), where 34 coals of different ranks were tested for gasification reactivity, the Calcium and Sodium content was found to correlate well with the reactivity. However, mineral matter is general is found to have a detrimental impact on the reactivity, as the higher concentration minerals would impede the active sites in the coal matrix. The mineral matter effect was significant for the lower ranked coals, however, had no effect the reactivity in anthracites (106). Furthermore, a few reports in literature such as (105) and (108) correlate the reactivity of chars as a function of the carbon content in the parent coal, and found that as the carbon content increases, the reactivity drops. Moreover, there is further experimental evidence presented in (106) showing earlier transition of lignites from the pore diffusional kinetic phase to the chemically controlled kinetic phase. During gasification, at initial stages the gases would diffuse into the pore structure and then react, subsequently, as the reaction proceeds, the pore structure would disintegrate, resulting in the reaction being limited by the chemical interaction alone. Thus, if a coal transitions faster, it would indicate higher reactivity. Similarly, a study evaluating the gasification reactivity through chemisorption parameters by (104)shows that the in the lower rank coals, such as lignites, the gases after adsorbing on the surface would react before desorbing from the surface. However, in the case of higher rank coals, the gases would desorb before reacting on the surface, thus resulting in lower reactivity. Sakawa et. al (109) found that the increasing inertinite content increases the reactivity among coals with almost same reflectance.

## 6.4 Surface Area

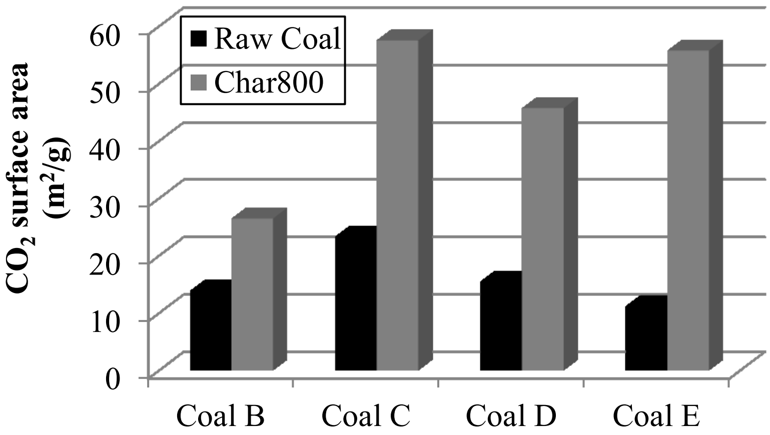

**Figure 6.4:** Comparison of the surface area of raw coal and gasified coal for the four coals tested.

It was noted in the last paragraph that the conversion of the char would affect the surface area and in turn the surface of the raw coal would influence the rate of conversion of chars. Figure 6.4 compares the $CO_2$ surface areas for the raw coal and the coal char gasified in $CO_2$ atmosphere at 800°C. The surface areas reported have been calculated from the DFT methods. It can be seen that for all the coal samples, the surface area of the gasified coal is significantly higher than the raw coals. Among the raw coals, coal C has the highest surface area at 23 $m^2/g$ followed by coals D, E and B with surface areas of 15, 13 and 11 $m^2/g$. On the other hand, among the char800 species, coal C char has the higher surface area with 57 $m^2/g$ followed by coal E and D char at 55 and 45 $m^2/g$. Coal B char 800 has the least surface area among the chars with 26 $m^2/g$. It should be noted that there is a change in the trend with regard to coal E. It was noted in the raw coals that coal E has the least surface area but in the case of char800 coal E has the highest surface area. Moreover, it is obvious from figure 6.4 that the percentage increase in the surface area is higher for coal E followed by coals D, C and B. This trend in the development of surface area in the coal chars is similar to that noted in the previous chapter with pyrolysed coal char. The increase in the surface area of the char800 species is because of the enlarged pores that result as consequence of extensive decomposition of the crosslinks in the coal matrix. At higher temperatures, typically around 600-800°C, structural realignment of the aromatics takes place resulting in an orderly arrangement of layers and loss in the surface area (68). In the case of coal B, the coking coal even in the case of gasification, the metaplast that is formed would plug the micropores that were previously formed during volatile release, thus, resulting in the loss of surface area (75). This hypothesis is consistent with the observation in this study as the percentage increase in the surface area of the char compared to the raw coal is the least in the case of coal B. However, it is to be noted that the conversion level in coal B is only 20% (See Figure 6.3), which is relatively less to have any significant difference from the pyrolysis conditions. There could be a much greater increase in the surface area and a better understanding when surface analysis would be carried out at higher burn-outs.

## 6.5 Pore size distributions

The pore size distribution of coal/chars has been obtained through the application of DFT methods on the low pressure isotherms of $CO_2$ adsorption (See figure 6.5). In all the raw coals, the surface area contributions by pores with less than 6 Å pore width do not contribute to the surface. In the range of 6 -8 Å, there is a sharp rise in the dS/dr curve to reach a maximum in the range of 10-12 Å. Where, *S* and *r* are the surface area and the half pore width respectively. There after the surface area contribution decreases steadily before a slight distortion in the range of 12-15 Å. The slight distortion brings a bimodal nature to the microporous region of the pore size distribution. The mesopore region, 20 -500 Å, the surface area contribution decreases as the half pore width increases. In general, the surface area contribution is negligible for pores with size greater than 50 Å. Moreover, for all the raw coals, most of the surface area has been contributed by the pores that are present in the range of 5- 20 Å, i.e., the micropores. The contribution of pores in the size range of 20 -500 Å, the mesopores to the total surface is limited to 20%. The macropores on the other hand, did not contribute much to the total surface area in raw coals. In the case of raw coals, coal C has the highest micropore surface area followed by coals D, B and E. However, the mesopore contribution to the total surface area is highest in coal C, followed by coal B, D and E. The distribution of the micro-, meso-, and macropores in coals may be a function of the maceral components. It can be seen from Table that the vitrinite content in the raw coals is in the order coal C> coal D> coal B> coal E. Thus, implying that greater vitrinite content results in greater fraction of micropores. This observation corroborates other reports in literature on the influence of vitrnite content on microporosity (59). As in the case of raw coals, in gasified char800 samples, there is generally a single sharp peak in the micropore region around half pore width of 10-12 Å. In addition, the start point of the peak is in chars is also around 6 Å. However, the distortion that was observed in the case of raw coals around 12-15 Å becomes more prominent in char800 (prominent in coal D char800). In the case of char800 species, the coal D has the highest micropore surface area followed by coals C, E and B. In the case of mesopores, the surface area contribution is highest in the case of coal C char 800 followed by coal D, E and B. Interestingly, the mesopore contribution to the total surface area has not increased from the raw coal. In other words, the higher surface area in coal B char 800 compared to raw coal is only due to the micropores. Moreover, it is surprising to note the

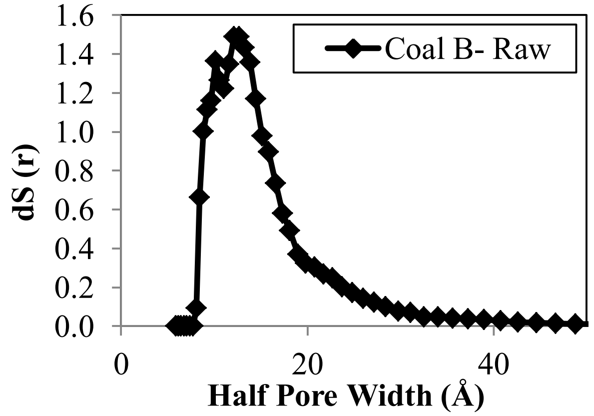

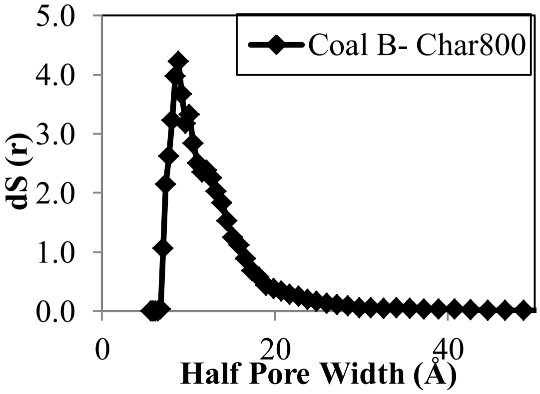

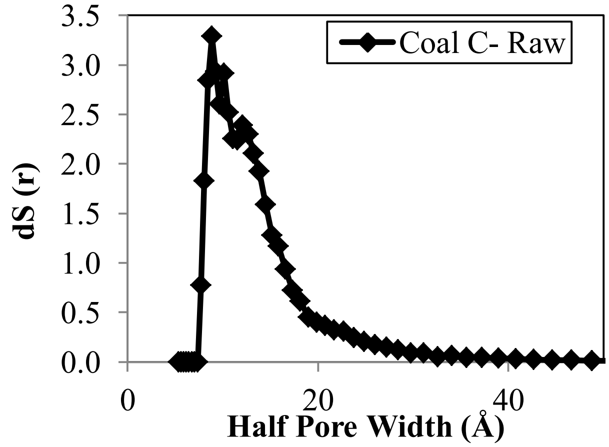

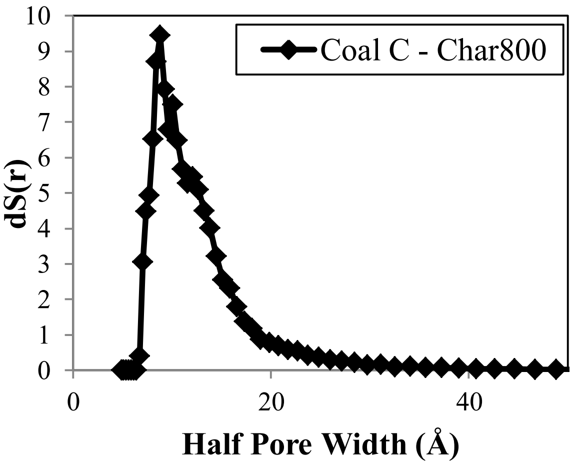

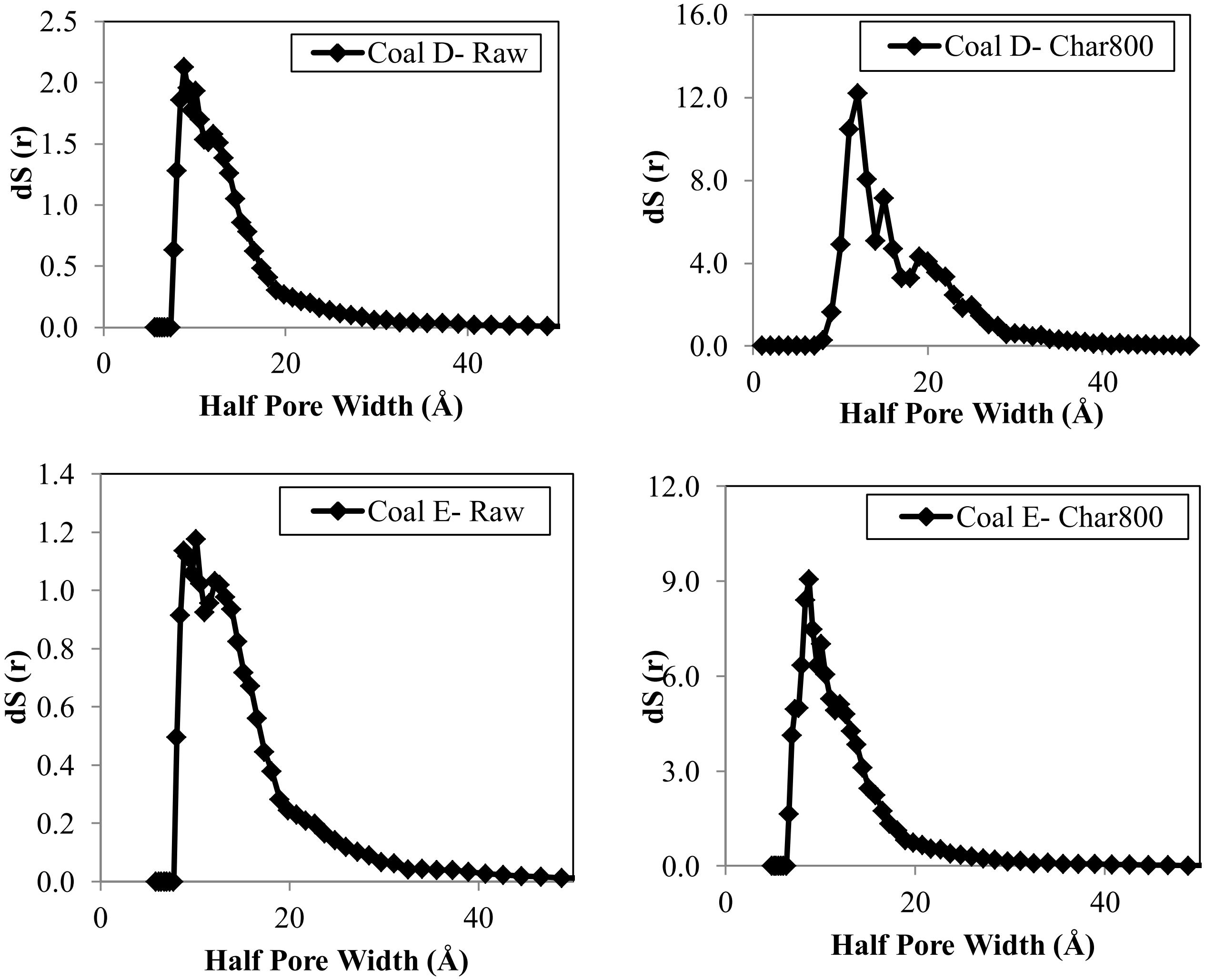

**Figure 6.5:** Comparison of the pore size distribution of the raw coals (figures to the left) and gasified coal chars (figures to the right).

greater mesopore surface area in coal D. It is a lower rank sub-bituminous coal. From figure 6, it can be seen that the coal D char 800 has lesser surface area than coal E char 800 inspite of having greater micropore contribution. This might be due to the greater fraction of mesopores formed, thus effectively decreasing the surface area when the char would only be composed of micropores.

## 6.6 Surface Morphology

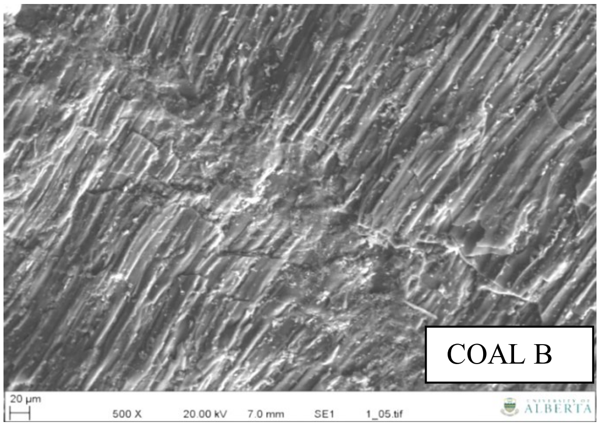

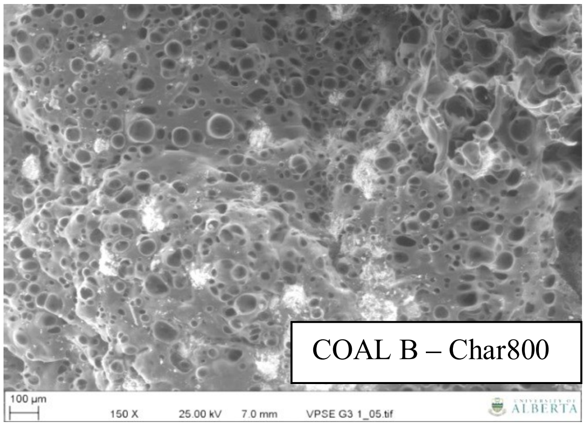

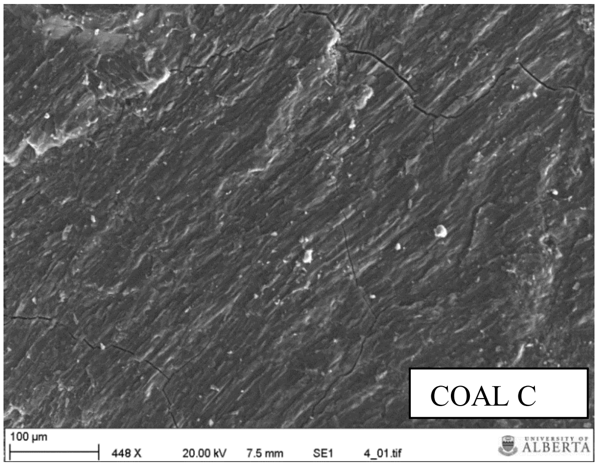

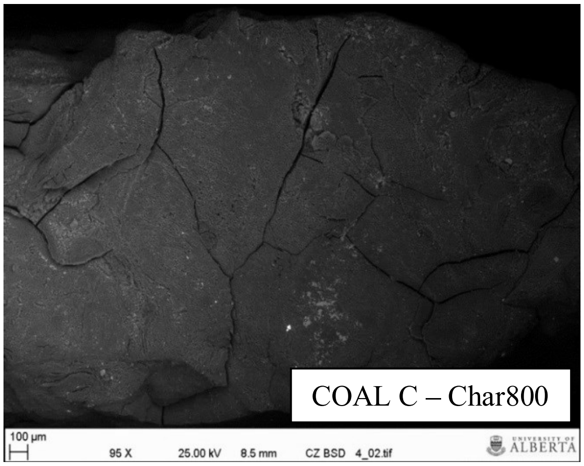

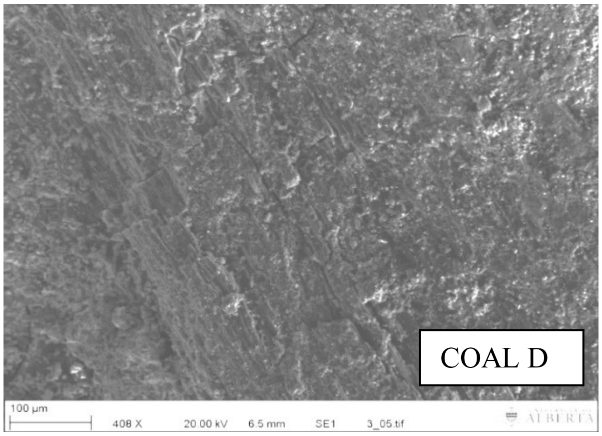

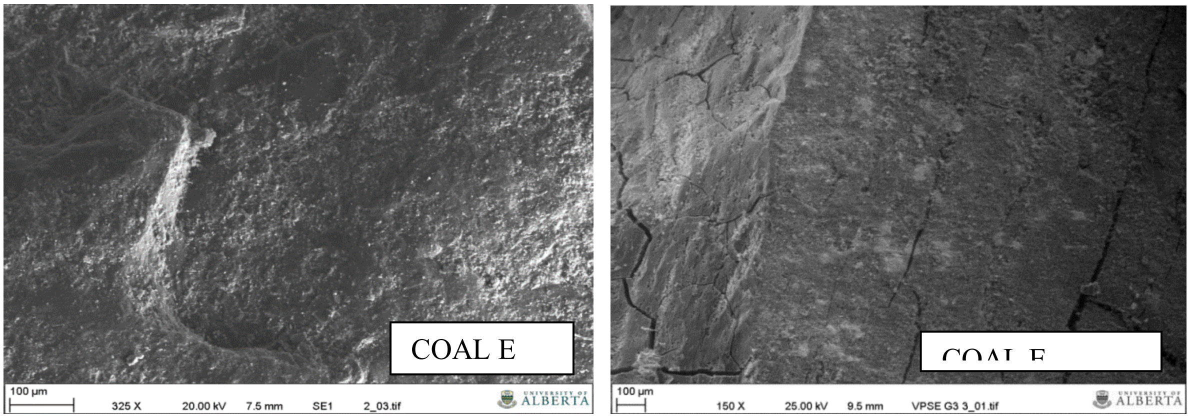

**Figure 6.6:** Scanning Electron Micrographs of the raw coal and gasified coal chars at 800$^{o}$C.Images to the left are the raw coals; the ones to the right are the gasified chars.

In figure 6.6, the scanning electron micrographs for all the eight samples used in this study have been compiled. The first row of images compares raw coal B and its gasified char. It can be seen form the images that the raw coal B looks dense, with a lot of striations parallel to each other with no observable fractures on the surface. The char800 of coal B looks drastically different with a lot of 'bubbles' appearing on the surface. The image was taken at 150X zoom, indicating that the bubbles were fairly large in size; they were also visible when viewed with the naked eye. The bubbles are characteristic of a coking coal with the tar condensing on the surface. On the other hand, the raw coal C also is characterised by parallel striations, however, the density of these striations is much lesser. There are also a few fractures visible at 448X in the scanned raw coal particle. The coal C gasified char particle, looked different from its coal B counterpart. No bubbles were observed on the surface, and at 95X zoom, several large fractures appeared on the surface of the particle. The particle however did not disintegrate. For Coal D raw coal, there were no striations that were observed on the surface, however, the surface of the particle appeared to be rough compared to coal C and D. In the case of Coal E, a lot of fractures appeared on the surface of the coal particle. There were also parallel striations that are faintly visible. In the case of coal E char 800, large fractures were visible on the surface of the particle at 150X. Considering the different nature of the char particles, it would be possible that the gasified chars would have better diffusivities in the case of raw coals. Moreover, it would also be pertinent to look at the diffusivity variation within the char species.

## 6.7 Diffusivity of raw coals and coal chars

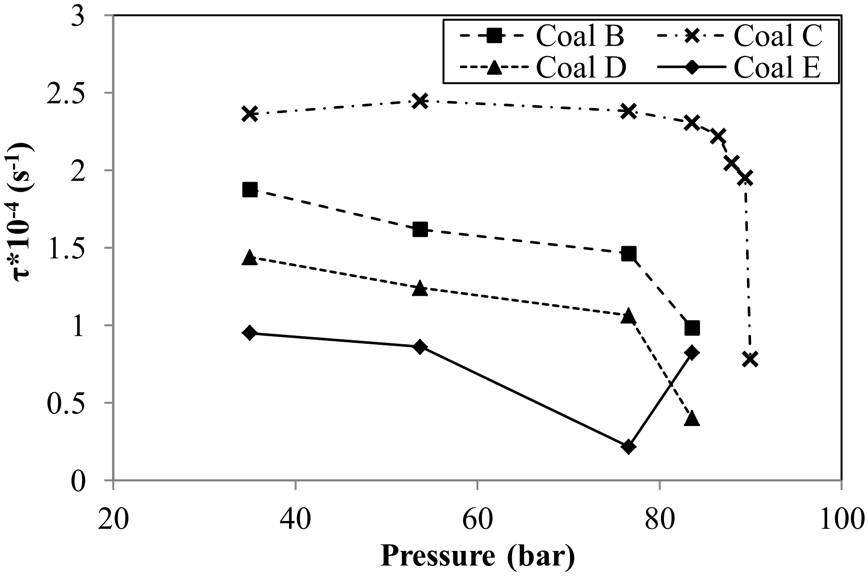

**Figure 6.7** Comparison of effective diffusivities of the four raw coals.

Figure 6.7 compares the effective diffusivities of the raw coals used in this study. The effective diffusivities have been estimated by fitting the unipore diffusion model (90) to the $CO_2$ adsorption rate curve (t < 500s). The procedure has been detailed in section 3.2.1. It has been observed that the unipore diffusion model as shown in equation 3.9 is only applicable to $\frac{V_t}{V_\infty}$ <0.5 and the model is only used for getting a rough estimate of the effective diffusivities. Better estimates of the diffusivity can be obtained by making use of numerical models such as the bi-disperse model (110) and Isotherm and Adsorption rate model (44). However, the unipore model was used in this study to only obtain rough estimates of diffusivity of all the coal types and make qualitative assessments on the influence of coal properties on sorption kinetics. From Figure 5.8, it can be seen that in general the diffusivity decreases with pressure for all the coals. The trend and magnitude is similar to that observed in earlier reports for $CO_2$ diffusivity in dry coal (44, 111) . The decrease in the diffusivity with increase in pressure can be attributed to the transition from lower pressure to bulk diffusion at higher pressures (111, 112). Further, among the coals tested, coal C was observed to have the highest diffusivity with 2.5 $*10^{-4}$ $s^{-1}$ at 50 bar, followed by coals B, D and E with 1.6 $*10^{-4}s^{-1}$, 1.4 $*10^{-4}$ $s^{-1}$ and 0.9 $*10^{-4}$ $s^{-1}$ respectively. The variation in the diffusion with coal type would be a function of physical and chemical composition of the coal. In particular, the maceral components have been found to greatly influence the nature of pores in the coal (84, 113). Greater the vitrinite content the greater is the fraction of micropores in the coal (59). The inertinite and the liptinite are composed for both micro/meso and macropores. The trend observed in the diffusivity of $CO_2$ in raw coal correlates well with the mesoporosity content solids. However, there was no visible trend with respect to the distribution of prominent macerals such as vitrinite, inertinite and liptinite. It can only be speculated that since the liptinite content, responsible for the greater fraction of macropores in the coal, is not significantly different in the coal, the effect on diffusivity is not discernible. Smith and Williams (114) suggest an increasing pore size, hence better diffusivity with decreasing in rank. However, the results in this study and in (54) suggest no clear relationship between rank and the diffusivity in coal. In addition, it is also to be noted that there is an abrupt decrease in the diffusivity around 80 bar for all the coals. This might be due to the bulk diffusion being hindered by the capillary condensation of the supercritical fluid occurring in the narrow pores. However, it could also be possible that the diffusive coefficients estimated by the unipore model may not be accurate, and the trends observed may deviate considerably. Analysis using numerical models has to be carried out in order to establish better relationships between the coal property and the diffusivity.

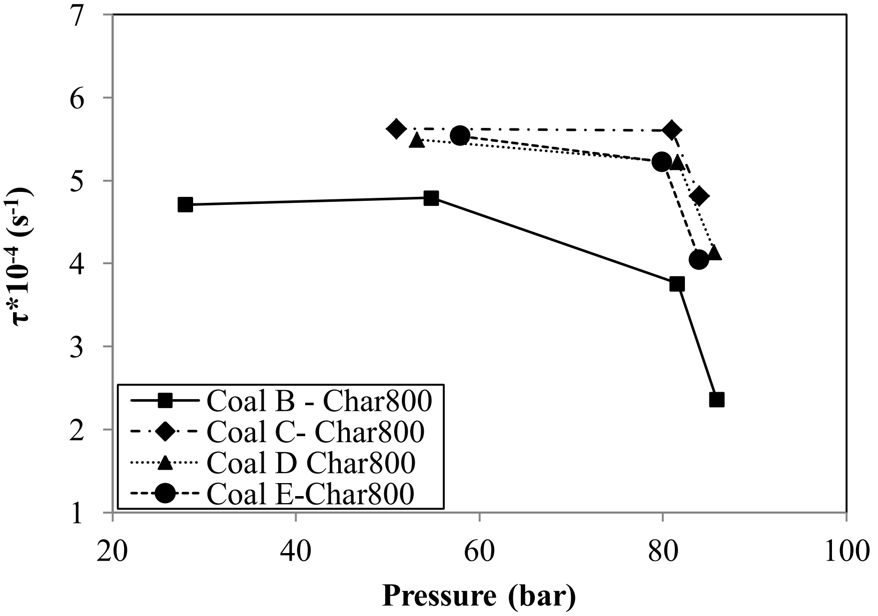

**Figure 6.8** Comparison of effective diffusivities of the gasified coal chars.

Figure 6.8 shows the effective diffusivities of the gasified coal chars. Effective diffusivity in the chars, as in the case of raw coals, has also been obtained by the fitting the sorption versus time data with the unipore model. The diffusivities in the case of gasified chars decrease with pressure. At pressures above 80 bar, the diffusivity goes through the sudden decrease. Such trends have not been observed previously in literature. The reason could be same as in the case of raw coals. In addition, within the coal chars, coal C has the highest diffusivity followed by coal E, D and B char800. This trend is the opposite when the raw coals are considered. Moreover, it can be seen that the effective diffusivities of the coal chars are higher (more than 3 times) in magnitude than the respective raw coals. Obviously, the reason for the increase in the effective diffusivity would be the enhanced microporous surface area, increase in pore volume due to the evolution in volatile matter. Further, in the case of coal B, which is a coking coal, the excessive tar that is deposited on the surface would result in plugging of several pores, leading to lesser diffusion rates. Moreover, from Figure 5.6, it can be seen that coal the order of diffusivities in the char species is the same as their mesoporous surface areas.

## 6.8 Adsorption models

Figure 6.9 shows the comparison of the experimental isotherms with the isotherms estimated by the Langmuir, DR, and DA models. It can be seen that all the three models closely match the experimental isotherms. However, among the three plots the isotherm generated by the DA model parameters is the closest to the experimental data. In addition, it is to be noted that the models in the supercritical region of $CO_2$ do not match the abrupt peak in the isotherm which is observed in all the cases except coal C raw. As noted earlier, the Dubinin models are based on the mechanism that adsorption in very fine pores takes place through pore filling as opposed to the Langmuir theory where the sorption is considered to occur in layers. Among the Dubinin models, the DR equation assumes that the pore size distribution in the adsorbent follows a Gaussian distribution whereas in the DA equation pore size distribution is assumed to follow a Weibull distribution.

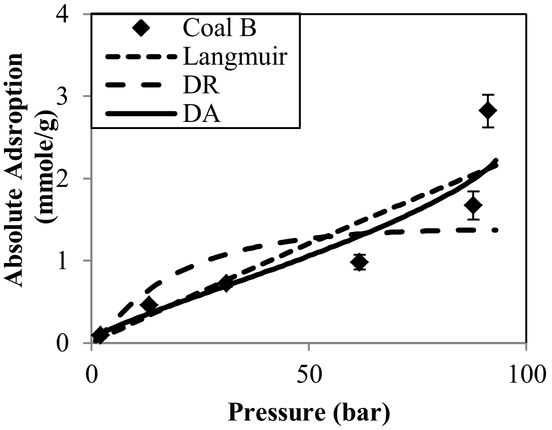
Coal B
Langmuir
DR
DA
Absolute Adsroption (mmole/g)
Pressure (bar)
0
1
2
3
4
0
50
100

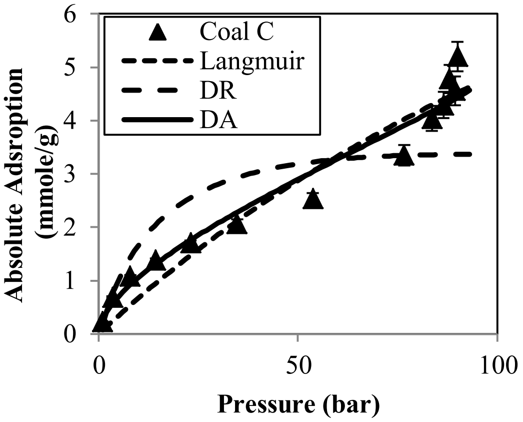
Coal C
Langmuir
DR
DA
Absolute Adsroption (mmole/g)
Pressure (bar)
0
1
2
3
4
5
6
0
50
100

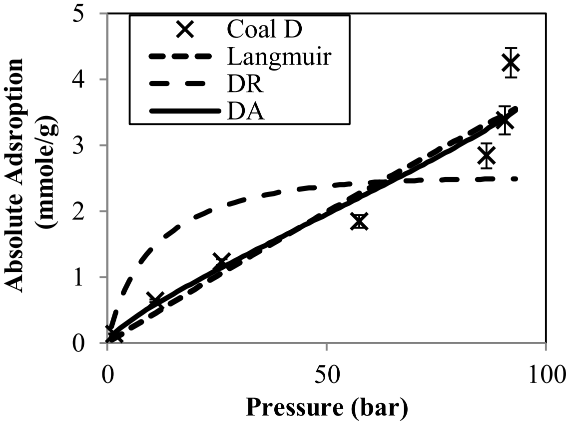
Coal D
Langmuir
DR
DA
Absolute Adsroption (mmole/g)
Pressure (bar)
0
1
2
3
4
5
0
50
100

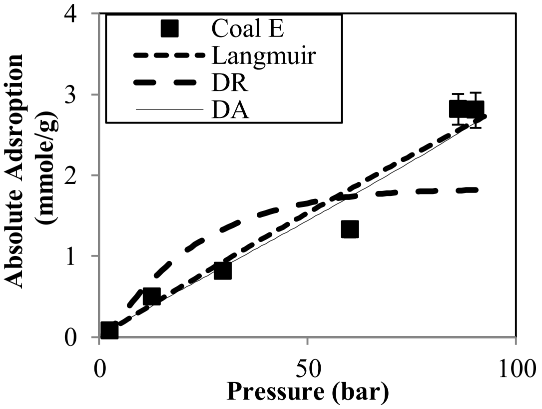
Coal E
Langmuir
DR
DA
Absolute Adsroption (mmole/g)
Pressure (bar)
0
1
2
3
4
0
50
100

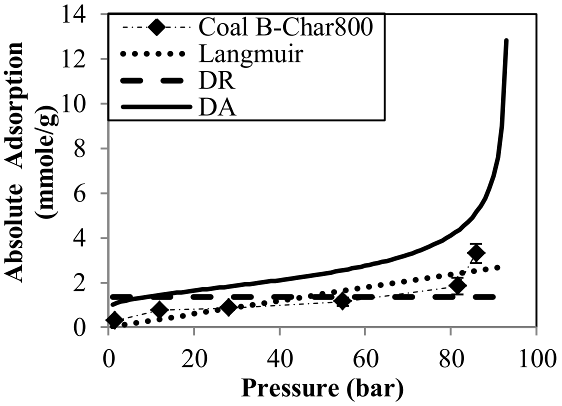
Coal B-Char800
Langmuir
DR
DA
Absolute Adsorption (mmole/g)
Pressure (bar)
0
2
4
6
8
10
12
14
0
20
40
60
80
100

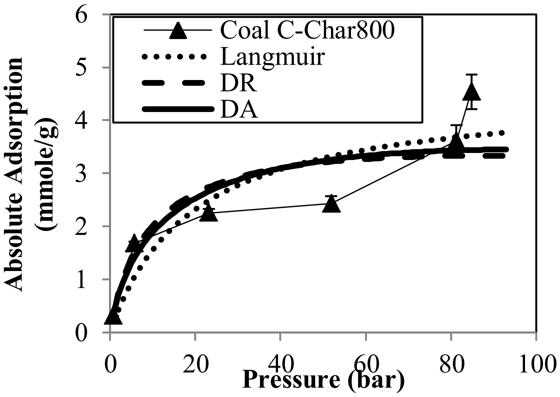
Coal C-Char800
Langmuir
DR
DA
Absolute Adsorption (mmole/g)
Pressure (bar)
0
1
2
3
4
5
6
0
20
40
60
80
100

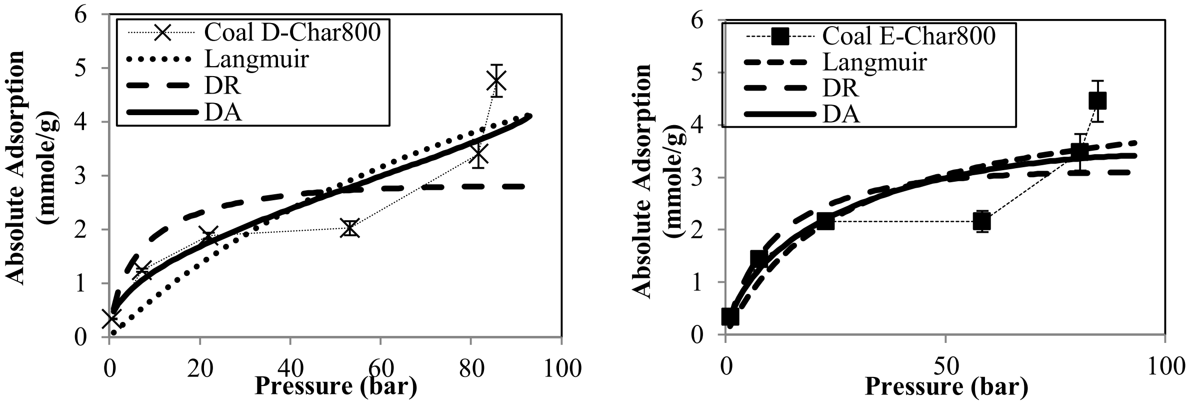

**Figure 6.9:** Comparison of the experimentally measured sorption isotherm with the isotherms estimated from model parameters

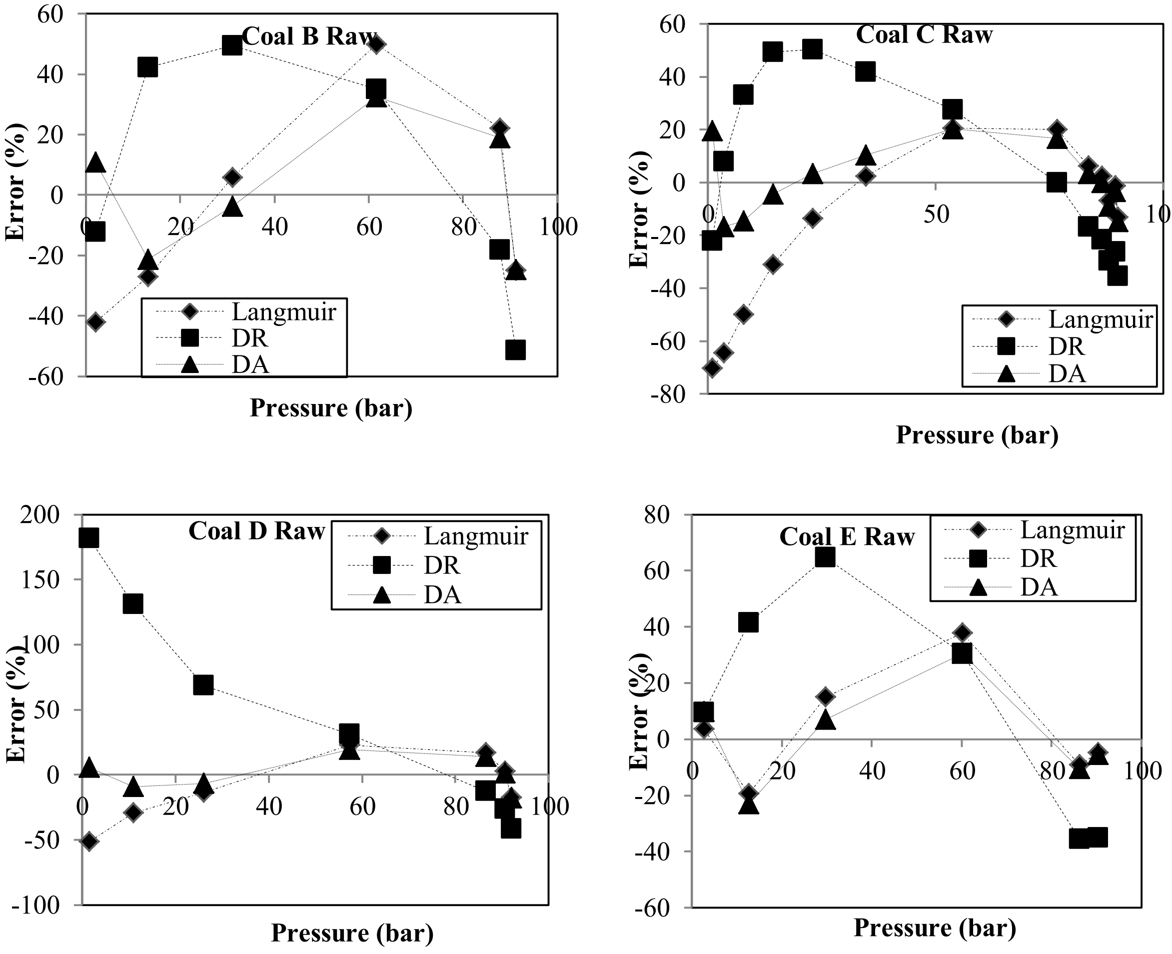

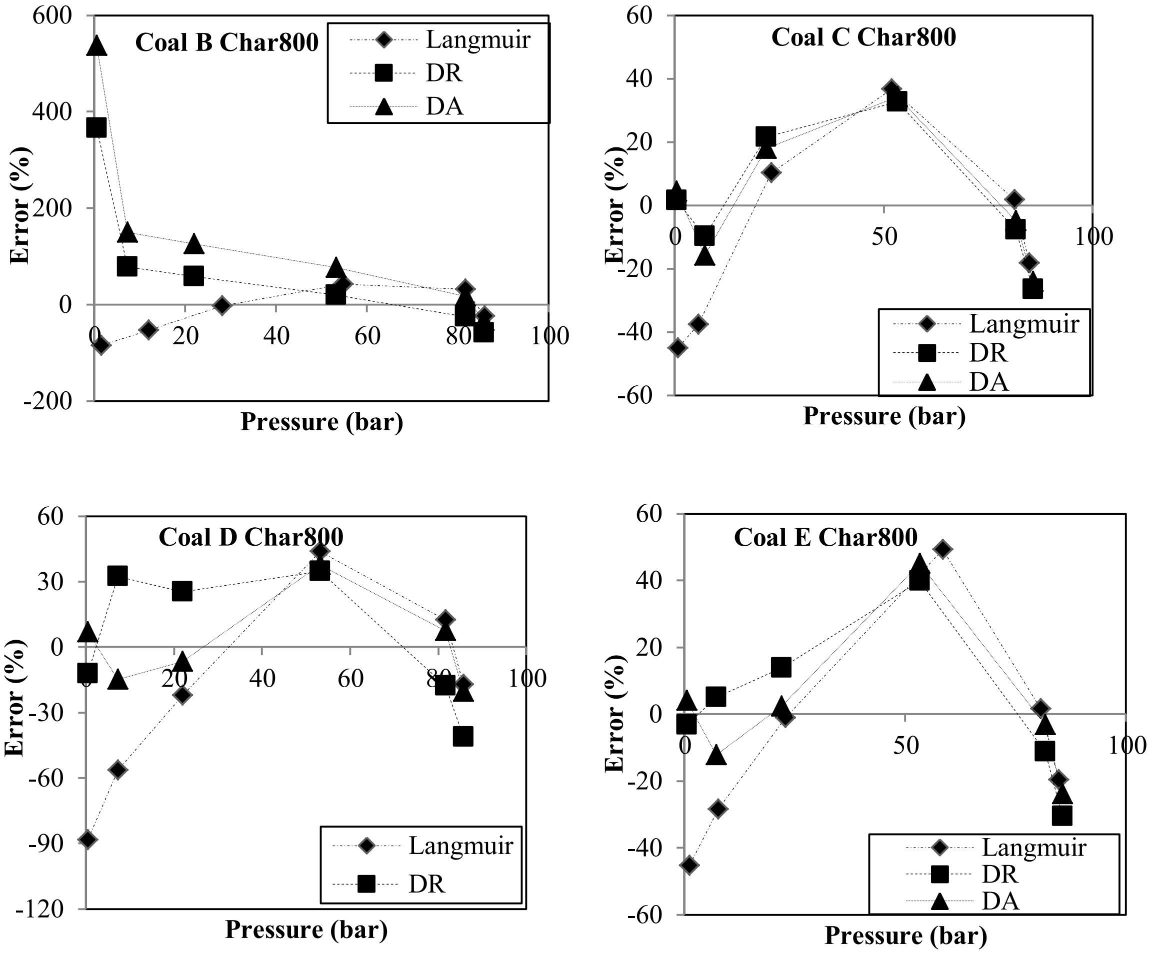

**Figure 6.10** Comparison of the experimentally measured sorption isotherm with the isotherms estimated from model parameters

Moreover, the DA equation is the general form and the DR equation is a special case when the factor n = 2. Thus regression model for DA equation would require the optimization of three parameters compared to the two parameters in the case of Langmuir and DR. The accuracy of the models can also be assessed through the plots presented in Figure 5.11. In figure 5.11, the percentage deviation of the predicted sorption from the model to the actual experimental data is plotted against pressure for all the samples. It is observed that in most cases the error is of similar magnitudes for all the three models. In general, the maximum deviation for all the models is around 30% except for Langmuir in coal D, coal B char800 and coal D char800 where the error reached more than 50% at 2 bar pressure. Moreover, it is also observed from the coal C plot that the error initial pressures are not predicted well by the DA equation. Furthermore, in coal E the

Langmuir estimate of sorption is off by 30% for the sorption magnitude at 2 bar. In general, it is observed that the predictions in the initial and final points give the highest errors. The DA equation was found fit experimental data best for both methane and CO2 sorption in many cases (41-43). The efficacy of the model in most of these reports was tested by plotting characteristic curves of the model parameters for isotherms at different temperatures (41). However, in this study, the percentage deviation was used due to the absence of isotherms at different temperatures.

# Chapter – 7

# Conclusions and Future Work

The thesis has dealt with the estimation of sorption capacities of gasified char and further correlating them to the raw coal properties for the purpose of understanding the storage capabilities of a post-UCG site. The determination of the sorption isotherms was carried through a volumetric adsorption apparatus at 45.5°C. The temperature was chosen to represent the temperature of the gasified bed that been abandoned and cooled subsequently. In addition, during the study, techniques and protocols were developed for obtaining reliable measurements on a volumetric apparatus. These protocols led to the design of better apparatus on which the sorption measurements on coal char were carried out. The char samples were obtained from large coal samples (2.2-4.75 mm) being gasified/pyrolysed at higher than 800°C particularly at low heating rates in order to replicate the UCG conditions to the maximum extent possible. Moreover, several characterization techniques such as the proximate and ultimate analysis, petrographic analysis, surface morphology and area, pore size distribution were employed to correlate the sorption to the raw coal properties.

From the chapter 4, it was understood that the sensitivity of the $CO_2$ density curve is maximum around 80 bar, even at temperatures 15°C above the critical temperature. As a consequence, the accuracy of the pressure transducer would play a pivotal role in determining the reliability of adsorption isotherms. Apart from this the temperature sensitivity, void volume, and volume calibration errors play significant roles. The performance evaluation was conduction through the blank isotherms, inert samples and silica gel isotherms. It was concluded from the analysis that in a volumetric apparatus, the errors would be minimal if the injection was in single pressure mode instead of cumulative. The volumetric adsorption measurement possesses inherent inaccuracies owing to the stated above; errors in adsorption isotherms being similar in nature and magnitude allow comparisons to be made between samples.

In chapter 5, pyrolysed coal chars obtained from two different coal samples were tested for $CO_2$ sorption capacities. In order to understand the effect of coal properties, the sorption capacities of chars were in turn correlated with the raw coal properties. In addition, the sorption capacities of four raw coals were also correlated to the coal properties to understand the influence of mineral and maceral components. It was observed from the experimental results that the adsorption magnitude is influenced by coal rank and coal properties. Within the coal properties, the vitrinite, volatile matter, and ash content showed a consistent trend for the studied samples with literature data. It was particularly noted that the maceral distribution on the coal samples has a pivotal role in determining the adsorption capacities of virgin coals. From the four coal samples, coal A (a coking coal) and coal B (a non-coking coal) were chosen for the comparison of adsorption capacity with their respective pyrolysed coal chars at 800°C and 1000°C. Results suggest that adsorption capacity of coal char samples is significantly higher than virgin coal samples. This increase in adsorption in coal chars is because of the enhanced surface area, which is a strong function of coal nature and pyrolysis temperature. Further, pore size distribution studies provided a fundamental understanding about the adsorption behaviour in coal A and coal B. From the studies, it was understood that the char obtained from non-coking coal (coal A) are more microporous than coking coal (coal B), thus leading to greater adsorption due to enhanced surface area.

In chapter 6, the sorption capacities of gasified char obtained from different coal samples were quantified. A significant increase in the sorption capacity was observed in the gasified chars compared to the respective raw coals. However, the increase in sorption was a function of the coal type and the conversion of the coal in 10 mins of gasification at $800^{o}C$ under $CO_2$ atmosphere at 2 liter/min. It was observed that the chars from the sub-bituminous coal tested (characteristic of very high vitrinite content) had the highest sorption capacity among the four coals followed by the lignite and bituminous char respectively. Moreover, effective diffusivities were estimated and were found to decrease with pressure. In addition, the diffusivities were a function of the mesoporous content in the raw coals. The diffusivity in the chars was a function of coal type. For instance, it was particularly noted that the bituminous coal had higher diffusivity than lignite in the raw form, however the trend reversed in the case chars. The sorption isotherms for all the samples were fit to the Langmuir theory and the Adsorption potential theory models like the D-R and D-A equation. It was found that the D-A model yielded the best fit for the experimental data.

The experimental tools and results developed during the course of this work lay the background for undertaking further research in understanding the sorption behavior of gasified coal chars. Coals are known to swell upon adsorption of $CO_2$, however, gas sorption induced swelling has not been considered in this work. Swelling is an important parameter to consider in future studies for obtaining reliable estimates of sorption capacity. The effect of conversion and temperature on the surface area development in large coal particles still remains an area which has not been quantified. The results presented in this work do provide fundamentals on sorption in gasified particles; however, sorption and diffusion measurements on coal cores would be more meaningful for scale up or simulation purposes. The effect of overburden pressure on the sorption behavior of chars is also an area that can be looked at.

# References

1. Metz B, Davidson O, De Coninck H C, Loos M, and Meyer L A. Special report on carbon dioxide capture and storage. IPCC, Cambridge University Press, Cambridge, United Kingdom and NewYork; 2005.

2. IPCC (Intergovernmental panel on climate change). Climate change : The physical science basis. Geneva, Switzerland, 2007

3. Bachu S, Bonijoly D, Bradshaw J, Burruss R, Holloway S, Christensen NP. CO $_2$ storage capacity estimation: Methodology and gaps. International Journal of Greenhouse Gas Control. 2007 10;1(4):430-43.

4. Pro Oxygen.$CO_2$Now; Pro Oxygen: Victoria, British Columbia, Canada, 2013; www.co2now.org (accessed Nov 4, 2013).

5. Huesemann M. The limits of technological solutions to sustainable development. Clean Technologies and Environmental Policy. 2003 03/01;5(1):21-34.

6. Bachu S. CO $_2$ storage in geological media: Role, means, status and barriers to deployment. Progress in Energy and Combustion Science. 2008 4; 34(2):254-73.

7. IEA. Energy technology perspectives: Scenarios and strategies. France: International Energy Association; 2010.

8. Seibel BA, Walsh PJ. Potential impacts of CO $_2$ injection on deep-sea biota. Science. 2001 October 12;294(5541):319-20.

9. Klara SM, Srivastava RD, McIlvried HG. Integrated collaborative technology development program for CO2 sequestration in geologic formations—United states department of energy R&D. Energy Conversion and Management. 2003 10;44(17):2699-712.

10. Simon R, Graue DJ. Generalized Correlations for predicting solubility, swelling and viscosity behavior of CO2 -crude oil. Journal of Petroleum Technology. 1965;17(1):102.

11. Mastalerz M, Gluskoter H, Rupp J. Carbon dioxide and methane sorption in high volatile bituminous coals from indiana, USA. International Journal of Coal Geology. 2004 10/22;60(1):43-55.

12. Bhutto AW, Bazmi AA, Zahedi G. Underground coal gasification: From fundamentals to applications. Progress in Energy and Combustion Science. 2013 2;39(1):189-214.

13. Couch GR. Underground coal gasification. IEA Clean Coal Centre; 2009.

14. Klimenko A. Early ideas in underground coal gasification and their evolution. Energies. 2009;2(2):456-76.

15. Liu S, Li J, Mei M, Dong D. Groundwater pollution from underground coal gasification. Journal of China University of Mining and Technology. 2007 12;17(4):467-72.

16. - Underground coal gasification: A brief review of current status. - Ind Eng Chem Res. (-17):- 7865.

17. Larsen JW. Sorption of carbon dioxide by coals. Fuel Chemistry Division Preprints. 2003;48(1):112.

18. Day S, Duffy G, Sakurovs R, Weir S. Effect of coal properties on CO2 sorption capacity under supercritical conditions. International Journal of Greenhouse Gas Control. 2008 7;2(3):342-52.

19. Mahajan OP, Walker Jr. PL. Chapter 4 - Porosity of coals and coal products. In: Analytical Methods for Coal and Coal Products, editor: Clarence Karr, Jr. Academic Press; 1978. p. 125-62.

20. Burton E, Friedmann J, Upadhye R. Best practices in underground coal gasification. Lawrence Livermore National Laboratory; Report No.: DOE Contract No: W-7405-Eng-48.

21. Kurt Kleiner. Coal-to-gas: The answer for a low-emissions future?. 2008 print(0803).

22. Younger P. Hydrogeological and geomechanical aspects of underground coal gasification and its direct coupling to carbon capture and storage. Mine Water and the Environment. 2011 06/01;30(2):127-40.

23. Roddy DJ, Younger PL. Underground coal gasification with CCS: A pathway to decarbonising industry. Energy Environ Sci. 2010;3(4):400-7.

24. Self SJ, Reddy BV, Rosen MA. Review of underground coal gasification technologies and carbon capture. International Journal of Energy and Environmental Engineering. 2012;3(16).

25. Friedmann SJ, Upadhye R, Kong F. Prospects for underground coal gasification in carbon-constrained world. Energy Procedia. 2009 2;1(1):4551-7.

26. Kempka T, Steeger TF, Li DY, Schulten M, Schluter R, Krooss BM. Carbon dioxide sorption capacities of coal gasification residues. - Environ Sci Technol. 2011;45(4):1719.

27. Sircar S. Gibbsian surface excess for gas adsorption- revisited. - Ind Eng Chem Res. 1999;38(10):3670.

28. Rajendran A. Adsorption and chromatography under supercritical conditions , PhD Dissertation. ETH Zurich; 2004.

29. Menon PG. Adsorption at high pressures. - Chem Rev. 1968;68(3):277.

30. Sircar S. Recent developments in macroscopic measurement of multicomponent gas adsorption equilibria, kinetics, and heats. Ind Eng Chem Res. 2007 05/01; 2014/09;46(10):2917-27.

31. Pini R. Enhanced coal bed methane recovery finalized to carbon dioxide storage , PhD Dissertation. ETH ZURICH; 2009.

32. Bhebhe S. The effect of coal composition on carbon dioxide adsorption, PhD Dissertation. University of the Witwatersrand; 2008.

33. Goodman AL, Busch A, Duffy GJ, Fitzgerald JE, Gasem KAM. An inter-laboratory comparison of $CO_2$ isotherms measured on argonne premium coal samples. Energy Fuels. 2004;18(4):1175.

34. Clarkson CR, Bustin RM. Binary gas adsorption/desorption isotherms: Effect of moisture and coal composition upon carbon dioxide selectivity over methane. International Journal of Coal Geology. 2000 3;42(4):241-71.

35. Mohammad S, Fitzgerald J, Robinson RLJ, Gasem KAM. Experimental uncertainties in volumetric methods for measuring equilibrium adsorption. - Energy Fuels. 2009(5):2810.

36. Langmuir I. Journal of American Chemical Society. 1916;38:2221.

37. Gregg SJ, Sing KSW. Adsorption, surface area and porosity. London: Academic Press; 1982.

38. Dubinin MM. Adsorption in micropores. J Colloid Interface Sci. 1967 4;23(4):487-99.

39. Dubinin MM, Radushkevich LV. Equation of the characteristic curve of activated charcoal. Proc. Acad. Sci. Phys. CHem. Sect. USSR. 1947;55.

40. Hutson ND, Yang RT. Theoretical basis for the Dubinin-Radushkevitch (D-R) adsorption isotherm equation. Adsorption; 3, 3; 189-195. 1997;3(3):189.

41. Agarwal RK, Schwarz J.A. Analysis of high pressure adsorption of gases on activated carbon by potential theory. Carbon. 1988;26(6).

42. Clarkson CR, Bustin RM. The effect of pore structure and gas pressure upon the transport properties of coal: A laboratory and modeling study. 1. isotherms and pore volume distributions . Fuel. 1999;78(11).

43. Marsh H. Adsorption methods to study microporosity in coals and carbons—a critique. Carbon. 1987;25(1):49-58.

44. Clarkson CR, Bustin RM. The effect of pore structure and gas pressure upon the transport properties of coal: A laboratory and modeling study-1. Isotherms and pore volume distributions. Fuel. 1999 9;78(11):1333-44.

45. Li M, Gu AZ. Determination of the quasi-saturated vapor pressure of supercritical gases in the adsorption potential theory application. Journal of Colloid and Interface Science. 2004;273:356.

46. R. Reich, W.T. Ziegier, K.A. Rogers,. Ind. Eng. Chem. Process Des. Dev. 1980;19:336.

47. - Advanced coal characterization:  A review. Energy Fuels. (- 2):- 451.

48. McCartney JT, Teichmüller M. Classification of coals according to degree of coalification by reflectance of the vitrinite component. Fuel. 1972 1;51(1):64-8.

49. Gan H, Nandi SP, Walker Jr PL. Nature of the porosity in American coals. Fuel. 1972 10;51(4):272-7.

50. Larsen JW, Hall P, Wernett PC. Pore structure of the argonne premium coals. Energy Fuels. 1995;9(2):324.

51. Mahajan OP. $CO_2$ surface area of coals: The 25-year paradox. Carbon. 1991;29(6):735-42.

52. Prinz D, Littke R. Development of the micro- and ultramicroporous structure of coals with rank as deduced from the accessibility to water. Fuel. 2005 9;84(12–13):1645-52.

53. Ozdemir E, Morsi BI, Schroeder K. $CO_2$ adsorption capacity of argonne premium coals. Fuel. 2004 5;83(7–8):1085-94.

54. Saghafi A, Faiz M, Roberts D. CO2 storage and gas diffusivity properties of coals from sydney basin, australia. International Journal of Coal Geology. 2007 4/2;70(1–3):240-54.

55. Jian X, Guan P, Zhang W. Carbon dioxide sorption and diffusion in coals: Experimental investigation and modeling. Science China Earth Sciences. 2012;55(4):633-643.

56. Laxminarayana C, Crosdale PJ. Role of coal type and rank on methane sorption characteristics of bowen basin, australia coals. International Journal of Coal Geology. 1999 7;40(4):309-25.

57. Clarkson CR, Marc Bustin R. Variation in micropore capacity and size distribution with composition in bituminous coal of the western Canadian sedimentary basin: Implications for coalbed methane potential. Fuel. 1996 10;75(13):1483-98.

58. Gürdal G, Yalçın MN. Gas adsorption capacity of carboniferous coals in the zonguldak basin (NW turkey) and its controlling factors. Fuel. 2000 12;79(15):1913-24.

59. Perera MSA, Ranjith PG, Choi SK, Airey D, Weniger P. Estimation of gas adsorption capacity in coal: A review and an analytical study. - International Journal of Coal Preparation and Utilization. 2012;32(1):25.

60. Carroll RE, Pashin JC. Relationship of sorption capacity to coal quality: $CO_2$ sequestration potential of coalbed methane reservoirs in the black warrior basin. International coalbed methane symposium proceedings; Alabama. ; 2003.

61. Crosdale PJ, Beamish BB, Valix M. Coalbed methane sorption related to coal composition. International Journal of Coal Geology. 1998 2;35(1–4):147-58.

62. Harris LA, Yust CS. Transmission electron microscope observations of porosity in coal. Fuel. 1976 7;55(3):233-6.

63. Hessley KR, Reasoner JW, Riley JT. Coal science - an introduction to chemistry, technology, and utilization. Canada: Wiley-Interscience; 1986.

64. Yu J, Lucas JA, Wall TF. Formation of the structure of chars during devolatilization of pulverized coal and its thermo properties: A review. Progress in Energy and Combustion Science. 2007 4;33(2):135-70.

65. Saxena SC. Devolatilization and combustion characteristics of coal particles. Progress in Energy and Combustion Science. 1990;16(1):55-94.

66. De Koranyi A, Balek V. Structural changes in coals during pyrolysis. Thermochimica Acta. 1985 9/15;93(0):737-40.

67. Balek V, De Koranyi A. Diagnostics of structural alterations in coal: Porosity changes with pyrolysis temperature. Fuel. 1990 12;69(12):1502-6.

68. Yu J, Strezov V, Lucas J, Liu G, Wall T. A mechanistic study on char structure evolution during coal devolatilization - Experiments and model predictions. Proceedings of the Combustion Institute. 2002;29(1):467-73.

69. Miura S, Silveston PL. Change of pore properties during carbonization of coking coal. Carbon. 1980;18(2):93-108.

70. Wei De Jiang, Lee I, Yang RYK. Microstructural variations of lignite, subbituminous and bituminous coals and their high temperature chars. Fuel Process Technol. 1988 3;18(1):11-23.

71. Gutierrez M, Cukierman AL, Lemcoff NO. Study of subbituminous coal chars: Effect of heat treatment temperature on their structural characteristics. Journal of Chemical Technology & Biotechnology. 1988(2):85.

72. Razouk RI, Saleeb FZ, Youssef AM. The effect of thermal treatment on the surface area of coal. Carbon. 1968 6;6(3):325-31.

73. Toda Y, Hatami M, Toyoda S, Yoshida Y, Honda H. Fine structure of carbonized coals. Carbon. 1970 10;8(4):565-71.

74. Solomon PR, Serio MA, Despande GV, Kroo E. Cross-linking reactions during coal conversion. - Energy Fuels. 1990(1):42.

75. Suuberg EM, Lee D, Larsen JW. Temperature dependence of crosslinking processes in pyrolysing coals. Fuel. 1985 12;64(12):1668-71.

76. Matsuoka K, Akiho H, Xu W, Gupta R, Wall TF, Tomita A. The physical character of coal char formed during rapid pyrolysis at high pressure. Fuel. 2005 1;84(1):63-9.

77. De Koranyi A. The relationship between specific reactivity and the pore structure of coal chars during gasification. Carbon. 1989;Volume 27, Issue 1, 1989, Pages 55–61(1):55.

78. Walker PL. The scientific base for coal gasification. Seminar on combustion technology; Pennsylvania State University. ; 1977.

79. Adschiri T, Furusawa T. Relation between $CO_2$ reactivity of coal char and BET surface area. Fuel. 1986;65, 927.

80. Piero S, Osvalda S, Sabato M. Gasification of a coal char by oxygen and carbon dioxide. Carbon. 1998;36(4):443.

81. Feng B, Bhatia SK. Variation of the pore structure of coal chars during gasification. Carbon. 2003;41(3):507-23.

82. Roberts DJH. Char gasification in mixtures of $CO_2$ and $H_2O$: Competition and inhibition ; 2007.

83. Batchelder HR, Busche RM, Armstrong WP. Kinetics of coal gasification- proposed mechanism of gasification. Industrial and engineering chemistry. 1953;45(9):1856.

84. Ramasamy S, Sripada PP, Khan MM, Tian S, Trivedi J, Gupta R. Adsorption behavior of CO2 in coal and coal char. Energy and Fuels. 2014; 28(8):5241.

85. Chilev C, Pentchev I, Weinberger B, Lamari B. A comparison between the different methods for the measurement of excess adsorption of pure gases on porous adsorbents at high pressure. Journal of the University of Chemical Technology and Metallurgy. 2007;42(1):77-84.

86. Malbrunot P, Vidal D, Vermesse J, Chahine R, Bose TK. Adsorbent helium density measurement and its effect on adsorption isotherms at high pressure. - Langmuir. 1997;13(3):539.

87. Maggs F, Schwabe P, Williams J. Adsorption of helium on carbons: Influence on measurement of density. Nature. 1960 06/18;186(4729):956-8.

88. Kini KA, Stacy W. The adsorption of helium by carbonaceous solids. Carbon. 1963 10;1(1):17-24.

89. Ramasamy S, Tian S, Khan MM, Trivedi J, Gupta R. Assessing $CO_2$ storage potential in coal chars for UCG-CCS system. IEA 2nd underground coal gasification network workshop, Banff, Alberta, Canada. ; 2012.

90. Crank J. The mathematics of diffusion. 1-7; 1975.

91. Lemmon EW, McLinden MO, Friend DG. Thermophysical properties of fluid systems. In: Linstrom PJ, Mallard WG, editors. NIST Chemistry WebBook, NIST Standard Reference Database Number 69. Gaithersburg MD: National Institute of Standards and Technology; Retrieved September 2013.

92. Tian S. Fragmentation of large coal particles at high temperature in a drop tube furnace , PhD Dissertation, Canada: University of Alberta (Canada); 2011.

93. Solomon PR, Serio MA, Suuberg EM. Coal pyrolysis: Experiments, kinetic rates and mechanisms. Progress in Energy and Combustion Science. 1992;18(2):133-220.

94. Carles P. A brief review of the thermophysical properties of supercritical fluids. The Journal of Supercritical fluids. 2010;2(11).

95. Rajendran A, Hocker T, Di Giovanni O, Mazzotti M. Experimental observation of critical depletion: Nitrous oxide adsorption on Silica gel. Langmuir 2002**,** 18*,* 9726-9734

96. Gilgen, R., R. Kleinrahm, and W. Wagner. Supplementary measurements of the (pressure, density, temperature) relation of carbon dioxide in the homogeneous region at temperatures from 220 K to 360 K and pressures up to 13 MPa. . The Journal of Chemical Thermodynamics. 1992;24(12):1243.

97. Di Giovanni O, Dorfler W, Mazzotti M, Morbidelli M. Adsorption of supercritical carbon dioxide on silica. Langmuir. 2001, 17, 4316-4321.

98. Krooss BM, van Bergen F, Gensterblum Y, Siemons N, Pagnier HJM, David P. High-pressure methane and carbon dioxide adsorption on dry and moisture-equilibrated pennsylvanian coals. International Journal of Coal Geology. 2002 7;51(2):69-92.

99. Songolzadeh M, Ravanchi MT, Soleimani M. Carbon dioxide capture and storage: A general review on adsorbents. World Academy of Science, Engineering and Technology. 2012;70:225.

100. Pashin JC, Carroll RE, Groshong RHJ, Raymond DE, McIntyre M, Payton WJ. Geologic screening criteria for sequestration of CO2 in coal: Quantifying potential of the black Warrior coalbed methane fairway, alabama:, Annual Technical Progress Report. U.S. Department of Energy, National Technology Laboratory; 2003. Report No.: Contract DE-FC-00NT40927.

101. Ryan B, Richardson D. The potential for $CO_2$ sequestration in British Columbia coal seams. In: Legg JF, Campbell FR, editors. Carbon Dioxide Capture and Storage: A Compendium of Canada's Participation. Ontario: Office of Energy Research and Development Natural Resources Canada; 2005.

102. Gluskoter H, Mastalerz M, Stanton R. The potential for carbon dioxide sequestration in coal beds: New evidence from methane and carbon dioxide adsorption analysis for coals from lignite to anthracite. Geological association of America, Annual meeting, ; 2002.

103. Malekshahian M, Hill JM. Effect of pyrolysis and $CO_2$ gasification pressure on the surface area and pore size distribution of petroleum coke. Energy & Fuels. 2011;25(5250).

104. Jing X, Wang Z, Zhang Q, Yu Z, Li C, Huang J, et al. Evaluation of CO2 gasification reactivity of different coal rank chars by physicochemical properties. Energy and Fuels:7287.

105. Ng SH, Fung PCD, Kim SD. Study of pore structure and reactivity of Canadian coal derived chars. Fuel. 1988;67(5):700.

106. Van Heek KH, Muhlen H. Aspects of coal properties amd composition important for gasification. Furl. 1985;64(10):1405.

107. Miura K, Hashimoto K, Silveston PL. Factors affecting the reactivity of coal chars during gasification, and indexes representing reactivity. Fuel. 1989;68(11):1461.

108. Takarada T, Tamai Y, Tomita A. Reactivities of 34 coals under steam gasification. Fuel. 1985;64(10):1438.

109. Sakawa M, Sakurai Y, Hara Y. Influence of coal characteristics on CO2 gasification. Fuel. 1982;61(8):717.

110. Runkenstein E, Vaidyanathan AS, Younquist GR. Sorption by solids with bidisperse pore structures. Chemical Engineering Science. 1971;26:1305.

111. Pillalamarry M, Harpalani S, Liu. Gas diffusion behavior of coal and its impact on production from coalbed methane reservoirs. International Journal of Coal Geology. 2011;86:342.

112. Siemons N, Wolf KAA, Bruining J. Interpretation of carbon dioxide diffusion behavior in coals. International Journal of Coal Geology. 2007;72:315.

113. Weishauptova Z, Sykorova I. Dependence of carbon dioxide sorption on the petrographic composition of bituminous coals from the Czech part of the upper Silesian basin, Czech republic . Fuel. 2011;90(1):312.

114. Smith DM, Williams FL. Diffusion models for gas production from coal. Fuel. 1984;63:256

# Appendix – A
# Error and Sensitivity Analysis

## A.1 Sensitivity Analysis

This section details the parameters in the error propagation models used for carrying out the sensitivity analysis.

### A.1.1 Pressure Sensitivity

**Table A.1:** Simulation parameters used for pressure sensor sensitivity

| **Parameter** | **Value** |
|---|---|
| Temperature | 45.5$^{o}$C |
| Standard Volume Used in Pycnometer | 26.43135087 cc |
| Reference Cell volume | 24.09723316 cc |
| Sample Cell Volume | 39.88943627 cc |
| Sample skeletal volume | 0 cc |
| Accuracy of pressure sensor (eps) | 0.01, 0.011, 0.02, 0.06 bar |
| Temperature variation (ets) | 0.1 $^{o}$C |
| Error in calibrated volume (eVstd) | 0.05 cc |

**Table A.2:** Pressure Sensitivity Analysis

| Pressure Sensitivity | | | | | | | | | |
|---|---|---|---|---|---|---|---|---|---|
| Pressure (bar) | **Total Error (mmole)** | **Total Error (mmole)** | **Total Error (mmole)** | **Total Error (mmole)** | **Total Error (mmole)** | **Percentage Increase 1%** | **Percentage Increase 10%** | **Percentage Increase 100%** | **Percentage Increase 200%** |
| | eps=0.01 | eps=0.0101 | eps=0.011 | eps=0.02 | eps=0.03 | eps=0.0101 | eps=0.011 | eps=0.02 | eps=0.03 |
| 4 | 0.22 | 0.22 | 0.22 | 0.24 | 0.27 | 0.07 | 0.69 | 9.45 | 23.60 |
| 8 | 0.22 | 0.22 | 0.23 | 0.25 | 0.28 | 0.07 | 0.72 | 9.86 | 24.58 |
| 12 | 0.24 | 0.24 | 0.24 | 0.26 | 0.29 | 0.07 | 0.74 | 10.04 | 25.00 |
| 17 | 0.25 | 0.25 | 0.25 | 0.28 | 0.31 | 0.07 | 0.73 | 10.02 | 24.95 |
| 22 | 0.27 | 0.27 | 0.27 | 0.30 | 0.34 | 0.07 | 0.72 | 9.83 | 24.49 |
| 28 | 0.30 | 0.30 | 0.30 | 0.33 | 0.37 | 0.07 | 0.69 | 9.50 | 23.72 |
| 35 | 0.34 | 0.34 | 0.35 | 0.38 | 0.42 | 0.06 | 0.67 | 9.18 | 22.96 |
| 43 | 0.41 | 0.41 | 0.41 | 0.45 | 0.50 | 0.06 | 0.66 | 9.01 | 22.57 |
| 55 | 0.52 | 0.53 | 0.53 | 0.58 | 0.65 | 0.07 | 0.70 | 9.62 | 24.00 |
| 70 | 0.72 | 0.73 | 0.73 | 0.79 | 0.88 | 0.06 | 0.61 | 8.39 | 21.10 |
| 78 | 0.86 | 0.86 | 0.86 | 0.91 | 1.00 | 0.04 | 0.46 | 6.34 | 16.14 |
| 81 | 0.93 | 0.93 | 0.93 | 0.98 | 1.06 | 0.04 | 0.40 | 5.51 | 14.11 |
| 83 | 0.97 | 0.97 | 0.97 | 1.01 | 1.09 | 0.03 | 0.36 | 4.97 | 12.76 |
| 84 | 1.00 | 1.00 | 1.00 | 1.04 | 1.11 | 0.03 | 0.33 | 4.58 | 11.80 |
| 85 | 1.02 | 1.02 | 1.02 | 1.06 | 1.13 | 0.03 | 0.30 | 4.23 | 10.93 |

## A.1.2 Temperature Sensitivity

**Table A.3:** Simulation parameters used for temperature sensitivity

| **Parameter** | **Value** |
|---|---|
| Temperature | 45.5$^{o}$C |
| Standard Volume Used in Pycnometer | 26.43135087 cc |
| Reference Cell volume | 24.09723316 cc |
| Sample Cell Volume | 39.88943627 cc |
| Sample skeletal volume | 0 cc |
| Accuracy of pressure sensor (eps) | 0.01 bar |
| Temperature variation (ets) | 0.1, 0.0101, 0.11, 0.2, 0.3 $^{o}$C |
| Error in calibrated volume (eVstd) | 0.05 cc |

**Table A.4:** Temperature Sensitivity Analysis

| Temperature Sensitivity | | | | | | | | |
|---|---|---|---|---|---|---|---|---|
| Pressure (bar) | **Total Error (mmole)** | **Total Error (mmole)** | **Total Error (mmole)** | **Total Error (mmole)** | **Total Error (mmole)** | **Percentage Increase 1%** | **Percentage Increase 10%** | **Percentage Increase 100%** | **Percentage Increase 200%** |
| | ets=0.1 | ets=0.101 | ets=0.11 | ets=0.2 | ets=0.3 | ets=0.101 | ets=0.11 | ets=0.2 | ets=0.3 |
| 4 | 0.22 | 0.22 | 0.23 | 0.39 | 0.58 | 0.75 | 7.58 | 80.19 | 164.41 |
| 8 | 0.22 | 0.23 | 0.24 | 0.40 | 0.59 | 0.73 | 7.34 | 78.17 | 160.75 |
| 12 | 0.24 | 0.24 | 0.25 | 0.41 | 0.60 | 0.69 | 6.94 | 74.70 | 154.41 |
| 17 | 0.25 | 0.25 | 0.27 | 0.43 | 0.61 | 0.63 | 6.39 | 69.85 | 145.48 |
| 22 | 0.27 | 0.27 | 0.29 | 0.45 | 0.64 | 0.56 | 5.73 | 63.80 | 134.27 |
| 28 | 0.30 | 0.30 | 0.32 | 0.47 | 0.67 | 0.49 | 4.99 | 56.85 | 121.23 |
| 35 | 0.34 | 0.35 | 0.36 | 0.51 | 0.71 | 0.41 | 4.21 | 49.28 | 106.79 |
| 43 | 0.41 | 0.41 | 0.42 | 0.58 | 0.78 | 0.33 | 3.43 | 41.33 | 91.31 |
| 55 | 0.52 | 0.53 | 0.54 | 0.70 | 0.92 | 0.26 | 2.66 | 33.08 | 74.81 |
| 70 | 0.72 | 0.73 | 0.74 | 0.92 | 1.17 | 0.20 | 2.06 | 26.28 | 60.81 |
| 78 | 0.86 | 0.86 | 0.88 | 1.05 | 1.32 | 0.17 | 1.74 | 22.57 | 52.95 |
| 81 | 0.93 | 0.93 | 0.94 | 1.11 | 1.36 | 0.15 | 1.53 | 19.97 | 47.36 |
| 83 | 0.97 | 0.97 | 0.98 | 1.14 | 1.38 | 0.13 | 1.36 | 17.92 | 42.88 |
| 84 | 1.00 | 1.00 | 1.01 | 1.16 | 1.39 | 0.12 | 1.22 | 16.23 | 39.14 |
| 85 | 1.02 | 1.02 | 1.03 | 1.17 | 1.38 | 0.11 | 1.11 | 14.82 | 35.98 |

## A.1.3 Volume Calibration Sensitivity

**Table A.5:** Simulation parameters used for volume calibration sensitivity

| **Parameter** | **Value** |
|---|---|
| Temperature | $45.5^{o}$C |
| Standard Volume Used in Pycnometer | 26.43135087 cc |
| Reference Cell volume | 24.09723316 cc |
| Sample Cell Volume | 39.88943627 cc |
| Sample skeletal volume | 0 cc |
| Accuracy of pressure sensor (eps) | 0.01 bar |
| Temperature variation (ets) | $0.1^{o}$C |
| Error in calibrated volume (eVstd) | 0.05, 0.0505, 0.055, 0.1, 0.15 cc |

**Table A.6:** Volume Calibration Sensitivity Analysis

| Volume Calibration Sensitivity | | | | | | | | | |
|---|---|---|---|---|---|---|---|---|---|
| **Pressure (bar)** | **Total Error (mmole)** | **Total Error (mmole)** | **Total Error (mmole)** | **Total Error (mmole)** | **Total Error (mmole)** | **Percentage Increase 0.5 %** | **Percentage Increase 5%** | **Percentage Increase 50%** | **Percentage Increase 100%** |
| | eVstd=0.05 | eVstd=0.0505 | eVstd=0.055 | eVstd=0.1 | eVstd=0.15 | eVstd=0.0505 | eVstd=0.055 | eVstd=0.1 | eVstd=0.15 |
| 4 | 0.22 | 0.22 | 0.22 | 0.22 | 0.23 | 0.01 | 0.10 | 1.48 | 3.91 |
| 8 | 0.22 | 0.22 | 0.23 | 0.24 | 0.26 | 0.04 | 0.44 | 6.08 | 15.51 |
| 12 | 0.24 | 0.24 | 0.24 | 0.27 | 0.31 | 0.10 | 1.00 | 13.45 | 32.86 |
| 17 | 0.25 | 0.25 | 0.25 | 0.31 | 0.38 | 0.17 | 1.76 | 22.79 | 53.42 |
| 22 | 0.27 | 0.27 | 0.28 | 0.36 | 0.48 | 0.26 | 2.67 | 33.17 | 74.99 |
| 28 | 0.30 | 0.30 | 0.31 | 0.43 | 0.59 | 0.36 | 3.67 | 43.75 | 96.05 |
| 35 | 0.34 | 0.35 | 0.36 | 0.53 | 0.74 | 0.46 | 4.68 | 53.90 | 115.63 |
| 43 | 0.41 | 0.41 | 0.43 | 0.67 | 0.95 | 0.56 | 5.67 | 63.24 | 133.23 |
| 55 | 0.52 | 0.53 | 0.56 | 0.90 | 1.30 | 0.65 | 6.56 | 71.38 | 148.30 |
| 70 | 0.72 | 0.73 | 0.78 | 1.29 | 1.89 | 0.73 | 7.37 | 78.41 | 161.17 |
| 78 | 0.86 | 0.87 | 0.93 | 1.57 | 2.31 | 0.78 | 7.86 | 82.57 | 168.74 |
| 81 | 0.93 | 0.93 | 1.00 | 1.71 | 2.53 | 0.81 | 8.13 | 84.89 | 172.93 |
| 83 | 0.97 | 0.97 | 1.05 | 1.80 | 2.67 | 0.83 | 8.34 | 86.57 | 175.97 |
| 84 | 1.00 | 1.00 | 1.08 | 1.87 | 2.77 | 0.84 | 8.49 | 87.89 | 178.33 |
| 85 | 1.02 | 1.03 | 1.11 | 1.92 | 2.85 | 0.86 | 8.63 | 88.97 | 180.29 |

# Appendix – B
# Adsorption Isotherms and Estimation of Model Parameters

## B1. Adsorption Isotherms

The $CO_2$ adsorption isotherms for the raw coals B, C, D and E have been presented in table B1. In addition, the isotherms for the gasified chars have been presented in table B2. The isotherms for all the samples have been obtained at 45.5°C.

**Table B.1**: Adsorption isotherms for raw coals at 45.5°C

| Coal B | | | Coal E | | | Coal C | | | Coal D | | |
|---|---|---|---|---|---|---|---|---|---|---|---|
| **Pressure (bar)** | **Excess (mmole/g)** | **Error** | **Pressure (bar)** | **Excess (mmole/g)** | **Error** | **Pressure (bar)** | **Excess (mmole/g)** | **Error** | **Pressure (bar)** | **Excess (mmole/g)** | **Error** |
| 2.14 | 0.09 | 0.00 | 2.62 | 0.08 | 0.00 | 0.97 | 0.23 | 0.01 | 1.59 | 0.13 | 0.00 |
| 13.24 | 0.44 | 0.02 | 12.62 | 0.48 | 0.02 | 3.52 | 0.68 | 0.01 | 10.96 | 0.62 | 0.02 |
| 31.12 | 0.65 | 0.04 | 29.76 | 0.73 | 0.04 | 7.93 | 1.05 | 0.03 | 26.06 | 1.12 | 0.04 |
| 61.67 | 0.73 | 0.09 | 60.20 | 1.01 | 0.10 | 14.34 | 1.31 | 0.04 | 57.36 | 1.43 | 0.09 |
| 87.85 | 0.80 | 0.17 | 86.14 | 1.43 | 0.19 | 23.10 | 1.58 | 0.05 | 86.45 | 1.42 | 0.18 |
| 91.22 | 1.15 | 0.20 | 90.34 | 1.20 | 0.21 | 34.76 | 1.83 | 0.08 | 90.60 | 1.42 | 0.21 |
| | | | | | | 53.74 | 2.01 | 0.12 | 92.00 | 1.65 | 0.22 |
| | | | | | | 76.64 | 2.10 | 0.19 | | | |
| | | | | | | 83.59 | 2.20 | 0.23 | | | |
| | | | | | | 86.54 | 2.15 | 0.25 | | | |
| | | | | | | 87.98 | 2.27 | 0.26 | | | |
| | | | | | | 89.43 | 2.03 | 0.27 | | | |
| | | | | | | 90.00 | 2.26 | 0.28 | | | |

**Table B.2**: Adsorption isotherms for gasified char800 at 45.5$^{o}$C

| **Coal B Char800** | | | **Coal E Char800** | | | **Coal C Char800** | | | **Coal D Char800** | | |
|---|---|---|---|---|---|---|---|---|---|---|---|
| **Pressure (bar)** | **Excess (mmole/g)** | **Error** | **Pressure (bar)** | **Excess (mmol/g)** | **Error** | **Pressure (bar)** | **Excess (mmol/g)** | **Error** | **Pressure (bar)** | **Excess (mmole/g)** | **Error** |
| 1.45 | 0.29 | 0.01 | 1.10 | 0.33 | 0.01 | 0.76 | 0.31 | 0.01 | 0.48 | 0.33 | 0.01 |
| 12.00 | 0.74 | 0.04 | 7.72 | 1.40 | 0.04 | 5.72 | 1.65 | 0.03 | 7.24 | 1.21 | 0.03 |
| 28.15 | 0.79 | 0.09 | 22.82 | 2.00 | 0.08 | 23.17 | 2.09 | 0.07 | 21.93 | 1.75 | 0.06 |
| 54.77 | 0.91 | 0.19 | 58.43 | 1.65 | 0.20 | 51.92 | 1.95 | 0.15 | 53.22 | 1.61 | 0.13 |
| 81.60 | 1.05 | 0.37 | 80.70 | 2.03 | 0.35 | 81.29 | 2.08 | 0.29 | 81.63 | 1.95 | 0.26 |
| 85.89 | 1.69 | 0.43 | 84.71 | 2.35 | 0.39 | 84.83 | 2.39 | 0.33 | 85.67 | 2.45 | 0.30 |

## B2. Helium Void Volume Estimation

The helium void volume in this study was estimated by the helium expansion method described in Chapter -3. In essence, a known quantity of helium is let into the sample cell containing the sample, based on the equilibrium pressure obtained and with the assumption that helium does not adsorb on the samples, the void volume is estimated. Table shows a typical helium void volume experiment for a coal sample. The void volume is calculated from the equation 3.20.

**Table B3.** Typical Helium void volume measurement in coal

| Initial pressure (psia) | Final Pressure (psia) | Density Initial (mmole/cc) | Density Final (mmole/cc) | Void Volume in the Cell (cc) |
|---|---|---|---|---|
| 1501.4 | 699.5 | 3.7409 | 1.7836 | 26.4439978 |
| 1599.5 | 750.65 | 3.9742 | 1.9112 | 26.01119298 |
| 1697.3 | 789.8 | 4.2054 | 2.0086 | 26.35507409 |
| 1797.3 | 841.7 | 4.4407 | 2.1373 | 25.9699466 |
| 1901 | 887.7 | 4.6775 | 2.2301 | 26.44525736 |
| 1999.9 | 921.8 | 4.9129 | 2.3353 | 26.59745138 |
| | | | Average | 26.30382003 |

The helium density of the sample can be calculated by quotient of the mass of the sample and the sample volume. The sample volume is estimated by subtracting the helium void volume from the sample cell volume.

## B3. Langmuir Model Parameters

The Langmuir equation is of the form:

$$\frac{n}{V} = \frac{Bp}{1 + Bp} \qquad (B.1)$$

Where, $B$ is a product of the constants in the condensation and the evaporation terms. $n$ is the absolute amount adsorbed per unit mass, $V$ is the monolayer capacity and $p$ is the pressure. The equation was rearranged and regression was performed with n versus p. The absolute amount adsorbed is calculated by using the adsorbed phase density $\rho_a$ equal to the density of liquid $CO_2$ 541.88 kg/m$^3$ in the equation B.2:

$$n_{absolute} = \frac{n_{excess}}{(1 - \frac{\rho_1^*}{\rho_a})} \qquad \text{(B.2)}$$

Non-linear regression was employed in the curve fit toolbox of Matlab. The 95% confidence intervals for the parameter estimates have been depicted as P- and P+. Where P is the parameter and P- and P+ are the lower and upper limit of the interval.

**Table B.4**: Langmuir Model Parameters for raw coals

| Coal | B | B- | B+ | V | V- | V+ | SSE | R-square |
|---|---|---|---|---|---|---|---|---|
| Coal B | 0.001 | -0.024 | 0.026 | 567.300 | -12690.000 | 13820.000 | 447.127 | 0.817 |
| Coal E | 0.001 | -0.012 | 0.014 | 721.400 | -7915.000 | 9358.000 | 180.392 | 0.948 |
| Coal C | 0.004 | -0.004 | 0.013 | 357.100 | -137.500 | 851.700 | 1063.667 | 0.939 |
| Coal D | 0.001 | -0.012 | 0.014 | 932.700 | -10470.000 | 12330.000 | 514.191 | 0.925 |

**Table B.5**: Langmuir Model Parameters for gasified char800

| Coal | B | B - | B+ | V | V- | V+ | SSE | R-square |
|---|---|---|---|---|---|---|---|---|
| Coal B Char800 | 0.000 | -0.026 | 0.027 | 2000 | -149900 | 153900.000 | 701.281 | 0.760 |
| Coal E Char800 | 0.036 | -0.057 | 0.128 | 106.4 | 12.900 | 200.000 | 1042.075 | 0.805 |
| Coal C Char800 | 0.052 | -0.072 | 0.176 | 101.8 | 33.000 | 170.600 | 985.223 | 0.820 |
| Coal D Char800 | 0.008 | -0.031 | 0.047 | 210.9 | -403.600 | 825.300 | 1197.488 | 0.809 |

## B.4 Dubinin - Radushkevich (D-R) Model Parameters

The DR formulation is as follows,

$$W = W_o \exp\{-(\frac{RT}{\beta E}\ln\frac{p^o}{p})^2\} \qquad \text{(B.3)}$$

Where, W is the absolute adsorbed volume of the adsorbate, $W_o$ is the micropore volume, $\beta$ is the affinity coefficient, E is the characteristic energy, T is the temperature, R is the universal gas constant and $p^o$ is the saturation vapor pressure. For the calculation of absolute adsorbed volume the adsorbed phase density was set to 581.44 kg/m3 and used in equation B.2. The regression has been performed on the equation after applying natural log on both sides. The final equation is of the form

$$y = \ln W_o - D * x^2 \qquad \text{(B.4)}$$

It is to be noted that the constant $(\frac{RT}{\beta E})^2$ has been replaced with D and x is $\ln\frac{p^o}{p}$. The saturation vapor pressure $p^o$has been calculated to be 93.4581 bar, based on the Antoine equation at 318.5K given by equation B.4

$$\ln P^o = B - C/(D + T) \qquad \text{(B.5)}$$

Where, B= 10.085 C= 1647.77 D= -21.62. The 95% confidence intervals for the parameter estimates have been depicted as P- and P+. Where P is the parameter and P- and P+ are the lower and upper limit of the interval.

**Table B.6**: D-R Model Parameters for raw coals

| Coal | D | D - | D+ | ln(W) | ln(W)- | ln(W)+ | SSE | R-square |
|---|---|---|---|---|---|---|---|---|
| Coal B | 0.198 | 0.089 | 0.306 | 3.425 | 2.769 | 4.080 | 0.953 | 0.865 |
| Coal E | 0.254 | 0.145 | 0.363 | 3.706 | 3.108 | 4.304 | 0.771 | 0.913 |
| Coal C | 0.141 | 0.107 | 0.174 | 4.323 | 4.094 | 4.552 | 1.156 | 0.886 |
| Coal D | 0.186 | 0.113 | 0.259 | 4.019 | 3.540 | 4.499 | 0.909 | 0.895 |

**Table B.7**: D-R Model Parameters for gasified char800

| Coal | D | D - | D+ | ln(W) | ln(W)- | ln(W)+ | SSE | R-square |
|---|---|---|---|---|---|---|---|---|
| Coal B Char800 | 0.000 | 0.000 | 0.001 | 3.424 | 2.683 | 4.164 | 1.413 | 0.586 |
| Coal E Char800 | 0.115 | 0.073 | 0.158 | 4.237 | 3.877 | 4.598 | 0.280 | 0.934 |
| Coal C Char800 | 0.101 | 0.069 | 0.134 | 4.314 | 3.988 | 4.641 | 0.230 | 0.949 |
| Coal D Char800 | 0.080 | 0.038 | 0.123 | 4.138 | 3.642 | 4.634 | 0.555 | 0.873 |

## B.5 Dubinin - Astakhov (D-A) Model Parameters

The Dubinin- Astakhov (DA) equation is of the form:

$$W = W_o \exp \{-(\frac{RT}{\beta E} \ln \frac{p^o}{p})^n\} \qquad \text{(B.5)}$$

The DA equation is a generalization of the DR equation (where *n*=2). *n* in the is referred to as the heterogeneity factor. As in the case of DR equation, the DA equation is also rearranged after applying natural logarithm on both sides of the equation before regression is performed.

$$\mathrm{y} = \ln W_o - D * x^{\,n} \qquad \text{(B.3)}$$

It is to be noted that the constant $(\frac{RT}{\beta E})^n$ has been replaced with D and x is $\ln \frac{p^o}{p}$. The saturation vapor pressure $p^o$has been calculated to be 93.4581 bar. For the calculation of absolute adsorbed volume the adsorbed phase density was set to 581.44 kg/m3 and used in equation B.2. The 95% confidence intervals for the parameter estimates have been depicted as P- and P+. Where P is the parameter and P- and P+ are the lower and upper limit of the interval.

**Table B.8**: D-A Model Parameters for raw coals

| Coal | D | D - | D+ | W | W- | W+ | n | n- | n+ | SSE | R-square |
|---|---|---|---|---|---|---|---|---|---|---|---|
| Coal B | 1.093 | -0.098 | 2.284 | 3.923 | 3.070 | 4.776 | 0.780 | 0.058 | 1.502 | 0.258 | 0.963 |
| Coal E | 1.018 | 0.143 | 1.892 | 4.125 | 3.500 | 4.750 | 0.954 | 0.336 | 1.571 | 0.168 | 0.980 |
| Coal C | 0.706 | 0.467 | 0.945 | 4.633 | 4.466 | 4.799 | 0.912 | 0.688 | 1.136 | 0.198 | 0.980 |
| CoalD | 0.911 | 0.460 | 1.362 | 4.376 | 4.074 | 4.677 | 0.897 | 0.561 | 1.234 | 0.106 | 0.987 |

**Table B.9**: D-A Model Parameters for gasified char800

| Coal | D | D - | D+ | ln (Wo) | ln (Wo)- | ln (Wo)+ | n | n- | n+ | SSE | R-square |
|---|---|---|---|---|---|---|---|---|---|---|---|
| Coal B Char800 | 6.211 | -2.559000 | 2561000 | 10 | -2559000 | 2561000. | 0.067 | 0.030 | 0.105 | 0.458 | 0.86 |
| Coal E Char800 | 0.265 | -0.379 | 0.909 | 4.337 | 3.742 | 4.932 | 1.449 | -0.138 | 3.036 | 0.233 | 0.94 |
| Coal C Char800 | 0.144 | -0.300 | 0.588 | 4.347 | 3.809 | 4.886 | 1.777 | -0.153 | 3.708 | 0.225 | 0.95 |
| Coal D Char800 | 0.634 | -0.407 | 1.674 | 4.529 | 3.705 | 5.352 | 0.816 | -0.066 | 1.699 | 0.193 | 0.95 |

# Appendix – C
# Transformed Diffusivity

The transformed diffusivity of $CO_2$ has been determined by fitting the unipore diffusion model to the $CO_2$ sorption kinetic data.

$$\frac{V_t}{V_\infty} = 6(\frac{D_e t}{\pi})^{\frac{1}{2}} \qquad (C.1)$$

$V_t$ is the total amount of gas adsorbed at time t, $V_\infty$ is the total volume adsorbed. The transformed diffusivity depicted by $D_e$ . In addition, the 95% confidence intervals for the diffusivity estimates have been given in the tables as De- and De+. De- refers to the lower liomit of the interval and De+ is the upper limit of the interval.

**Table C.1**: Transformed diffusivity of $CO_2$ for raw Coal B

| **Pressure (bar)** | **De** | **De-** | **De+** | **SSE** | **R-square** |
|---|---|---|---|---|---|
| 35 | 0.0001878 | 0.0001827 | 0.0001928 | 6.307283314 | 0.410964894 |
| 54 | 1.62E-04 | 1.59E-04 | 1.65E-04 | 3.298945532 | 0.789805667 |
| 77 | 0.0001465 | 0.0001437 | 0.0001493 | 2.446537275 | 0.86088324 |
| 84 | 9.83E-05 | 9.60E-05 | 1.01E-04 | 2.58789003 | 0.668502773 |

**Table C.2**: Transformed diffusivity of $CO_2$ for raw Coal C

| **Pressure (bar)** | **De** | **De-** | **De+** | **SSE** | **R-square** |
|---|---|---|---|---|---|
| 35 | 0.0002364 | 0.0002296 | 0.0002432 | 9.059364709 | 0.30117188 |
| 54 | 0.0002447 | 0.000238 | 0.0002514 | 8.520134348 | 0.473177131 |
| 77 | 0.0002382 | 0.0002323 | 0.0002442 | 6.875717332 | 0.711269143 |
| 84 | 0.0002308 | 0.0002249 | 0.0002367 | 7.052444241 | 0.657726921 |
| 87 | 0.0002221 | 0.0002168 | 0.0002275 | 5.967661304 | 0.710672635 |
| 88 | 0.0002046 | 0.0002001 | 0.000209 | 4.486270518 | 0.76839185 |
| 89 | 0.0001952 | 0.0001906 | 0.0001999 | 5.046905164 | 0.714463324 |
| 90 | 7.83E-05 | 7.70E-05 | 7.95E-05 | 0.95191154 | 0.887724884 |

**Table C.3**: Transformed diffusivity of $CO_2$ for raw Coal D

| Pressure (bar) | De | De- | De+ | SSE | R-square |
|---|---|---|---|---|---|
| 35 | 0.0001441 | 0.0001425 | 0.0001457 | 0.843107138 | 0.952858911 |
| 54 | 0.0001241 | 0.0001229 | 0.0001253 | 0.528764343 | 0.970684928 |
| 77 | 0.0001064 | 0.0001057 | 0.000107 | 0.204564559 | 0.9884081 |
| 84 | 4.02E-05 | 3.99E-05 | 4.05E-05 | 0.119407941 | 0.983098428 |

**Table C.4**: Transformed diffusivity of $CO_2$ for raw Coal E

| Pressure (bar) | De | De- | De+ | SSE | R-square |
|---|---|---|---|---|---|
| 35 | 9.50E-05 | 9.37E-05 | 9.64E-05 | 0.868377634 | 0.911488418 |
| 54 | 8.62E-05 | 8.52E-05 | 8.71E-05 | 4.83E-01 | 0.96571957 |
| 77 | 2.17E-05 | 2.15E-05 | 2.19E-05 | 0.092689393 | 0.969537977 |
| 84 | 8.23E-05 | 8.17E-05 | 8.30E-05 | 2.41E-01 | 0.982095872 |

**Table C.5**: Transformed diffusivity of $CO_2$ for Coal B Char800

| Pressure (bar) | De | De- | De+ | SSE | R-square |
|---|---|---|---|---|---|
| 28 | 0.0004709 | 0.0004555 | 0.0004863 | 1.492590307 | 0.762496202 |
| 55 | 4.79E-04 | 0.0004637 | 0.0004943 | 1.434218214 | 0.831722038 |
| 82 | 0.0003758 | 0.0003632 | 0.0003883 | 1.236601187 | 0.821155219 |
| 86 | 2.36E-04 | 0.000227 | 0.0002447 | 0.974407186 | 0.630178266 |

**Table C.6**: Transformed diffusivity of $CO_2$ for Coal C Char800

| Pressure (bar) | De | De- | De+ | SSE | R-square |
|---|---|---|---|---|---|
| 51 | 0.0005623 | 0.0005471 | 0.0005776 | 1.217656622 | 0.892917062 |
| 81 | 0.0005602 | 0.0005404 | 0.00058 | 2.054522249 | 0.805148718 |
| 84 | 0.000481 | 0.0004662 | 0.0004958) | 1.343291748 | 0.878955416 |

**Table C.7**: Transformed diffusivity of $CO_2$ for Coal D Char800

| Pressure (bar) | De | De- | De+ | SSE | R-square |
|---|---|---|---|---|---|
| 53 | 0.0005493 | 0.0005318 | 0.0005668 | 1.644244921 | 0.814230845 |
| 82 | 0.0005217 | 0.0005042 | 0.0005391 | 1.722316915 | 0.874694748 |
| 86 | 4.14E-04 | 4.01E-04 | 4.26E-04 | 1.130593873 | 0.884093877 |

**Table C.8**: Transformed diffusivity of $CO_2$ for Coal E Char800

| Pressure (bar) | De | De- | De+ | SSE | R-square |
|---|---|---|---|---|---|
| 58 | 5.53E-04 | 5.36E-04 | 5.71E-04 | 1.659250529 | 0.848347724 |
| 80 | 0.0005221 | 5.03E-04 | 5.41E-04 | 2.002947749 | 0.774790442 |
| 84 | 0.0004043 | 3.92E-04 | 4.17E-04 | 1.155604392 | 0.879043097 |